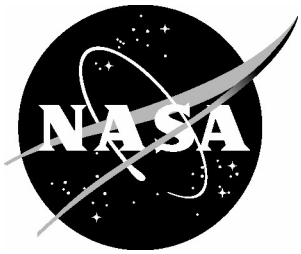
NASA/TM–20250000107 Corrected Copy



Uncertainty Quantification for Empirical X-59 Sonic Boom Loudness Levels

Jacob Klos
Langley Research Center, Hampton, Virginia

January 2025

NASA STI Program . . . in Profile

Since its founding, NASA has been dedicated to the advancement of aeronautics and space science. The NASA scientific and technical information (STI) program plays a key part in helping NASA maintain this important role.

The NASA STI program operates under the auspices of the Agency Chief Information Officer. It collects, organizes, provides for archiving, and disseminates NASA's STI. The NASA STI program provides access to the NTRS Registered and its public interface, the NASA Technical Reports Server, thus providing one of the largest collections of aeronautical and space science STI in the world. Results are published in both non-NASA channels and by NASA in the NASA STI Report Series, which includes the following report types:

- TECHNICAL PUBLICATION. Reports of completed research or a major significant phase of research that present the results of NASA Programs and include extensive data or theoretical analysis. Includes compilations of significant scientific and technical data and information deemed to be of continuing reference value. NASA counter-part of peer-reviewed formal professional papers but has less stringent limitations on manuscript length and extent of graphic presentations.

- TECHNICAL MEMORANDUM. Scientific and technical findings that are preliminary or of specialized interest, e.g., quick release reports, working papers, and bibliographies that contain minimal annotation. Does not contain extensive analysis.

- CONTRACTOR REPORT. Scientific and technical findings by NASA-sponsored contractors and grantees.

- CONFERENCE PUBLICATION. Collected papers from scientific and technical conferences, symposia, seminars, or other meetings sponsored or co-sponsored by NASA.

- SPECIAL PUBLICATION. Scientific, technical, or historical information from NASA programs, projects, and missions, often concerned with subjects having substantial public interest.

- TECHNICAL TRANSLATION. English-language translations of foreign scientific and technical material pertinent to NASA's mission.

Specialized services also include organizing and publishing research results, distributing specialized research announcements and feeds, providing information desk and personal search support, and enabling data exchange services.

For more information about the NASA STI program, see the following:

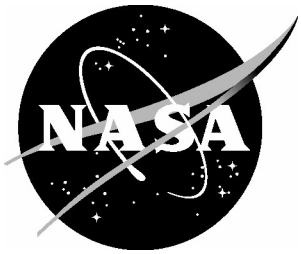
- Access the NASA STI program home page at http://www.sti.nasa.gov

- E-mail your question to help@sti.nasa.gov

- Phone the NASA STI Information Desk at 757-864-9658

- Write to:
  NASA STI Information Desk
  Mail Stop 148
  NASA Langley Research Center
  Hampton, VA 23681-2199

NASA/TM–20250000107 Corrected Copy



Uncertainty Quantification for Empirical X-59 Sonic Boom Loudness Levels

Jacob Klos
Langley Research Center, Hampton, Virginia

National Aeronautics and
Space Administration

Langley Research Center
Hampton, Virginia 23681-2199

January 2025

The use of trademarks or names of manufacturers in this report is for accurate reporting and does not constitute an official endorsement, either expressed or implied, of such products or manufacturers by the National Aeronautics and Space Administration.

Available from:

NASA STI Program / Mail Stop 148
NASA Langley Research Center
Hampton, VA 23681-2199
Fax: 757-864-6500

This page intentionally left blank.

Table of Contents

Table of Figures iii
Table of Tables v
List of acronyms and symbols vi
Abstract vii
I. INTRODUCTION 1
A. Planned X-59 field test campaigns 3
B. GRS hardware and software 3
II. INVARIABLE SOURCES OF UNCERTAINTY 5
A. Microphone calibration 5
B. Microphone ambient temperature 8
C. Microphone ambient humidity 8
D. Microphone ambient (barometric) pressure 9
E. GRS ADC gain 9
III. VARIABLE SOURCES OF UNCERTAINTY 10
A. Background noise 12
B. GRS ADC sample rate 21
C. Windscreen insertion loss and sonic boom elevation angle 24
D. Boom finder induced window position jitter 27
E. Metric software numeric precision 30
IV. METHODS USED TO COMBINE THE SOURCES OF UNCERTAINTY 32
V. RESULTS 34
A. Total measurement error 34
B. Contribution proportions 38
C. Effects of reduced uncertainty 40
VI. CONCLUSIONS 50
A. Caveats and future work 50
1. GRS analog to digital converter 50
2. Microphone 50
3. Field test location 51
4. Ground impedance 52
5. Turbulence 52
B. Summary 52

Acknowledgements 54
References 54
Appendix 1: Calculation of corrected SNR with representative data plots 57
Appendix 2: Plots of total measurement error for eight different noise metrics 68
Appendix 3: Tabulated total measurement error for eight different noise metrics 77
Appendix 4: Plots of the proportion of the total variance explained by each uncertainty source for eight different noise metrics 86
Appendix 5: Tabulated proportion of the total variance explained by each uncertainty source for eight different noise metrics 95

Table of Figures

Figure 1: In-situ calibration levels relative to original manufacturer's calibration value for 390 in-situ calibrations of 24 Brüel and Kjær Type 4193 microphones..... 7

Figure 2: Summary of simulated background noise measurement error versus metric type and corrected signal to noise ratio, where both the mean bias and 68.3% confidence interval are plotted, and where the purple arrows in the upper left subplot highlight the expected measurement error for the 5th percentile and median on-design X-59 mock sonic boom recordings (see also Figure 3). 16

Figure 3: Summary of corrected SNR values observed in the on-design and off-design X-59 mock acoustic waveform datasets for the eight metrics identified in the subplot titles, where the purple arrows in the upper left subplot highlight the expected measurement error for the 5th percentile and median on-design X-59 mock sonic boom recordings. 17

Figure 4: Bivariate histograms of Perceived Level versus corrected SNR, where the waveform case is indicated in the subplot title and bin counts are indicated by color as shown in the color bars. 18

Figure 5: Example histograms of on-design measurement errors falling within in the 2 dB wide corrected SNR bin identified in legend; where the metric type, the number of observations, and the corrected SNR bin limits are identified in the legend along with the plot features. 20

Figure 6: Assumed sample rate uncertainty effects versus metric type, where both the standard deviation and the mean bias of the measurement error are plotted. .. 23

Figure 7: Insertion loss versus frequency and elevation angle, where solid lines indicate the subset of angles that were used to estimate windscreen effects (data source: Ref [23]). 25

Figure 8: Assumed windscreen insertion loss and elevation angle uncertainty effects versus metric type, where both the standard deviation and the mean bias of the measurement error are plotted. 26

Figure 9: Summary of simulated window jitter related measurement error versus metric type and corrected signal to noise ratio, where both the standard deviation and the mean bias of the error are plotted. 29

Figure 10: Intermediate result showing combined measurement error for only the invariable sources, which does not include the effects of variable sources like background noise (see Section V.A for results that include the variable sources). 33

Figure 11: Total measurement error for the PL noise metric versus the PL corrected SNR, a) shows the total measurement error and b) shows the observed distribution of corrected SNR for the on-design and off-design X-59 mock acoustic recordings. 36

Figure 12: Total combined measurement error standard deviation..... 37

Figure 13: Proportion of the total variance explained by each uncertainty source for the PL noise metric versus the PL corrected SNR of the mock recording. 39

Figure 14: Comparison of baseline measurement error estimate and SNR ranges (left-hand subplots) versus error estimates and SNR ranges while using attenuated background noise levels and smaller microphone-related uncertainties (right-hand subplots). 45

Figure 15: Comparison of baseline proportional contributions and SNR ranges (left-hand subplots) versus proportional contributions and SNR ranges while using smaller microphone-related uncertainties and attenuated background noise levels (right-hand subplots). 46

Figure 16: Comparison of the measurement error standard deviations for the baseline values versus using updated values; a) measurement error for three different cases, b) range of corrected SNR with baseline background noise levels, and c) range of corrected SNR with attenuated background noise levels..... 47

Figure 17: Comparison of the measurement error mean bias for the baseline values versus using updated values; a) measurement error for three different cases, b) range of corrected SNR with baseline background noise levels, and c) range of corrected SNR with attenuated background noise levels..... 48

Table of Tables

Table 1: Listing of the sources of uncertainty, the assumed effect, and whether the source was determined to be significant. 2

Table 2: Assumed microphone calibration effects on measurement chain gain. 7

Table 3: Assumed ambient temperature effects[7] on measurement chain gain. 8

Table 4: Assumed ambient humidity effects[7] on measurement chain gain. 8

Table 5: Assumed ambient (barometric) pressure effects[7] on measurement chain gain. 9

Table 6: Assumed GRS ADC gain uncertainty effects[7] on measurement chain gain. 9

Table 7: Noise metric types considered here. 11

Table 8: Coefficient of determination for linear fit of loudness level versus corrected SNR for each of eight noise metrics (source data found in Appendix 1)..... 19

Table 9: Summary of mean bias and standard deviation[7] for sample rate effects on measurement error versus noise metric type (effect does not vary with level). 23

Table 10: Summary of mean bias and standard deviation[7] for windscreen effects on measurement error versus noise metric type (effect does not vary with level). 26

Table 11: Summary of mean bias and standard deviation[7] for numerical precision effects on measurement error versus noise metric type (effect does not vary with level)..... 31

Table 12: Number and percentage of mock acoustic recordings, of the 43,200 mock recordings analyzed to assess background noise related measurement error, falling within each corrected SNR bin for the PL metric..... 49

List of acronyms and symbols

ADC	Analog-to-digital converter
ASEL	A-weighted sound exposure level
BSEL	B-weighted sound exposure level
CI	Confidence interval
C_i	One-third-octave band correction values
CSEL	C-weighted sound exposure level
DSEL	D-weighted sound exposure level
dB	Indicates units of decibels
ESEL	E-weighted sound exposure level
F_s	Sample rate
GRS	Ground Recording System
ISBAP	Indoor sonic boom annoyance predictor
i	Index corresponding to a particular one-third-octave band
L_A	One-third-octave band sound pressure level, preboom background noise
L_B	One-third-octave band sound pressure level, sonic boom
mic	Abbreviation for microphone
NOM	Narrow-band Octave-band Metrics (NASA's metrics software)
NASA	National Aeronautics and Space Administration
PL	Perceived level
ppm	Parts-per-million
SNR	Signal-to-noise ratio
SNR_c	Corrected signal-to-noise ratio
TEDS	Transducer electronic datasheet
X	Correction method constant chosen from Table 1 of Ref. [1]
Y	Correction method constant chosen from Table 1 of Ref. [1]
ZSEL	Z-weighted sound exposure level
σ	Measurement error standard deviation
μ	Mean value

Abstract

Estimates of the total uncertainty for empirically determined loudness levels are documented when GRS (Ground Recording System) noise monitors are used to record X-59 sonic boom waveforms. The total uncertainty is characterized by combining nine different sources of uncertainty that may affect the apparent gain of the measurement chain. These uncertainty estimates are presented as expected measurement error relative to the true loudness level, and separate error estimates are provided for eight different noise metrics in which NASA has interest. The behavior of the Perceived Level (PL) metric is studied within the report body, while the total uncertainties for the seven other noise metrics are summarized in appendices for brevity. The effects of four sources of uncertainty are estimated simply from information found on hardware specification sheets provided by the manufacturer. However, mock acoustic recordings are created to estimate the effects of other sources because those effects are expected to induce spectral coloration, so they may vary with noise metric type and sound level. These sources are not well modeled by simple gain adjustments. Importantly, measurement error is computable when processing mock recordings since the true levels are knowable, which is not the case when processing data recorded in the field. Specifically, the true levels are knowable because the components of the mock recordings are separable – e.g., loudness levels of booms can be computed with or without superimposed background noise. Mock acoustic recordings also have the benefit of allowing analysis of sonic booms from vehicles that are not yet flying, like the X-59, since the mock recordings are created by combining vehicle-specific predicted waveforms with other audio sources. The estimates of total measurement error are documented as a function of the signal-to-noise ratio (SNR) of the loudness level, where the corrected SNR is computed while accounting for the effects of the method that is used to correct for background noise contamination when computing the noise metric values. The corrected SNR calculations used here can be applied to both mock recordings and in-field measurements, so the uncertainty of in-field recordings can be found using pre-computed lookup tables that identify the relationship between metric type, corrected SNR, and the expected measurement error.

I. INTRODUCTION

NASA will use noise monitors to record acoustical data during overflights of the X-59 aircraft and will process those data to estimate the loudness levels of the sonic booms that are produced at ground level by the vehicle during supersonic flight. The loudness level values calculated from these audio recordings will be used:

- To verify that the aircraft can achieve the reduced loudness levels to which it was designed (e.g., see Ref. [2]), and
- As a component of the estimated noise dose assigned to respondents during tests of community annoyance to shaped sonic boom noise (e.g., see Refs. [3, 4, 5, 6]).

The planned field tests activities are summarized in the next subsection. Several sources of uncertainty in the measurement chain of the noise monitors will affect loudness levels that are computed from the measured waveforms, which will cause those empirical loudness levels to deviate from the true levels. The purpose of this document is to discuss the sources of uncertainty, estimate their magnitudes, and estimate the combined measurement error that is expected when GRS noise monitors – developed by Crystal Instruments – are used to record X-59 sonic boom waveforms and compute loudness levels.

The measurement chain and signal processing related sources of uncertainty considered here are listed in Table 1. The first five sources of uncertainty found in Table 1 are termed "invariable" since their effects are not expected to vary with metric type or the loudness level of the measured sonic boom. These effects are assumed to result in a simple change in overall gain, which is applied equally to all metric types and levels. In contrast, the last five sources listed in Table 1 are expected to vary with the choice of noise metric and the level since those sources may produce spectral coloration. It is expected that the unique weighting function of each noise metric type will interact differently with the spectral coloration effects to produce metric-specific, and possibly level-specific, uncertainty estimates. These five sources are termed "variable" sources of uncertainty here. Three of the variable sources are related to the GRS hardware components while two variable sources are related to the computational algorithms that are used to process the measured waveforms. The effects of all ten sources are quantified separately and then combined to estimate the total error, where the effect of each source is assumed to be independent of the other sources.

Also included in the fourth column of Table 1 is an indication of whether the effect of each source was found to contribute significantly to the total measurement error that is documented later. Specifically, if an effect was found in Section V to have a proportional contribution of 1% or more to the total measurement error variance for any metric or level, then the source is identified as significant in Table 1. Sources are indicated as not significant if they contributed less than 1% to the total variance across all levels and all metric types considered here.

The methods used to estimate the effect of each source of uncertainty are different for the invariable and variable sources of uncertainty. Generally, information found on the hardware specification sheets informs the effects of the invariable sources. The exception to that is the microphone calibration source, which is informed by past in-situ calibration

data for a set of NASA-owned microphones. For the variable sources, mock acoustic recordings are constructed and used to estimate the contribution from all five of those sources, where the effects are evaluated for different noise metric types and sound levels. The total uncertainty of all sources when combined will be a function of both metric type and level since the combined result will include the background noise source, whose effect is significant and varies with both metric and level (Table 1).

This document is organized as follows. The types of field tests during which booms from the X-59 aircraft will be measured are briefly discussed in Section I.A to give readers a general sense of test objectives. Section I.B documents the GRS hardware so readers have some basic knowledge of the noise monitor components that will be used during those field tests. Then the values assumed for the effects of the invariable and the variable sources of uncertainty are documented in Sections II and III, respectively. The approaches used to estimate the assumed values are documented in those sections. Next, the methods used to combine these different sources to compute the total measurement error are discussed in Section IV. Section V.A documents the outcome of combining all uncertainty sources, where the total measurement error is presented for the values assumed in Sections II and III. The measurement error is documented as a function of SNR and metric type. Then, the proportional contribution of each source to the total variance is documented in Section V.B, which gives some indication of the relative influence of each uncertainty source. The four sources that contribute most to the total measurement error are identified in that section. Changes in the total measurement error are studied in Section V.C to highlight how modest changes in test procedures and GRS placement choices might reduce the error for three of the four most significant sources as compared to the baseline results in Sections V.A and V.B. Finally, some caveats that readers should understand and possible future work to refine the uncertainty estimates are given in Section VI.

Table 1: Listing of the sources of uncertainty, the assumed effect, and whether the source was determined to be significant.

Source	**Effect varies with metric?**	**Effect varies with level?**	**Effect is significant?**
Microphone, calibration	No	No	Yes
Microphone, ambient temperature	No	No	Yes
Microphone, ambient humidity	No	No	Yes
Microphone, ambient pressure	No	No	Yes
GRS ADC, gain	No	No	Yes
Background noise	Yes	Yes	Yes
GRS ADC, sample rate	Yes	No	No
Windscreen, insertion loss/incident angle	Yes	No	Yes
Boom finder, window jitter	Yes	Yes	No
Metric code, numeric precision	Yes	No	No

A. Planned X-59 field test campaigns

The planned field tests are grouped into two long-duration flight test campaigns termed "phase 2" and "phase 3". The phase 2 flights will be conducted near NASA Armstrong Flight Research Center with up to 70 noise monitors arranged into one or more large arrays located in the Mojave Desert. During phase 2 flights, the sonic boom waveforms of the X-59 will be measured so the acoustical characteristics can be computed and compared to those of the aircraft design requirements and computer-based simulations (e.g., see Ref. [2]). The primary objective of phase 2 is to determine if the aircraft achieved the acoustical design requirements, specifically whether the sonic boom loudness level target is met. A secondary objective is to check the validity of the propagation tools that are used to simulate shaped sonic booms that are received at ground level (e.g., Ref. [7]) since these tools will be used in the design and analysis of phase 3 (discussed below). Thus, the expected uncertainty in the measurements is needed during phase 2 since it will inform the analysis of whether measured levels agree with target levels and predicted levels.

During phase 3 flights, the aircraft will fly over communities within the United States to gather data about how people in communities react to the sonic boom noise produced by the aircraft (e.g., see Refs. [3, 4, 5]). Phase 3 is planned to be divided into about five different tests, each about a month long, where X-59 will repeatedly overfly five communities within the United States and respondents will judge their annoyance to the sonic boom noise they experience. The objective of phase 3 is to educe a dose-response model from data that quantify community annoyance to shaped sonic boom noise. The data gathered in phase 3 will include both community annoyance data and outdoor noise dose data that is estimated, in part, using empirical loudness levels computed from the measured waveforms [6]. About 100 noise monitors will be placed outdoors within overflown communities to measure the booms received. Then, the measured levels will be combined with predicted levels using a Kalman filter method [6], the weightings of which will be informed by the estimated uncertainty of both noise dose data sources.

Thus, the uncertainty quantified in this report and the MATLAB® scripts used for that quantification (Sections II, III, and IV) are expected to help inform future analyses during both phase 2 and 3 X-59 field test campaigns. However, the input values assumed herein may need to be adjusted as calibration and field test procedures are refined.

B. GRS hardware and software

The acoustical measurement chain of the GRS noise monitors consists of four hardware components:

- The analog-to-digital converter (ADC) hardware inside the GRS[1] noise monitor manufactured by Crystal Instruments [8],
- A model 378M12 low-frequency capable, IEPE-powered microphone that is manufactured by PCB Piezotronics (specification sheet not available publicly),

[1] The GRS product link in Ref. [8] is provided for documentation purposes only. Each GRS input channel has two separate 24-bit ADCs that simultaneously digitize the microphone signal, which is powered by a 10 mA IEPE source. The low-range ADC input range is ±0.5 V. The high range ADC input range is ±10 V.

- A windscreen device[2] covering the microphone to reduce wind noise [9], and
- A cable that connects the PCB microphone located in the windscreen to the ADC input of the GRS unit.

The microphone cable is assumed to have no effect on the measurement chain gain since the cable lengths will be relatively short so should not attenuate the shaped sonic boom signal within the frequency range of interest[3]. Cables up to about 1000 feet in length are not expected to attenuate the signal[3]. The other three hardware components are assumed to contribute to variation in the measurement chain gain as summarized above in Table 1.

Loudness level values will be computed from the recorded waveforms using automated algorithms running off-board the GRS noise monitors during phase 2 and on-board them during phase 3. Two algorithm-based sources of uncertainty are included here to account for known computational effects (Table 1, last two sources listed). These two sources are: 1) the jitter that is expected to be introduced when a boom finder algorithm is used to locate an X-59 sonic boom in a recorded waveform, and 2) the numerical precision that is used when processing the waveform to compute loudness levels. These algorithm-based sources are discussed later in Section III. Neither effect was found to be a significant source of measurement error.

An important topic in the discussion of measurement chain uncertainty is how the microphone sensitivity will be determined. The sensitivity value is used to convert from units of voltage measured by the ADC to units of pressure, so an error in that conversion factor will affect the apparent measurement chain gain. It is assumed, and recommended here, that the sensitivity stored in the transducer electronic datasheet (TEDS) of the microphone will be used for that conversion. This is the method that has been chosen for X-59 community tests in phase 3. That sensitivity is assumed to be from a recent traceable calibration that was performed by a calibration "laboratory" while indoors at some ambient reference temperature, pressure, and humidity and while using an acoustical calibrator. Consequently, weather-based sources of sensitivity variation are expressed here relative to an assumed ambient reference condition, so the assumed decibel variations in gain will be expressed as both a range and bias. These reference conditions, the gain range, and the gain bias estimates are identified in the next section. Importantly, the uncertainty in the TEDS calibration value is approximated here. It is expected that the values assumed below may be refined once details about actual traceable calibration procedures are known.

---

[2] The windscreen, ground board, and microphone mounting hardware are similar in design to the "COUGAR Short" configuration discussed in Ref. [9]. A revised design named "COUGAR Gold" will be used during X-59 field tests.

[3] https://www.pcb.com/contentstore/mktgcontent/IMI_Downloads/TipfromTech-DrivingLongCableLengths.pdf, accessed November 2024. The shielded twisted pair cable is assumed to be a model 042M39 cable made by PCB Piezotronics with linear capacitance of 20 pF/ft, driven by 10 mA from the GRS IEPE current source. Assuming a 1 Volt (100 Pa) peak input from a 378M12 microphone (with a 10 mV/Pa sensitivity) gives a maximum frequency of 716 kHz for cables that are 100 ft long or 71.6 kHz for cables that are 1000 ft long. Cables used during phase 2 are expected to be shorter than 1000 ft. Cables used during phase 3 are expected to be shorter than 100 ft. Thus, cable lengths are not expected to limit the signal bandwidth since both maximum frequency values cited above exceed the maximum GRS Nyquist frequency, which is 51.2 kHz, and the upper frequency limit of the 378M12 microphone, which is about 20 kHz.

II. INVARIABLE SOURCES OF UNCERTAINTY

The sources of uncertainty whose effects are not expected to change significantly with either metric choice or sound level are documented in this section. The distribution type, the range, and the bias in gain assumed for each source are identified in subsections:

- Microphone calibration (Subsection II.A),
- Microphone ambient temperature (Subsection II.B),
- Microphone ambient humidity (Subsection II.C),
- Microphone ambient (barometric) pressure (Subsection II.D), and
- GRS ADC gain (Subsection II.E).

Some noise metrics, like Perceived Level (PL), use weighting functions that change with sound level. However, the variations in measurement chain gain caused by these sources of uncertainty are a few tenths of a dB or less. Consequently, the effects of non-linear weighting functions in metrics like PL are not expected to be significant. Also, the five invariable sources listed above are not expected to result in spectral coloration. Thus, the gain variations caused by these sources are applied equally to all noise metrics and all sonic boom loudness levels when combining the different sources of uncertainty.

A. Microphone calibration

The purpose of this subsection is to identify the variation in sensitivity that might be observed during calibration of a microphone. Specifically of interest is the uncertainty in the sensitivity value stored in TEDS, which will be determined during a traceable calibration by a qualified calibration laboratory during both phase 2 and phase 3. The intent of this subsection is not to identify effects caused by uncertainty sources related to changing ambient conditions, like temperature or humidity. Those ambient weather effects are incorporated into the uncertainty model separately and are discussed in the three subsections that follow.

To estimate the calibration effect, the outcome of 390 (total) calibrations of a set of 24 (count) Brüel and Kjær Type 4193 microphones was analyzed to estimate the variation expected during microphone calibration (Figure 1). Generally, a Brüel and Kjær Type 4231 acoustical calibrator was used when calibrating these Type 4193 microphones. While the GRS units will use a different model of microphone and the calibration of those microphones may be performed using a different model calibrator, the calibration dataset for the Type 4193 microphones is the best available real-world data for this uncertainty source. The values used for this uncertainty source can be updated in the future as in-situ and/or traceable calibration data and procedures for the GRS microphones become available. The distribution that is assumed here for this source of uncertainty is documented in Table 2, where a normal distribution is assumed based on visual inspection of Figure 1.

Only the standard deviation of the calibration data, 0.22 dB from Figure 1, is used to estimate calibration uncertainty effects here. This observed value is in close agreement

with the calibration accuracy of the Type 4231 calibrator, which is ±0.2 dB [10][4], and more generally the uncertainty that is expected when using an acoustical calibrator to determine sensitivity[5]. If traceable calibrations that set the TEDS value use a calibrator with better accuracy, then that may reduce the impact of this source. However, NASA currently does not know what calibrator will be used for traceable calibrations. The standard deviation value of 0.22 dB assumed here is expected to be a reasonable, if not conservative, estimate since a cursory survey of commercially available acoustical calibrator and pistonphone specifications indicates that most calibrators have accuracies of ±0.2 dB or better. Importantly, other methods[5] could be used to determine the microphone sensitivity during a traceable calibration – the reciprocity method, for example. Most of those other methods are expected to have better accuracy[5] than when using an acoustical calibrator to determine sensitivity. Thus, the variation assumed here, 0.22 dB (Table 2), should be conservative and the calibration component of the total uncertainty summarized later in Sections V.A and V.B might slightly overestimate the effect of this source. The magnitude of the overestimate will depend on the actual uncertainty of the calibration method used to determine the TEDS sensitivity of the GRS microphones. The analyses presented later can be updated when a better estimate becomes available. An example of reducing the effects of the calibration uncertainty component is included later in Section V.C.

A 0 dB bias is assumed for this uncertainty source (Table 2), not the –0.177 dB bias that is observed in the Type 4193 microphones calibration data (Figure 1). The observed bias of –0.177 dB (Figure 1) likely results from conversion from the open-circuit sensitivity, which is stored in the TEDS for the Type 4193 microphones, to the loaded sensitivity that is estimated when using a calibrator to calibrate the microphone and the preamplifier as an assembly. The loaded sensitivity accounts for the combined gain of the microphone cartridge and preamplifier assembly[6]. It is recommended that the loaded sensitivity be used for the 378M12 microphones when converting between voltage and pressure units, which should result in an unbiased uncertainty for the calibration component – a 0 dB bias like shown in Table 2. If the open-circuit sensitivity is stored in TEDS for the 378M12 microphones, then a correction[6] to convert between open-circuit sensitivity and loaded sensitivity should be applied when converting GRS recordings from voltage to pressure units during X-59 field tests.

[4] The Type 4231 product link in Ref. [10] is provided for documentation purposes only.

[5] See section 6.6 and Table 6.1 in the Brüel and Kjær "Microphone Handbook", February 1995, found at the following website: https://www.bksv.com/media/doc/be1373.pdf. [Accessed November 2024]

[6] See section 3.2 in the Brüel and Kjær "Microphone Handbook", February 1995, found at the following website: https://www.bksv.com/media/doc/be1373.pdf. [Accessed November 2024]

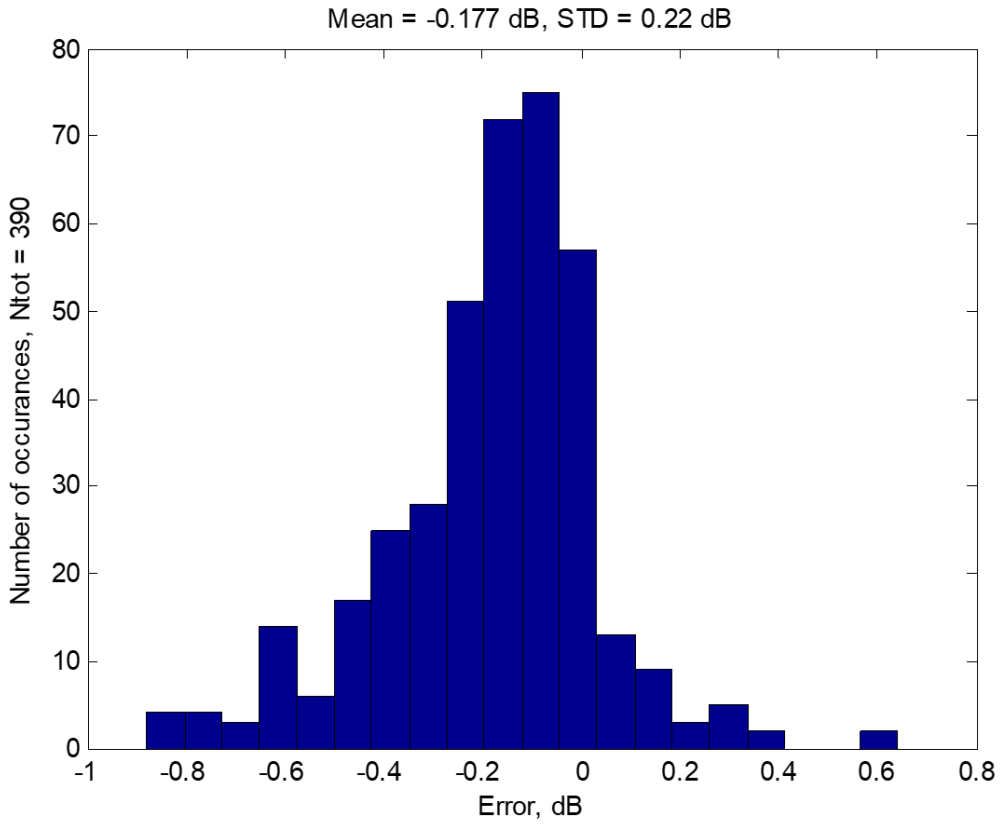


Figure 1: In-situ calibration levels relative to original manufacturer's calibration value for 390 in-situ calibrations of 24 Brüel and Kjær Type 4193 microphones.

Table 2: Assumed microphone calibration effects[7] on measurement chain gain.

Range, dB	Bias, dB	Dist. Type
0.2200	0.0000	Normal

[7] The cited "range" value is the standard deviation for normal distributions or the span between the upper and lower edges of uniform distributions. The "bias" value indicates the center of the symmetric distribution for both distribution types. Values are always cited in decibel units.

B. Microphone ambient temperature

The ambient temperature coefficient, 0.003 dB/°F, was taken from the microphone model 378M12 specification sheet revision A dated July 16th, 2021. That specification sheet is currently not publicly available. A range of temperatures from 35 to 110°F was assumed to determine the range and bias of the measurement chain gain, in decibels, that might result from changing ambient temperatures during X-59 measurements. The reference temperature is assumed to be 72°F. The distribution shape assumed in models here is uniform for the effects of ambient temperature on measurement chain gain. The assumed uniform distribution has the gain range and bias indicated at the right side in the table below.

Table 3: Assumed ambient temperature effects[7] on measurement chain gain.

Temperature			
dB/F	0.003		
Min	Ref	Max	
35	72	110	degree F
-0.111	0	0.114	dB gain

Range, dB	Bias, dB	Dist. Type
0.2250	0.0015	Uniform

C. Microphone ambient humidity

The ambient humidity coefficient, 0.002 dB/%RH, was taken from the microphone model 378M12 specification sheet (non-public) revision A dated July 16th, 2021. A range of humidities from 10 to 95 %RH was assumed to determine the range and bias of the measurement chain gain, in decibels, that might result from changing ambient humidity during X-59 measurements. The reference humidity is assumed to be 55%RH. The distribution shape assumed in models here is uniform for the effects of ambient humidity on measurement chain gain. The assumed uniform distribution has the gain range and bias indicated at the right side in the table below.

Table 4: Assumed ambient humidity effects[7] on measurement chain gain.

Relative humidity			
dB/%RH	0.002		
Min	Ref	Max	
10	55	95	% RH
-0.090	0.000	0.080	dB gain

Range, dB	Bias, dB	Dist. Type
0.1700	-0.0050	Uniform

D. Microphone ambient (barometric) pressure

The barometric pressure coefficient, –0.007 dB/kPa, was taken from the microphone model 378M12 specification sheet (non-public) revision A dated July 16th, 2021. A range of barometric pressures from 24 to 31 inHg was assumed to determine the range and bias of the measurement chain gain, in decibels, that might result from changing barometric pressure during X-59 measurements. The 24 inHg value is the floor of the minimum pressure, in units of inches Hg, observed in Denver, CO during October 2024 [11] and the larger value is the ceiling of the maximum pressure near costal Hampton, VA in the same month [12]. The floor and ceiling values were used to provide a more conservative range estimate. The reference pressure is assumed to be 30 inHg, which roughly corresponds to sea level pressure. The distribution shape assumed in models here is uniform for the effects of pressure on measurement chain gain. The assumed uniform distribution has the gain range and bias indicated at the right side in the table below.

Table 5: Assumed ambient (barometric) pressure effects[7] on measurement chain gain.

Pressure			
dB/kPa	-0.007		
Min	Ref	Max	
24	30	31	inHg
81.27	101.59	104.98	kPa
0.1422	0	-0.0237	dB gain

Range, dB	Bias, dB	Dist. Type
0.1659	0.0593	Uniform

E. GRS ADC gain

The tolerance in GRS ADC gain, ±1%, was taken from the GRS hardware specification sheet version 0.93 (non-public) dated May 28th, 2022. This corresponds to a range in voltage from 0.99 to 1.01 V for a 1 V reference input, which was used to determine the range and bias, in decibels, that might result from changing ADC gain. Assuming a different reference voltage, 10 V or 0.1 V for example, would yield the same decibel range and bias since those values are computed as a percentage of the reference. The distribution shape assumed in models here is uniform. The assumed uniform distribution has the gain range and bias indicated at the right side in the table below.

Table 6: Assumed GRS ADC gain uncertainty effects[7] on measurement chain gain.

ADC Gain			
Error, %	1		
Actual, V	1		
Min	Ref	Max	
0.990	1.000	1.010	Voltage
-0.0873	0	0.086427	dB gain

Range, dB	Bias, dB	Dist. Type
0.1737	-0.0004	Uniform

III. VARIABLE SOURCES OF UNCERTAINTY

The variable sources of uncertainty are expected to cause spectral coloration of the measured data. Thus, these sources cannot be modeled by a simple gain applied to the measured waveform or the loudness levels computed from them. Consequently, mock acoustic recordings were used to estimate the effects, which vary with metric type and/or level, caused by the last five sources of uncertainty listed in Table 1:

- Background noise (Subsection III.A),
- GRS ADC sample rate (Subsection III.B),
- Windscreen insertion loss and sonic boom elevation angle (Subsection III.C),
- Boom finder induced window position jitter (Subsection III.D), and
- Metric software numeric precision (Subsection III.E).

The mock acoustic recordings are assembled using the same methods and data discussed in Ref. [1]. Specifically, waveform "case A" and "case B" from Ref. [1] are used here. These two cases mix predicted sonic boom waveforms that are turbulized using filters from Ref. [13] with both background noise that was recorded during the NASA QSF18 test [14] and scaled post boom noise[8] that was recorded during the NASA SonicBAT test [13]. The details of how the mock recordings are constructed are left to Ref. [1] for brevity. The mock acoustic recordings are then manipulated in software to simulate the effect on loudness level that is expected from each source listed above. All mock recordings are synthesized at a sample rate of 24,000 Hz. Results found using this sample rate are expected to be similar to those of other sample rates like the 51,200 Hz rate that will be used during X-59 testing. Some implications of using the background noise from the QSF18 test are discussed later in Section VI.A.

Importantly, mock recordings are advantageous because the true loudness levels are computable since the mock recordings are built by superimposing different data sources, where the loudness levels of the constituent audio waveforms are known. However, what is assumed to be the "true" loudness level differs for each of the five sources of uncertainty listed above since we wish to separate uncertainty caused by background noise from uncertainty caused by sample rate variation, windscreen effects, etc. The assumed true level that is used as a reference and the observed uncertainty for each source is discussed in the next five subsections below. The eight noise metric types considered here are summarized in Table 7.

The distribution of observed measurement errors, in decibels, is found for each simulated source of uncertainty, metric type, and/or level. One of two distribution types – either normal or uniform – are fit to the data to estimate the mean bias and the range so these effects can be combined with the invariable effects documented in Section II. A uniform distribution was used in some cases since that type seemed, visually, to fit the data better than a normal distribution. A quantitative evaluation of which distribution type best fit the observed measurement error was not performed, only visual inspection was used. The range value that is documented corresponds to the standard deviation when a normal

[8] Post boom noise is long-duration, low-frequency oscillations that are observed in measured waveforms, are produced by the aircraft, but are not well modeled by the turbulence filters used in the present study.

distribution is assumed. For uniform distributions, the range indicates the span between the upper and lower edges of the distribution. The mean bias indicates the center of the distribution in both cases.

Table 7: Noise metric types considered here.

Noise metric name	Acronym	Units
Perceived level [15, 16, 17]	PL	decibels
Indoor sonic boom annoyance predictor [18]	ISBAP	decibels
A-weighted sound exposure level [19, 20]	ASEL	decibels
B-weighted sound exposure level [19, 20]	BSEL	decibels
C-weighted sound exposure level [19, 20]	CSEL	decibels
D-weighted sound exposure level [19, 20]	DSEL	decibels
E-weighted sound exposure level [19, 20]	ESEL	decibels
Z-weighted sound exposure level [19, 20]	ZSEL	decibels

The X-59 sonic boom waveforms that are used to create the mock recordings are taken from two prediction-based datasets using the C612A nearfield: an on-design (quiet) and an off-design (loud) set of sonic boom waveforms. The term "on-design" refers to a computer-based simulation case where the X-59 is cruising, virtually, at optimal conditions – e.g., trim, speed, and altitude. These optimal conditions correspond to settings where the aircraft was designed to produce a quiet, shaped sonic boom at ground level. The term "off-design" refers to a simulation case where the cruise conditions are non-optimal, so a louder boom is expected. Both on- and off-design booms are desirable and will be purposely produced by the X-59 aircraft during phase 3 community tests so the range in dose values is sufficiently large to educe a psychoacoustic model from the dose-response dataset.

The on- and off-design waveforms used here are predicted waveforms from a country-wide study of X-59 exposure, in which the effects of variable weather on these sonic boom signals were studied [21, 22]. The sets of boom waveforms used here are random subsets of 10,000 on-design and 10,000 off-design waveforms with varying loudness levels. Using a range from quiet to loud waveforms to create the mock recordings will help identify how empirical uncertainty is expected to vary over a broad range of sonic boom loudness levels. It also enables study of how boom type might affect the expected measurement uncertainty, where on-design booms might have more uncertainty than off-design booms since the signal-to-noise ratio (SNR) might be lower. Importantly, in cases documented below where more than 10,000 mock recordings were created to evaluate the effects of a source, the random sample of boom waveforms was drawn from the subset of 10,000 while allowing repeats. Since the randomly paired booms and background noise waveforms have varying levels, the signal-to-noise ratio is expected to vary widely across the different mock recordings, like it would in the real world.

NASA's metrics code NOM[9] was used to compute the loudness levels of all mock recordings here while correcting for background noise contamination using the "Custom F" method applied to the spectrum of the waveform [1]. The Custom F method was found in [1] to mitigate the effects of background noise in mock X-59 acoustic recordings. For brevity, a discussion of that correction method is left to Ref. [1]. Here, the corrected loudness levels of the mock acoustic recordings, and the error relative to the true levels, are used as a surrogate for the behavior of loudness levels that might be calculated from in-field noise monitor recordings. Similar studies of measurement error that use in-field recordings instead of mock recordings are not possible since the true loudness levels are unknowable for real measurements. Future uncertainty quantification studies should also use mock recordings, though maybe while using more representative data sources.

A. Background noise

Background noise effects were estimated using three sets of mock recordings. The first set was "case A" from Ref. [1] that contained randomly chosen on-design (quiet) X-59 booms that were mixed with a randomly chosen background noise snippet recorded during the QSF18 test. The second set was "case B" [1] that contained randomly chosen off-design (loud) X-59 booms mixed with randomly chosen background noise snippets from the QSF18 test. The third set was a contrived modification of "case A" [1], designed to better estimate uncertainty when SNR is low. Specifically, loudness levels were used as constraints when choosing the subsets of waveforms from which the mock recordings were assembled. In this third case, on-design X-59 booms were randomly chosen from the subset of booms with loudness levels less than 75 dB PL. These boom waveforms were then mixed with a randomly chosen background noise snippet from the subset of QSF18 data that had a loudness level of greater than 70 dB PL. This helped ensure the uncorrected SNR was low, typically less than 10 dB. For all three sets, the boom waveforms were modified using SonicBAT turbulence filters and mixed with randomly chosen post boom noise snippets prior to combining them with the background noise snippet.

Including the third case above improved the convergence of the measurement error estimates for low SNR values. Importantly, this third case is only included when computing and displaying measurement error results in this report. The third case is not included later when presenting loudness level distributions since this contrived case would overestimate the proportion of booms with low SNR if it were included. Sets 1, 2, and 3 had 14,400 mock recordings each, so a total of 43,200 mock recordings were used to estimate the measurement error caused by background noise. Loudness level distributions displayed later will be limited to sets 1 and 2 with 14,400 mock recordings each.

The loudness level error was computed for each mock recording relative to a truth value that was found when no background noise was mixed with the boom waveform. Also computed was the corrected SNR, which is an optional output of NASA's metrics code

[9] NASA's current sonic boom metrics software Narrow-band Octave-band Metrics, NOM, is released publicly as MATLAB® source code. The software can be located by searching for the software case number, LAR-20093-1, at the NASA online software catalog website: https://software.nasa.gov/search. Distribution restrictions may apply.

NOM[9] that accounts for the effects on SNR of correcting for background noise contamination using the methods in Ref. [1]. The corrected SNR is computed for the mock recording that includes background noise and can be computed for real recordings. The method to calculate the corrected SNR is documented in Appendix 1 below. This measure of SNR is a natural choice for independent variable since it is expected that uncertainty in loudness level should decrease with increasing SNR.

The measurement error statistical moments, the mean and standard deviation, were found by binning the observed errors using 2 dB wide bins of corrected SNR. Bin edges were aligned so one bin edge would fall at 0 dB SNR. The mean and standard deviation were only computed for bins that had more than 50 observations falling within them. For the mock recordings used here, generally only bins with a corrected SNR value greater than about 2 dB and less than about 44 dB had more than 50 observations fall within them, where the actual limiting bin decibel values depended on noise metric type. Bins falling below or above these limiting bins – e.g., when corrected SNR is less than 2 dB or corrected SNR is greater than 44 dB – were assigned the mean and standard deviation of the limiting bins.

The measurement error caused by background noise contaminating the mock measured signal is summarized in Figure 2 below for eight noise metrics. These data are for the case when a correction for background noise contamination is used – "Custom F" applied to the spectrum [1]. A separate subplot is provided for each metric type, where the mean bias and interval of the measurement error is plotted versus the corrected SNR of the mock measurements. The true level in this case is computed using the turbulized X-59 boom waveform mixed with post boom noise but not mixed with background noise, where the true value equals 0 dB along the ordinate for all SNR values along the abscissa. Text annotations are included along the ordinate to indicate when the loudness levels of the mock measurements are expected to overestimate versus underestimate the true level. As mentioned in the paragraph above, the plots in Figure 2 were created by binning the observed loudness level errors into 2 dB wide bins of corrected SNR. For example, many of the mock acoustic recordings will have a corrected SNR falling between +6 and +8 dB, depending on the level of both background noise and boom. Importantly, the measurement error values are assumed to be normally distributed along the ordinate within each bin along the abscissa. Thus, the red line indicates the mean value of the observations that fall within each bin and the green lines indicate the interval of ±1 standard deviation from the mean for those observations. Roughly 68.3% of the observations in each bin would fall within the confidence interval (CI) represented by the lower and upper green dashed lines. Other confidence intervals could be created by scaling the standard deviation when plotting the green lines. These mean and standard deviation data will be combined with the other uncertainty sources to compute the total measurement error in later sections.

It is useful to characterize how the corrected SNR behaves across all the mock X-59 acoustic recordings. Consequently, the distribution of corrected SNR that was observed within the on- and off-design datasets is plotted as separate box plots in Figure 3 for all eight metric types. Importantly, the contrived set of mock recordings discussed in the first paragraph of this subsection is excluded from Figure 3. A separate subplot is provided for

each metric type, wherein there is a separate box plot for each boom type: on- and off-design. The legend indicates the percentiles corresponding to each box plot feature. These box plots give a visual indication of how the SNR likelihood changes with both boom type and metric type. They are useful when interpreting the uncertainty data shown in Figure 2 since the box plots provide a visual indication of the likelihood of observing an SNR value. SNR likelihood can be related to the background noise uncertainty likelihood using both Figure 2 and Figure 3. For example, a corrected SNR value of about +9 dB PL corresponds to the 5th percentile of on-design X-59 booms (Figure 3, upper-left-most box plot, left-most black whisker). Similarly, a corrected SNR value of about +17 dB PL corresponds to the median on-design corrected SNR (Figure 3, upper-left-most box plot, red bar). These two features are highlighted by purple arrows in Figure 3 (upper-left subplot). The expected measurement error for the 5th percentile and median SNR cases can be inferred using the upper left plot in Figure 2 – the purple arrow annotations placed at +9 and +17 dB in that subplot. The mean bias at these two percentiles is very close in level (Figure 2, red line, comparing the two arrow-annotated bins) but the confidence interval is much larger for the 5th percentile case than the median case (Figure 2, green lines, comparing the two arrow-annotated bins). These box plots will be shown again when illustrating the combined effect of all uncertainty sources later in Sections V.A and V.B.

Using SNR for the independent variable is a better measure of uncertainty than if loudness level were used since a high loudness level does not necessarily imply a small uncertainty for the background noise component. For example, combining a loud sonic boom with loud background noise may still result in large uncertainty in the loudness level of the measured boom. Thus, an estimate of the SNR of the measurement is the preferred independent variable. The corrected SNR is used here because it accounts for the effects of correcting for background noise contamination when computing the loudness level of a measurement. That correction reduces the impact of the background noise on the computed loudness level value, effectively increasing the SNR compared to the case where no correction for background noise contamination was made. Using the corrected SNR instead of the SNR computed prior to correcting for background noise is highly recommended during X-59 field tests.

For information purposes, three bivariate histograms are plotted in Figure 4 for Perceived Level. The loudness levels and corrected SNR values are plotted along the ordinate and abscissa, respectively, for waveform “case C” and “case D” from Ref. [1], the distributions of which are nearly identical to those of waveform “case A” and “case B” for which the measurement error was shown previously. Color indicates the number of observations lying within each two dimensional bin. A separate subplot is provided for:

- The set of off-design mock acoustic recordings (Figure 4a),
- The set of on-design mock acoustic recordings (Figure 4b), and
- The combined on- and off-design dataset (Figure 4c),

where the third, contrived set of mock recordings discussed in the first paragraph of this subsection is excluded from Figure 4. A trend where loudness level increases with increased SNR is identifiable in Figure 4c. However, these variables are only moderately correlated (R^2 of 0.3 to 0.75). For example, when a best fit line is fit to the combined on- and off-design dataset – the raw observations underlying subplot 4c – the coefficient of

determination, R^2, is 0.539. The spread in observations visible in the Figure 4c histogram is the cause of this moderate correlation. Plots similar to Figure 4 are included in Appendix 1 for all eight noise metrics. The coefficients of determination for linear fits to the combined on- and off-design datasets (the "c" subplots in Appendix 1) are tabulated in Table 8 for all eight metrics. Because the correlation between loudness level and corrected SNR is weak ($R^2 < 0.3$) or moderate (from 0.3 to 0.75) for all eight metrics (e.g., Table 8), assignment of uncertainty using loudness level only is not recommended. For example, we should not assume that a loudness level of 75 dB PL that is computed from an in-field audio recording should have a well-defined uncertainty. Instead, it is recommended that the corrected SNR be computed for the empirical dataset and then uncertainty determined via lookup table using that corrected SNR value. This lookup process will be documented later in Section V, where the uncertainty of all sources once combined is presented.

Returning to the assumption of normality for the binned measurement errors (e.g., Figure 2), example histograms of the measurement errors are shown in Figure 5 for one bin of each of the eight noise metric types. Indicated in each legend are the metric type, the number of observations in the histogram, and the corrected SNR bin limits corresponding to the observations shown in the histogram. The bin identified was the lowest bin that has more than 2,000 observations falling within it for the data summarized in Figure 2. Importantly, the measurement error observations in Figure 5 were pooled across five repeat analyses while using a different random seed each time. Thus, there is about five times more data reported in each histogram in Figure 5 than in the corresponding bin in Figure 2. Repeating the analyses and pooling the estimated measurement error improved the smoothness of the histograms presented in Figure 5. However, the mean and interval estimates shown in Figure 2 do not change much with the increase in observation data, so only the first realization was used to estimate the mean and standard deviation values summarized in Figure 2. Also, the measurement errors for the on-design mock recordings only are included in Figure 5. The off-design waveforms were excluded while creating that figure for simplicity.

A normal distribution is fit to the observations in Figure 5 and displayed as the red line. Notably, the ranges on the abscissa and ordinate vary when comparing the different subplots of Figure 5. The scales are purposely different so readers can visualize differences between the fit (red curve) and the observations (blue bars). For example, the quality of the fit for CSEL would be difficult to visualize if plotted using the same abscissa range as PL. Based on visual inspection, a normal distribution is a reasonable fit to the observations (Figure 5). Some distributions do exhibit slight skewness, but the skewness magnitudes tend to be somewhat small compared to the standard deviations (widths) of the histograms. Thus, the properties of the normal distribution fits are believed to be reasonably representative of the observed distributions and the skewness is ignored here when combining the measurement error caused by background noise with the other sources of uncertainty.

The MATLAB® script named *BackgroundNoiseEffects_rev8.m* was used to create the data that appear in Figure 2. The script name is identified for documentation purposes only. It is not available for public distribution.

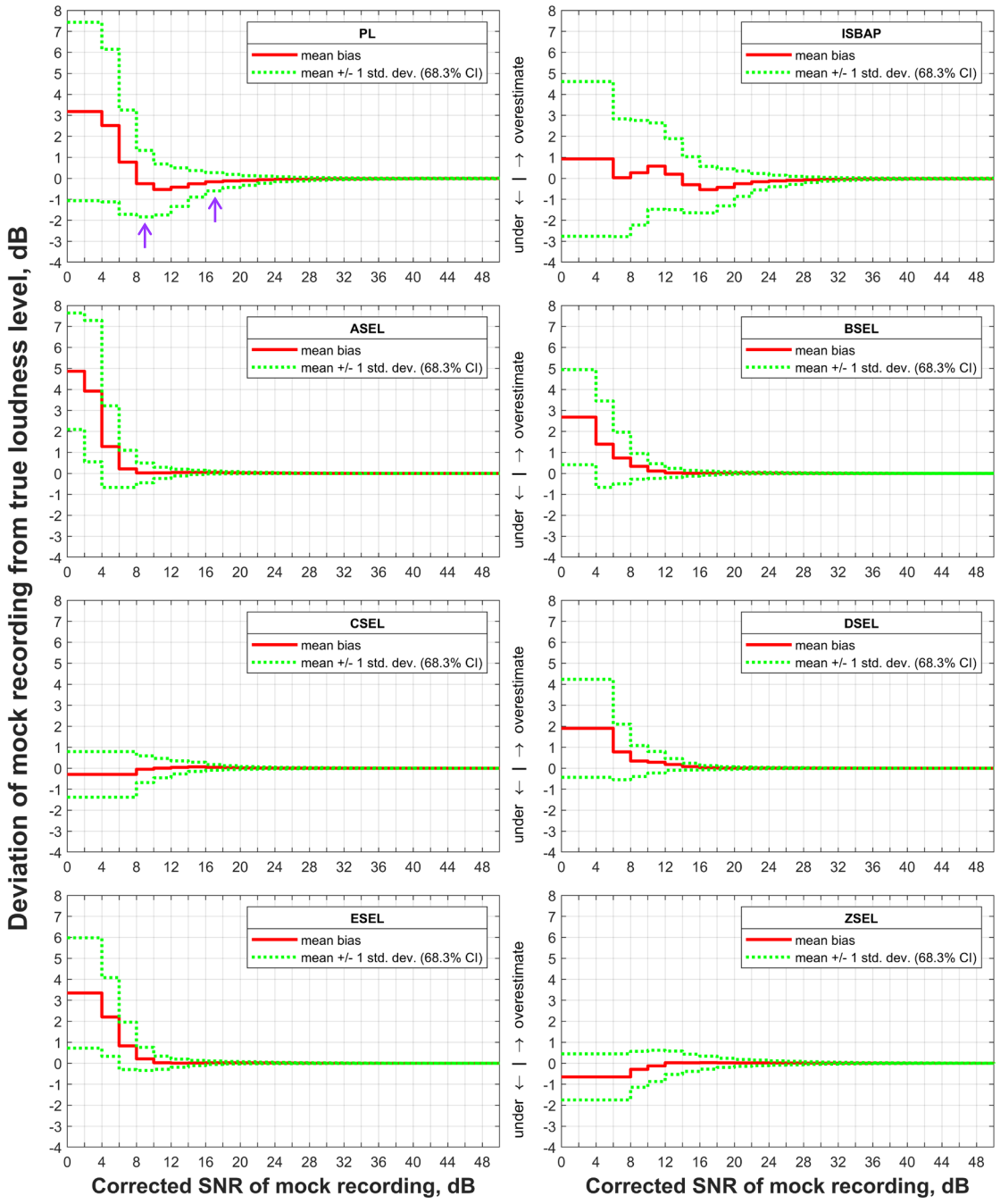


Figure 2: Summary of simulated background noise measurement error versus metric type and corrected signal to noise ratio, where both the mean bias and 68.3% confidence interval are plotted, and where the purple arrows in the upper left subplot highlight the expected measurement error for the 5th percentile and median on-design X-59 mock sonic boom recordings (see also Figure 3).

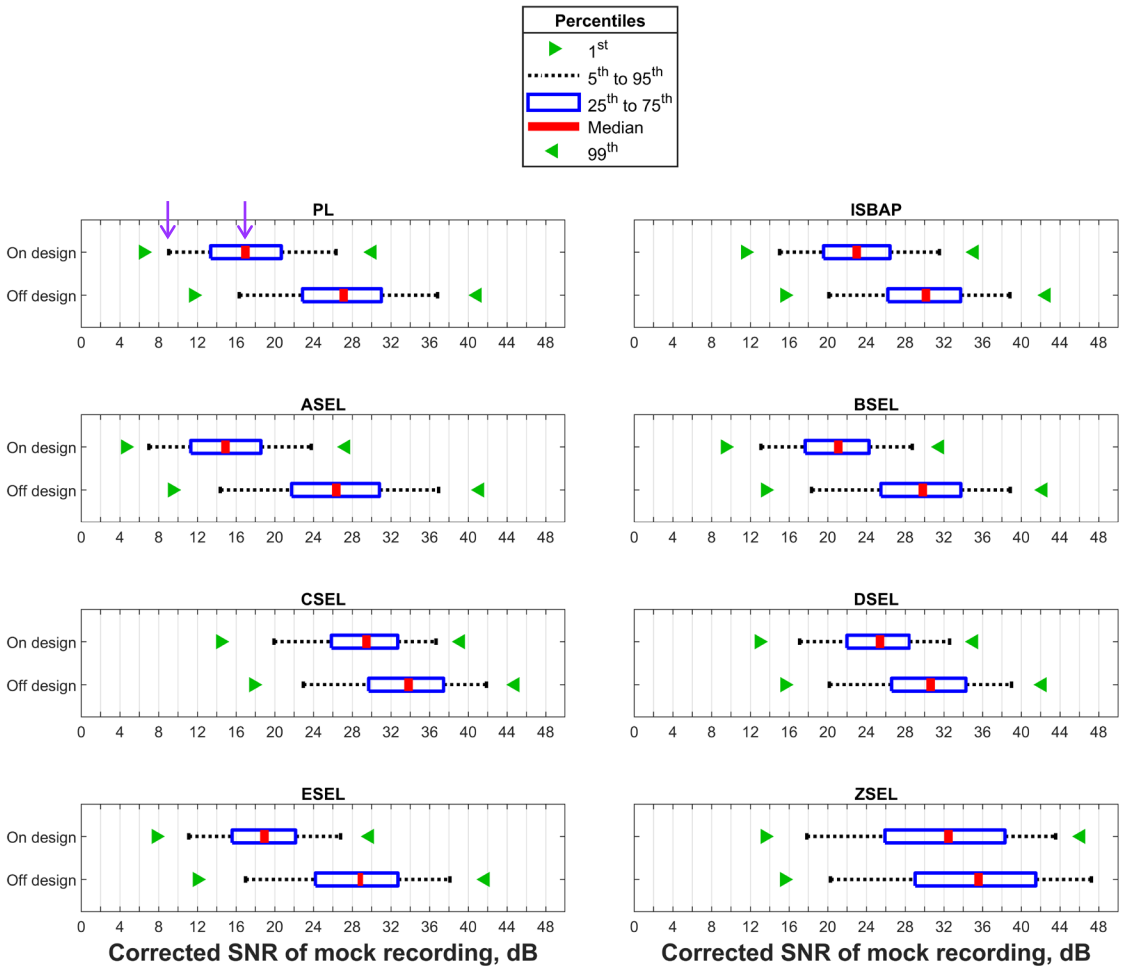


Figure 3: Summary of corrected SNR values observed in the on-design and off-design X-59 mock acoustic waveform datasets for the eight metrics identified in the subplot titles, where the purple arrows in the upper left subplot highlight the expected measurement error for the 5th percentile and median on-design X-59 mock sonic boom recordings.

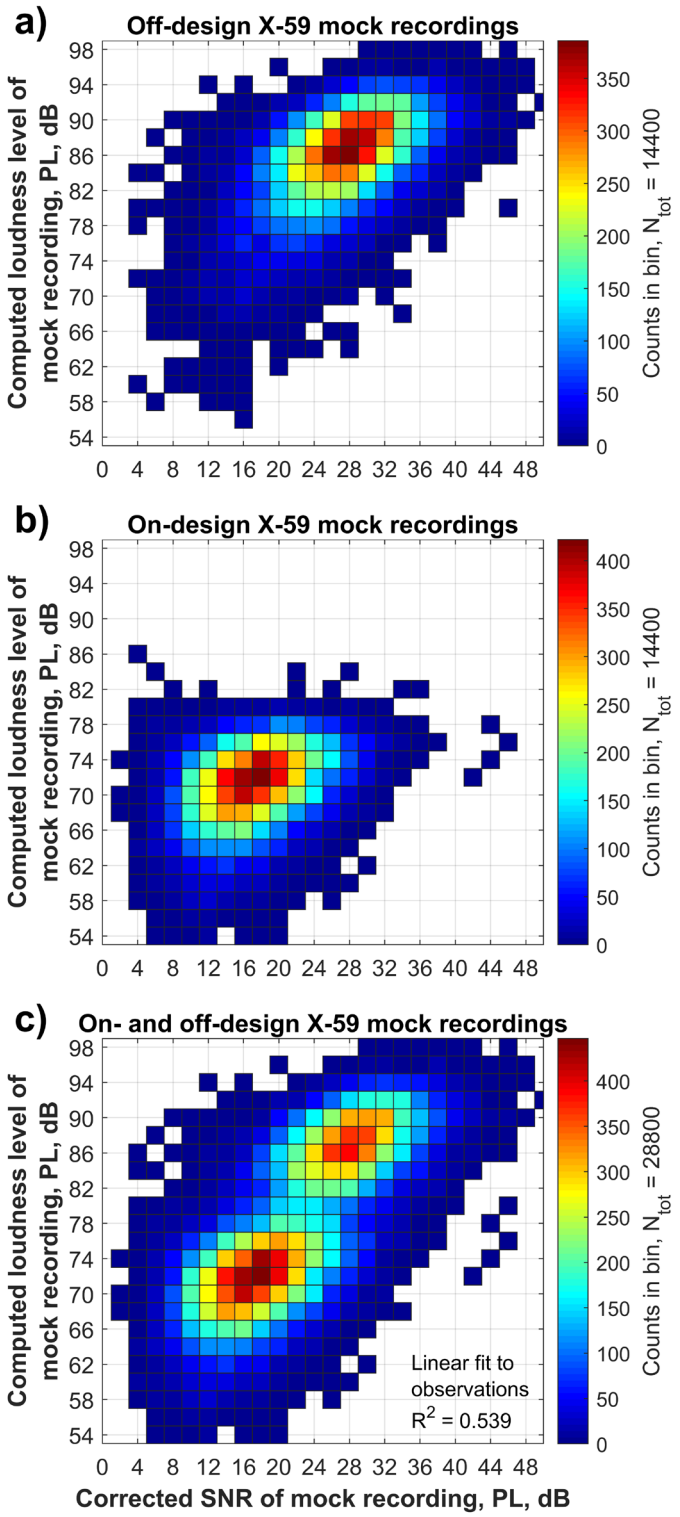


Figure 4: Bivariate histograms of Perceived Level versus corrected SNR, where the waveform case is indicated in the subplot title and bin counts are indicated by color as shown in the color bars.

Table 8: Coefficient of determination for linear fit of loudness level versus corrected SNR for each of eight noise metrics (source data found in Appendix 1).

Metric	R^2
PL	0.539
ISBAP	0.392
ASEL	0.65
BSEL	0.536
CSEL	0.269
DSEL	0.33
ESEL	0.578
ZSEL	0.09

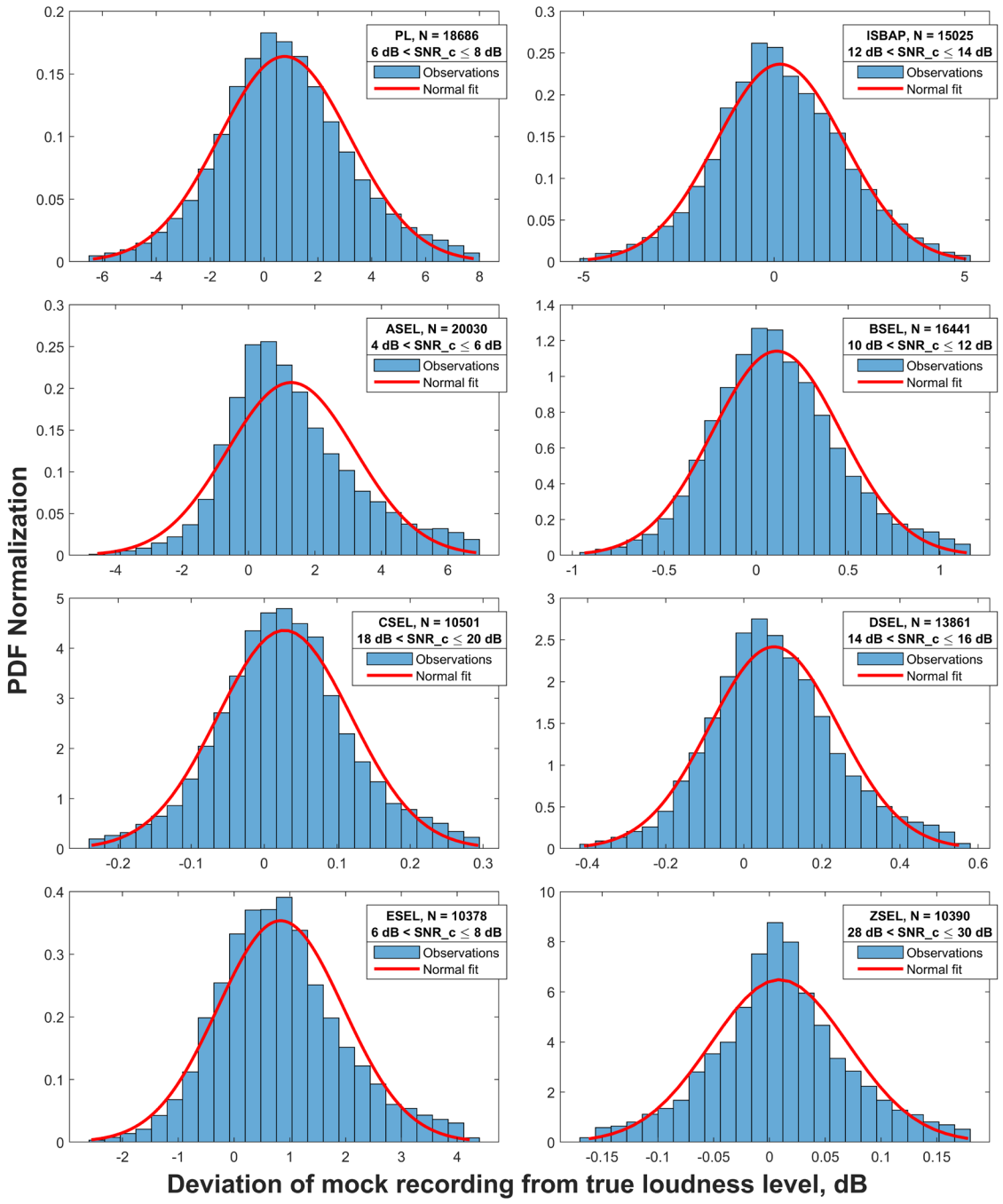


Figure 5: Example histograms of on-design measurement errors falling within in the 2 dB wide corrected SNR bin identified in legend; where the metric type, the number of observations, and the corrected SNR bin limits are identified in the legend along with the plot features.

B. GRS ADC sample rate

The sample rate effects were found by computing the loudness levels of mock acoustic recordings while perturbing the sample rate used for the signal processing steps by up to ±50 ppm (parts-per-million). That magnitude, ±50 ppm, was informed by the GRS hardware specifications version 0.93 dated May 28th, 2022. A uniform distribution between those limits is assumed.

To evaluate the effects of sample rate variation, 2,800 on-design and 2,800 off-design mock recordings were assembled. For each mock waveform and each of the eight metric types, two loudness levels are computed: one when using the proper sample rate and a second when using a sample rate perturbed by a random value chosen from the distribution cited above. The true levels in this case are from the analysis of the waveforms without the sample rate perturbations. That computation was repeated 400 times for each of the 5,600 mock recording while choosing a new random sample rate perturbation each time, giving a total of 2,800×2×400 = 2,240,000 perturbed mock recordings in the dataset. The mock recording waveforms used to compute both the perturbed loudness levels and the true loudness levels contained all four mock effects: sonic boom, turbulence effects, post boom noise, and background noise. The "Custom F" method [1] was used to correct for background noise contamination of all waveforms since we want to identify the effects of sample rate variation while processing the data like it will be processed during X-59 field tests. The metric-specific loudness level error, in decibels, is found by pairwise differencing the loudness levels computed with perturbations of sample rate and loudness levels found with no perturbations.

Sample rate effects are documented in Figure 6 and Table 9. The observed measurement error bias and standard deviation are documented in that figure and table, while assuming the measurement error is normally distributed. Results are shown for both the on- and the off-design waveform cases in Figure 6, and the average of those two cases is included in both the figure and the table. The expected loudness level error caused by ±50 ppm variation in sample rate is very small, where the observed standard deviation was 0.001 dB or less and depended on the metric type (Figure 6). Consequently, this source is unlikely to contribute significantly to the total uncertainty as compared to background noise effects discussed in the previous subsection and the invariable effects discussed earlier in Section II.

The sample rate error is applied as a ratio relative to the proper sample rate when computing the perturbed loudness levels. For example, a +17-ppm error is applied by scaling the sample rate, F_s, by a factor of (1 + 17÷1E+6) = 1.000017. Because the error is applied as a ratio, the effect does not depend on the chosen sample rate, F_s. The measurement error magnitudes, in decibels, that are found when analyzing mock recordings synthesized at a sample rate of 24,000 Hz will be the same as when analyzing similar mock recordings sampled at a rate of 51,200 Hz. Thus, the values presented here apply to all sample rates. A sample rate of 51,200 Hz is recommended for use during X-59 field tests so the spectra of both the sonic boom and the acoustical ambient can be accurately quantified.

The MATLAB® script named *SampleRateEffects_rev8.m* was used to create the data that appear in Figure 6 and Table 9. The script name is identified for documentation purposes only. It is not available for public distribution.

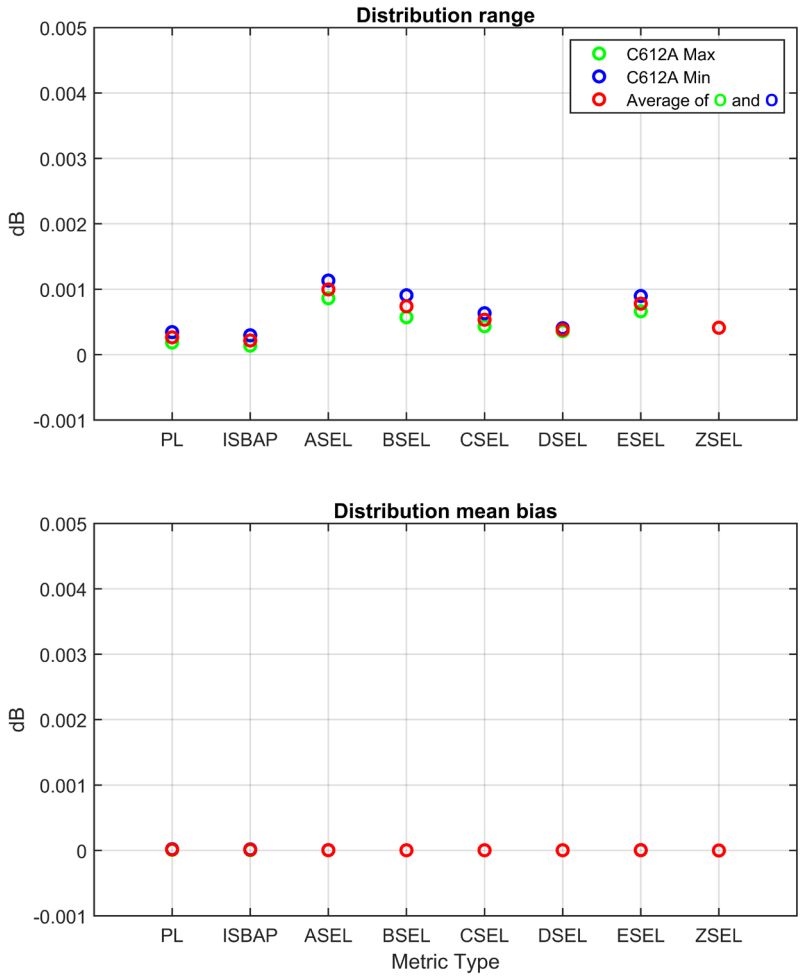


Figure 6: Assumed sample rate uncertainty effects versus metric type, where both the standard deviation and the mean bias of the measurement error are plotted.

Table 9: Summary of mean bias and standard deviation[7] for sample rate effects on measurement error versus noise metric type (effect does not vary with level).

Metric	Mean Bias dB	Range dB	Distribution Type
PL	1.6e-05	0.00027	normal
ISBAP	1.2e-05	0.00022	normal
ASEL	4.8e-06	0.001	uniform
BSEL	3.8e-06	0.00074	uniform
CSEL	3.8e-06	0.00053	uniform
DSEL	3.8e-06	0.00038	uniform
ESEL	4.8e-06	0.00078	uniform
ZSEL	0	0.00041	uniform

C. Windscreen insertion loss and sonic boom elevation angle

The effects of windscreen insertion loss and the boom elevation angle are informed by insertion loss measurements (Figure 7) of the COUGAR Gold windscreen[2], which were provided by BYU (Ref. [23], pending publication). These data are given at 5° increments for a range of elevation angles spanning from near grazing, 5°, to normal to the ground plane, 90°. Methods like those documented in Ref. [24] were used to generate these insertion loss estimates but while using the COUGAR Gold design instead of the designs from Ref. [24]. Importantly, the insertion loss data were only provided in the frequency range from 50 to 20,000 Hz (Figure 7). Consequently, the insertion loss values at frequencies less than 50 Hz were assumed to be zero for all elevation angles – the windscreens are assumed to be transparent at very low frequencies where unweighted sonic boom noise is high in level. The main effect of the windscreen on the measured signal is a spectral coloration from absorption and scattering effects that manifest as high frequency attenuation, as implied by the positive valued insertion loss data (Figure 7).

Two thousand eight hundred on-design and 2,800 off-design mock acoustic recordings were processed to estimate the insertion loss and elevation angle effects. For each mock recording, a random elevation angle was chosen assuming a uniform distribution ranging from 20° to 70° in 5° increments like the measured data. That limited range was used since X-59 booms are, generally, not expected to be near grazing or normal incidence when measured by the GRS noise monitors deployed for X-59 tests. For each mock recording, the insertion loss data corresponding to the chosen angle (e.g., a curve from Figure 7) was used to perturb the one-third-octave band spectrum of the waveform prior to computing loudness levels. These perturbations of the one-third-octave band spectrum approximate the spectral coloration that would be expected from covering the microphones with windscreens during the field tests. That process was repeated 100 times for each of the 5,600 mock recording while randomly choosing a new insertion loss curve each time, giving a total of 2,800×2×100 = 560,000 perturbed mock recordings in the dataset. To compute the measurement error, the loudness levels computed with spectral perturbations were differenced pairwise with the loudness levels found without the perturbations. In this case the true levels are from the waveforms without spectral perturbations caused by insertion loss effects. The mock recording waveforms used to compute both the perturbed loudness levels and the true loudness levels contained all four mock effects: sonic boom, turbulence effects, post boom noise, and background noise. The spectral perturbation was applied equally to all included mock effects. The “Custom F” method [1] was used to correct for background noise contamination of all waveforms.

The combined effects of windscreen insertion loss and elevation angle are documented in Figure 8 and Table 10. The observed measurement error mean bias and standard deviation are given while assuming the errors are normally distributed. The expected error caused by both insertion loss and variation in elevation angle is modest, where the observed standard deviation was less than 0.1 dB for all metric types (Figure 8). Consequently, this source is expected to contribute only slightly to the total uncertainty as compared to background noise effects discussed in the previous subsection and the invariable effects discussed in Section II.

The MATLAB® script named *WindscreenInsertionLossEffects_rev8.m* was used to create the data that appear in Figure 8 and Table 10. The script name is identified for documentation purposes only. It is not available for public distribution.

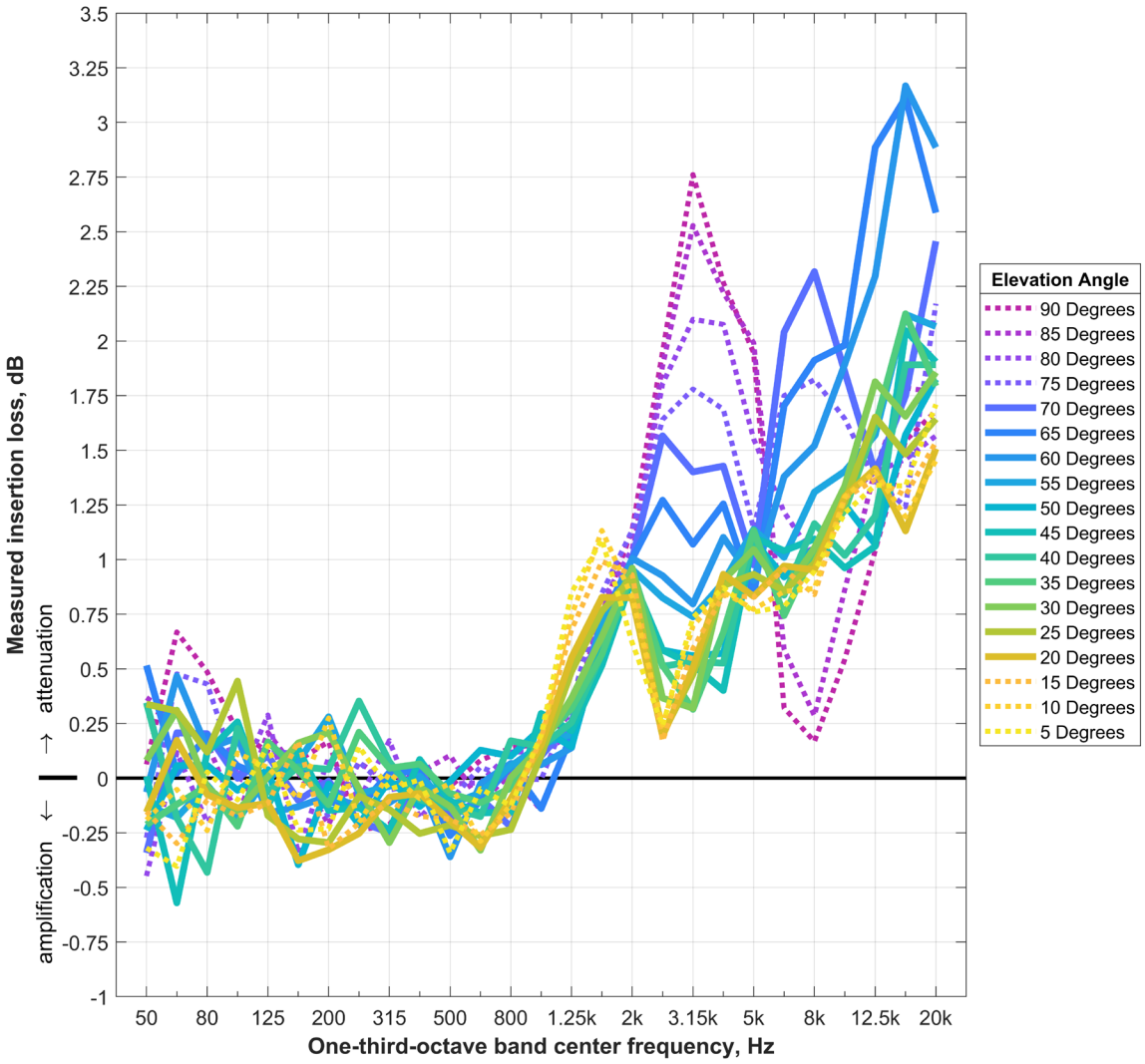


Figure 7: Insertion loss versus frequency and elevation angle, where solid lines indicate the subset of angles that were used to estimate windscreen effects (data source: Ref [23]).

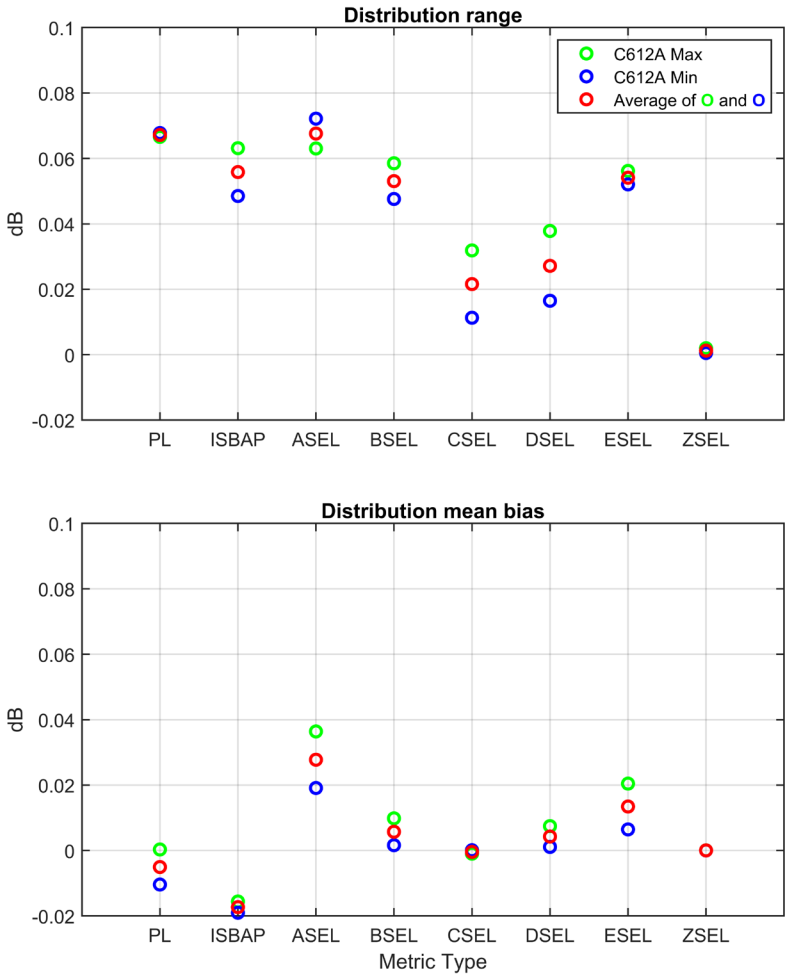


Figure 8: Assumed windscreen insertion loss and elevation angle uncertainty effects versus metric type, where both the standard deviation and the mean bias of the measurement error are plotted.

Table 10: Summary of mean bias and standard deviation[7] for windscreen effects on measurement error versus noise metric type (effect does not vary with level).

Metric	Mean Bias dB	Range dB	Distribution Type
PL	-0.0051	0.067	normal
ISBAP	-0.017	0.056	normal
ASEL	0.028	0.068	normal
BSEL	0.0057	0.053	normal
CSEL	-0.00044	0.022	normal
DSEL	0.0043	0.027	normal
ESEL	0.013	0.054	normal
ZSEL	3.3e-05	0.0012	normal

D. Boom finder induced window position jitter

Many acoustic recordings will be processed during X-59 field testing to compute loudness level values. One step in that signal processing path is to apply a taper window to the measured waveform prior to computing the sound pressure level spectrum, which is a precursor of the loudness levels. This step requires that the taper window be aligned properly with the sonic boom waveform to ensure the boom waveform will fall within the pass-portion of the window – the portion of the window function containing only unity values. The windowing function will be like the one discussed in Ref. [1].

The volume of data that will be processed and the need for timely results will necessitate use of computer-based algorithms to locate X-59 sonic boom waveforms within the recording files [25]. The locations provided by the boom-finder algorithm will introduce jitter error into the automated positioning of the window function. For example, the boom finder is not expected to determine the boom location exactly since things like background noise and turbulence effects will affect the algorithm accuracy. This jitter will materialize as a small, random time shift in the window position relative to the position if the boom location were known exactly. Consequently, this variation in the alignment of the window function will cause slight variations in the metric values relative to true metric values that would be computed if the exact boom locations were knowable. Importantly, small differences in the metric values are expected even if the sonic booms are always placed within the pass-portion of the window function since the windowed signals will also include background noise and post-boom noise effects, the level of which would be affected by this small-scale jitter. This is a source of uncertainty in the computed metric values that is expected to vary with both metric type and level.

Twenty-four thousand mock acoustic recordings, which included an equal number of on- and off-design X-59 booms, were processed to estimate the effects of window jitter. The true locations of the sonic boom waveforms and the true metric values of the mock acoustic recordings are known since the waveforms are assembled within these computer-based simulations. To estimate the measurement error due to window jitter, these true metric values were compared to the metric values computed when the window function was randomly shifted in time. The random jitter was drawn from a normal distribution with standard deviation of 25 msec and zero mean, which was rounded to a whole number of discrete-time samples to shift the taper window. That standard deviation is slightly larger than the expected accuracy of the boom finder algorithms that will be used during X-59 testing [25], so the results should provide a somewhat conservative estimate of the effects of jitter. The waveforms used to compute both the jittered and true loudness levels contained all four mock effects: a sonic boom, turbulence effects, post boom noise, and background noise. The “Custom F” method [1] was used to correct for background noise contamination of all waveforms.

The results of this study are summarized in Figure 9. The observed measurement error varies with both level and metric type, where signals with lower values of corrected SNR exhibit more error. Importantly, the distribution discussed above from which the jitter was chosen did not change with either SNR or the loudness level of the boom. The jitter

was always chosen from a normal distribution with standard deviation of 25 msec and zero mean. This may not be the case when processing real data since waveforms with high SNR or louder booms may be easier to locate algorithmically than quiet booms embedded in noisy recordings. However, the boom finder algorithms have not been finalized and delivered to NASA, so exercising them on these mock recordings is not currently practical. The observed effect of this source of variation is expected to be quite small (Figure 9) in comparison to many of the effects discussed in earlier sections, like background noise. Thus, this effect when combined with the other sources of uncertainty is not expected to contribute significantly to the total uncertainty of a loudness level computed from a recorded waveform. Consequently, the current simulations are believed to be sufficient for this report.

The MATLAB® script named *BoomFinderJitterEffects_rev8.m* was used to create the data that appear in Figure 9. The script name is identified for documentation purposes only. It is not available for public distribution.

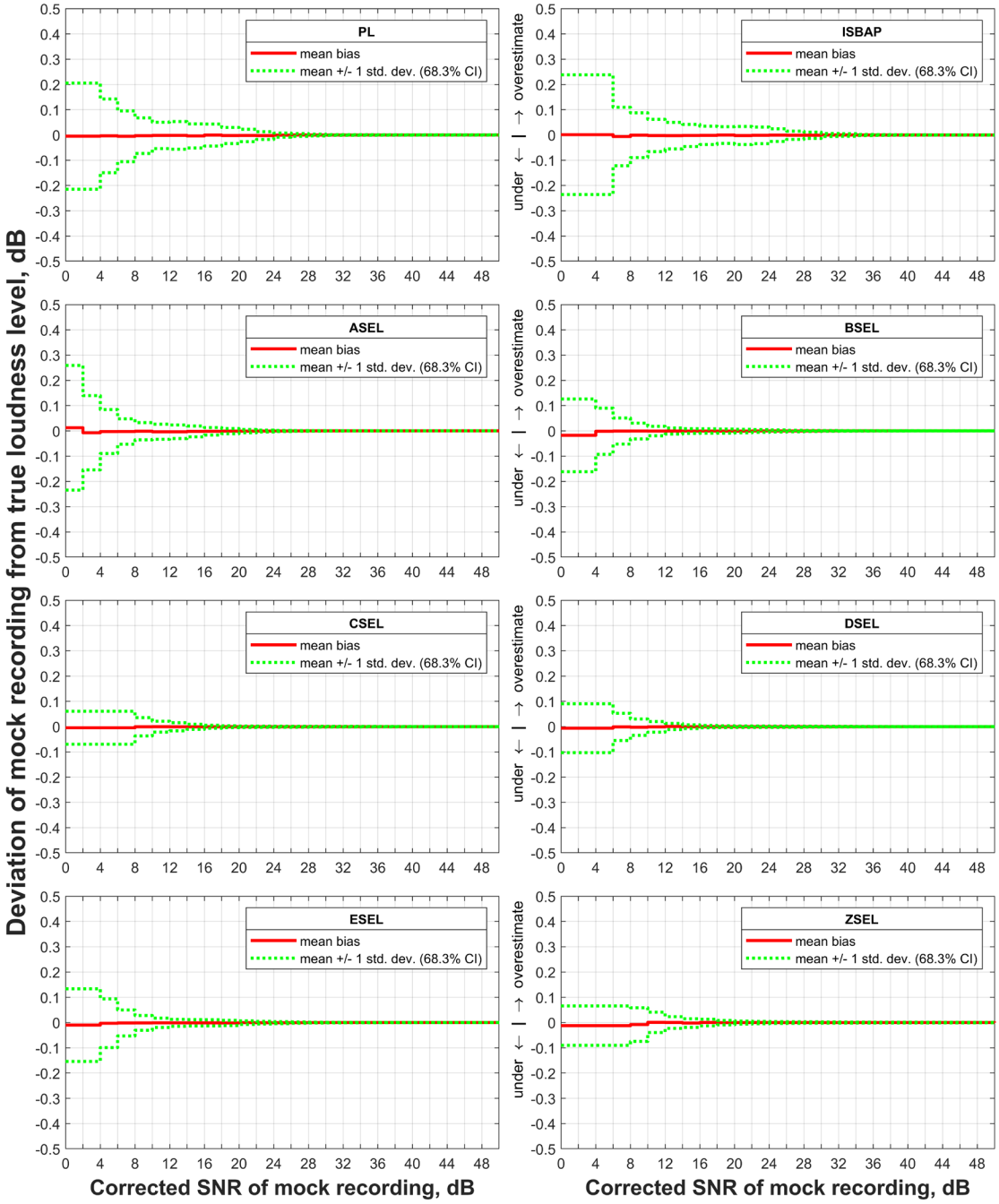


Figure 9: Summary of simulated window jitter related measurement error versus metric type and corrected signal to noise ratio, where both the standard deviation and the mean bias of the error are plotted.

E. Metric software numeric precision

The post-processing software that is used to compute loudness levels of recorded waveforms may introduce uncertainty due to numerical precision. For example, analysts may use single precision arrays and constants – instead of double precision data – to increase the computational speed and to reduce the memory used to processing large numbers of recorded waveforms. Hardware limitations may also force use of single precision data.

The expected error was quantified when using single precision versus double precision to compute loudness levels of 16,000 mock acoustic recordings, which included both on- and off-design X-59 sonic booms. The metric values computed when using double precision are assumed to be the true values. To estimate the effects of reduced precision, these true values were differenced with metric values found when using single precision for the computations. The waveforms used to compute both the single and double precision loudness levels contained all four mock effects: a sonic boom, turbulence effects, post boom noise, and background noise. The "Custom F" method [1] was used to correct for background noise contamination of all waveforms. The results are shown in Table 11.

These effects are significantly smaller when compared to the other effects discussed in earlier sections. For example, the measurement error standard deviation due to this effect is at most 0.00027 dB. Thus, this effect is assumed to be insignificant and will not be combined with the other effects when computing the total uncertainty to avoid unnecessary clutter when summarizing the total uncertainty in figures and tables. Of the other nine sources of uncertainty, the GRS sample rate uncertainty is closest in magnitude to this numerical precision effect (e.g., see Section III.B and Table 9 versus Table 11). Thus, the results for GRS sample rate presented in Sections V.A and V.B are representative of the results that would be expected if precision effects were also included. Importantly, sample rate effects were not found to be significant later in Section V.B, which motivated the exclusion of the precision effects when combining the different uncertainty sources.

The MATLAB® script named *PrecisionEffects_rev8.m* was used to create the data that appear in Figure 9. The script name is identified for documentation purposes only. It is not available for public distribution.

Table 11: Summary of mean bias and standard deviation[7] for numerical precision effects on measurement error versus noise metric type (effect does not vary with level).

Metric	Mean Bias dB	Range dB	Distribution Type
PL	2.7e-06	0.00027	normal
ISBAP	2.8e-06	0.00027	normal
ASEL	-2.6e-07	2.1e-06	normal
BSEL	-2.5e-07	1.9e-06	normal
CSEL	-2.1e-07	1.3e-06	normal
DSEL	-2.1e-07	1.3e-06	normal
ESEL	-2.5e-07	1.8e-06	normal
ZSEL	-2.1e-07	1.2e-06	normal

IV. METHODS USED TO COMBINE THE SOURCES OF UNCERTAINTY

A computer-based Monte Carlo approach was used to combine the different sources of uncertainty. A random perturbation of the measurement chain gain was drawn for each source of uncertainty using the assumed distribution types, the ranges, and the biases documented in Sections II.A to II.E and III.A to III.D. Each set of random gains was then summed across the different sources of uncertainty to determine the combined measurement chain gain across all sources. This process was repeated 3,000,000 times. Then, the variation of total gain across these realizations was studied to determine the statistical behavior of the measurement error when all sources of uncertainty are combined.

For example, the MATLAB® commands below would be used here to estimate the combined measurement error for three notional sources of uncertainty with the following distributions: 1) a normal distribution with mean +0.05 dB and standard deviation 0.2 dB, 2) a uniform distribution having a mean of +0.02 dB and range of 0.1 dB, and 3) a normal distribution with mean +0.00 dB and standard deviation 0.03 dB:

```
Ntot = 3e6;
dBRange1 = 0.2;
dBRange2 = 0.1;
dBRange3 = 0.03;
dBBias1 = +0.05;
dBBias2 = +0.02;
dBBias3 = +0.00;
Observations(:,1) = randn(Ntot,1)*dBRange1 + dBBias1;
Observations(:,2) = (rand(Ntot,1)-0.5)*dBRange2 + dBBias2;
Observations(:,3) = randn(Ntot,1)*dBRange3 + dBBias3;
CombinedObservations = sum(Observations,2);
CombinedMean = mean(CombinedObservations);
CombinedStDev = std(CombinedObservations);
```

Similar approaches are used to combine the nine sources discussed earlier, noting that some distributions may vary with metric or level and others may not. For the variable sources of uncertainty, the range and bias values are averaged across the on-design and off-design waveform cases (e.g., Figures 6 and 8, red circles) before combining them with the other sources of uncertainty. Furthermore, for the case where the effect of a variable source was binned (e.g., Figure 2), the number of off-design and on-design waveforms that fell within each bin was used to compute a weighted average across those two waveform cases. The resulting weighted average of bias and range in the data are plotted in Figures 2 and 9, which were used when combining those background noise effects with the other seven sources of uncertainty. The background noise effects and window jitter effects are a function of both corrected SNR and noise metric type, so the Monte Carlo simulations are performed for each metric type and level. Thus, the combined effect of all sources of uncertainty will also be a function of metric and SNR.

Because the distributions that are identified in Sections II and III include both uniform and normal distributions, readers may wonder how the combined gain error is expected to behave. An intermediate result is shown in Figure 10 to highlight the expected

behavior, where the total combined gain error of only the five invariable sources is displayed as a histogram. Importantly, that intermediate result does not include the variable sources of uncertainty identified in Section III. Consequently, the properties of the distribution are not identified since they have no practical use. Of the five sources included in Figure 10, only the microphone calibration component is assumed to be normal (Section II.A). A uniform distribution is assumed for the other four invariable sources of uncertainty (Sections II.B to II.E). Even so, a normal distribution (Figure 10, red line) fits well to the observed gain error (Figure 10, histogram) when using the Monte Carlo method outlined above to combine the sources. Thus, the combined gain error is expected to be well described by a calculated mean bias and standard deviation when the combined measurement error is assumed normal. Those two values will be cited in Section V below when discussing results that include both the invariable and variable sources of uncertainty.

The MATLAB® code used to combine the invariable and variable sources of uncertainty and create data plots is found in the m-file named *Compute_GRS_UQ_rev4.m*. The results of these simulations are documented in the next section. The script name is identified for documentation purposes only. It is not available for public distribution.

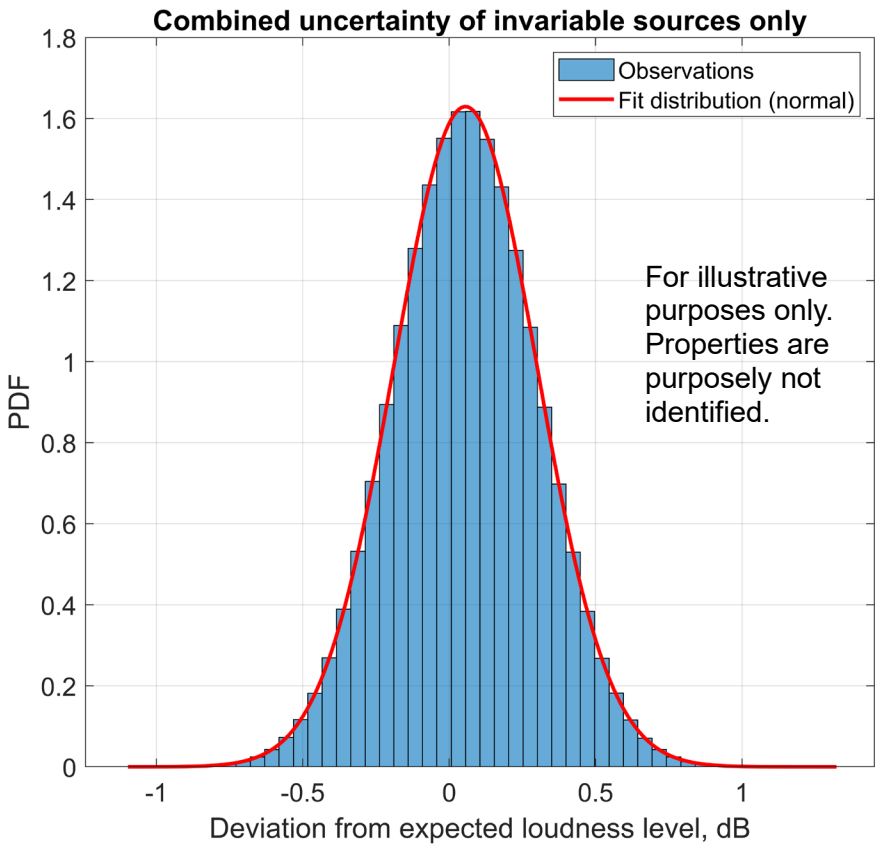


Figure 10: Intermediate result showing combined measurement error for only the invariable sources, which does not include the effects of variable sources like background noise (see Section V.A for results that include the variable sources).

V. RESULTS

A. Total measurement error

The results of combining the nine sources of uncertainty discussed above are plotted in Figure 11a below for the PL noise metric. As mentioned earlier, the numeric precision of the metrics computational software is not included in the total combined uncertainty since that effect is very small. Plotted in Figure 11a are the mean of the measurement error (solid red curve) and ±1 standard deviation interval about the mean (dotted green curves). The green dotted curves represent the 68.3% confidence interval of measurement error assuming a normal distribution. Other confidence intervals could be displayed by appropriate scaling of the standard deviation. For interested readers, the measurement error standard deviation is plotted directly in Figure 12, instead of as a confidence interval like in Figure 11a. The trend where the standard deviation smoothly decreases with increasing SNR is easier to identify visually in Figure 12. These data (Figures 11 and 12) are plotted versus the corrected SNR as discussed earlier in Section III.A. Please refer to that section for a discussion of why that independent variable was chosen. It is important to recognize that a single uncertainty value cannot be assigned to a measured loudness level a priori. The uncertainty must be assigned via lookup table after the measurement is made and the corrected SNR of that measurement is computed.

The distributions of corrected SNR observed in the mock acoustic recording datasets documented in III.A are plotted as box plots in Figure 11b. A separate box plot is given for the on- and off-design X-59 boom datasets. The black dashed whiskers indicate the 5^{th} to 95^{th} percentile data range and the blue box indicates the 25^{th} to 75^{th} percentile range. Markers identified in the legend locate the 1^{st}, 50^{th}, and 99^{th} percentile points. The horizontal alignment of the box plots in Figure 11b with the uncertainty plot shown in Figure 11a gives a visual indication of how the uncertainty may vary for each boom type. For example, the median corrected SNR for the on-design X-59 booms is about +16 dB, which corresponds to an expected bias error of about −0.213 dB and standard deviation of about 0.682 dB. On-design X-59 booms with an SNR of about +8.1 dB correspond to the 5^{th} percentile for that boom type and are expected to have a bias error of about −0.207 dB and standard deviation of about 1.60 dB. Comparing the box plots for the on- and off-design X-59 cases, the off-design waveforms are expected to have higher SNR so the uncertainty is expected to be smaller than the on-design waveforms at the same percentile. For example, the 5^{th} percentile of off-design booms has a corrected SNR value of about 16 dB, which would give the same uncertainty estimate as the median on-design boom.

Importantly, the behavior of the uncertainty and the corrected SNR are expected to change with the different metric types. Thus, separate plots like the one in Figure 11 are included in Appendix 2 for the PL, ISBAP, ASEL, BSEL, CSEL, DSEL, ESEL, and ZSEL metrics. Tabulated total uncertainty values for those metrics are included in Appendix 3, which were used to create the plots in Appendix 2. The tabulated data should be useful for analysts who wish to quantify the uncertainty of a measured sonic boom. Specifically, once the corrected SNR value is computed for a waveform measured in the field, the table data in Appendix 3 can be used to determine the expected combined bias error and standard

deviation. When the corrected SNR of a measured boom falls within the lower and upper edges of a tabulated bin from Appendix 3, then the values of bias and standard deviation for that bin should be used to compute the uncertainty. Those values were computed while using the "Custom F" spectral correction method [1]. Using a different method, or no correction, would require the tables to be recomputed. Importantly, the bias of truth relative to a measurement would be the negative of the measurement error bias that is tabulated in the "mean bias" column of the tables in Appendix 3.

For example, assume the calculated PL value of a measured waveform was 75 dB PL. Also assume that value was computed using NOM[9] after correcting for background noise contamination using the "Custom F" spectral correction method, and the corrected SNR was between +6 and +8 dB PL. That would correspond to an expected bias error of about +0.814 dB PL and standard deviation of 2.50 dB PL (looked up in Appendix 3, Table 3.1, Bin 4). Thus, the measured value with uncertainty might be expressed as $75^{+4.08}_{-5.71}$ dB PL at the 95% confidence level[10] when accounting for expected measurement error bias and range. Those values assume the 95% confidence interval is expressed as $\pm 1.959 \times \sigma + \mu$ with $\sigma = 2.50$ dB and $\mu = -0.814$ dB. The resulting confidence interval is not symmetric about the observed level, 75 dB PL, due to the mean bias, μ. For comparison, if the corrected SNR were higher, between say +14 and +16 dB PL for example, then the measured value with uncertainty might instead be expressed as $75^{+1.55}_{-1.12}$ dB PL at the 95% confidence level[11] (using Appendix 3, Table 3.1, Bin 8). Those limits are smaller and more symmetric than the prior example since the bias, +0.213 dB, is much smaller in this case. Inclusion of the expected bias error when assigning uncertainty may lead to counterintuitive confidence interval citations in some cases, where both limits are either positive or negative[12]. Analysts should be aware of this possibility. The likelihood of encountering such edge cases is not currently known, but depends on the ratio of μ to σ and the value that scales it. Finally, different confidence intervals can be cited by scaling the standard deviation, σ, differently. For example, scaling the standard deviation by 1.644 instead of 1.959 would give an estimate for the 90% confidence interval. Also, confidence intervals for different noise metrics can be found using the metric-specific tables in Appendix 3. For example, Table 3.4 would be used when computing intervals for BSEL.

[10] $-5.71 = -(1.959 \times 2.50) - 0.814$ and $+4.08 = (1.959 \times 2.50) - 0.814$, assuming the 95% confidence interval equals $\pm 1.959 \times \sigma + \mu$ with $\sigma = 2.50$ dB and $\mu = -0.814$ dB. Values taken from Appendix 3, Table 3.1, Bin 4.

[11] $-1.12 = -(1.959 \times 0.682) + 0.213$ and $+1.55 = (1.959 \times 0.682) + 0.213$, assuming the 95% confidence interval equals $\pm 1.959 \times \sigma + \mu$ with $\sigma = 0.648$ dB and $\mu = +0.213$ dB. Values taken from Appendix 3, Table 3.1, Bin 8.

[12] Depending on the chosen confidence interval, the value of σ, and the value of μ, it is possible the upper and lower bounds on the measured value could both be positive or both be negative, which might be counterintuitive. For example, a loudness level with uncertainty that looks something like $75^{-0.51}_{-8.37}$ dB might be possible in some cases, which would indicate that the true level is expected to be biased low compared to the measurement within the chosen confidence level. Such cases are only expected to occur when the mean bias is larger than the product of the standard deviation and the confidence interval scalar. Such edge cases will likely only occur in cases when the corrected SNR is very low in level, if at all.

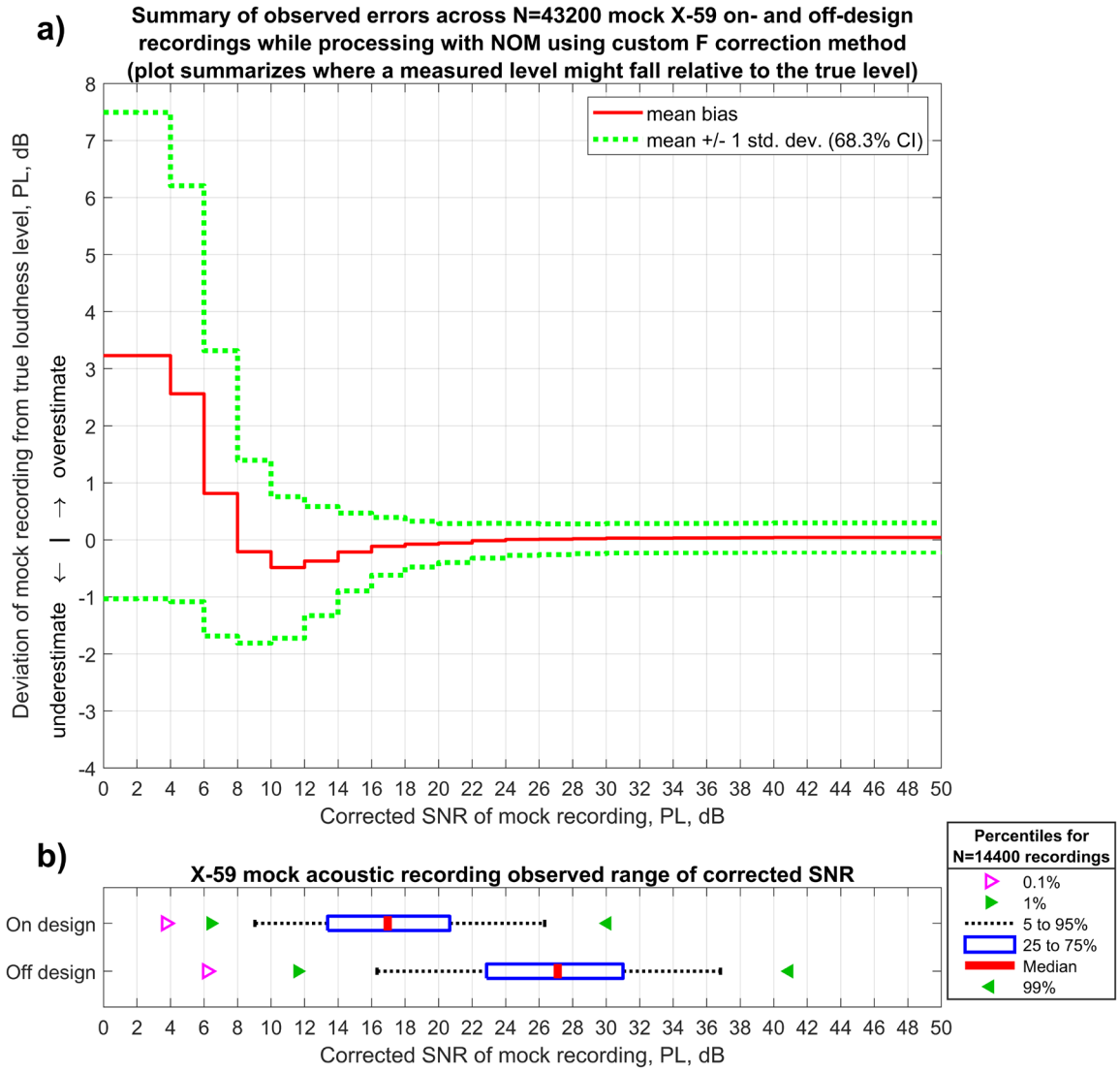


Figure 11: Total measurement error for the PL noise metric versus the PL corrected SNR, a) shows the total measurement error and b) shows the observed distribution of corrected SNR for the on-design and off-design X-59 mock acoustic recordings.

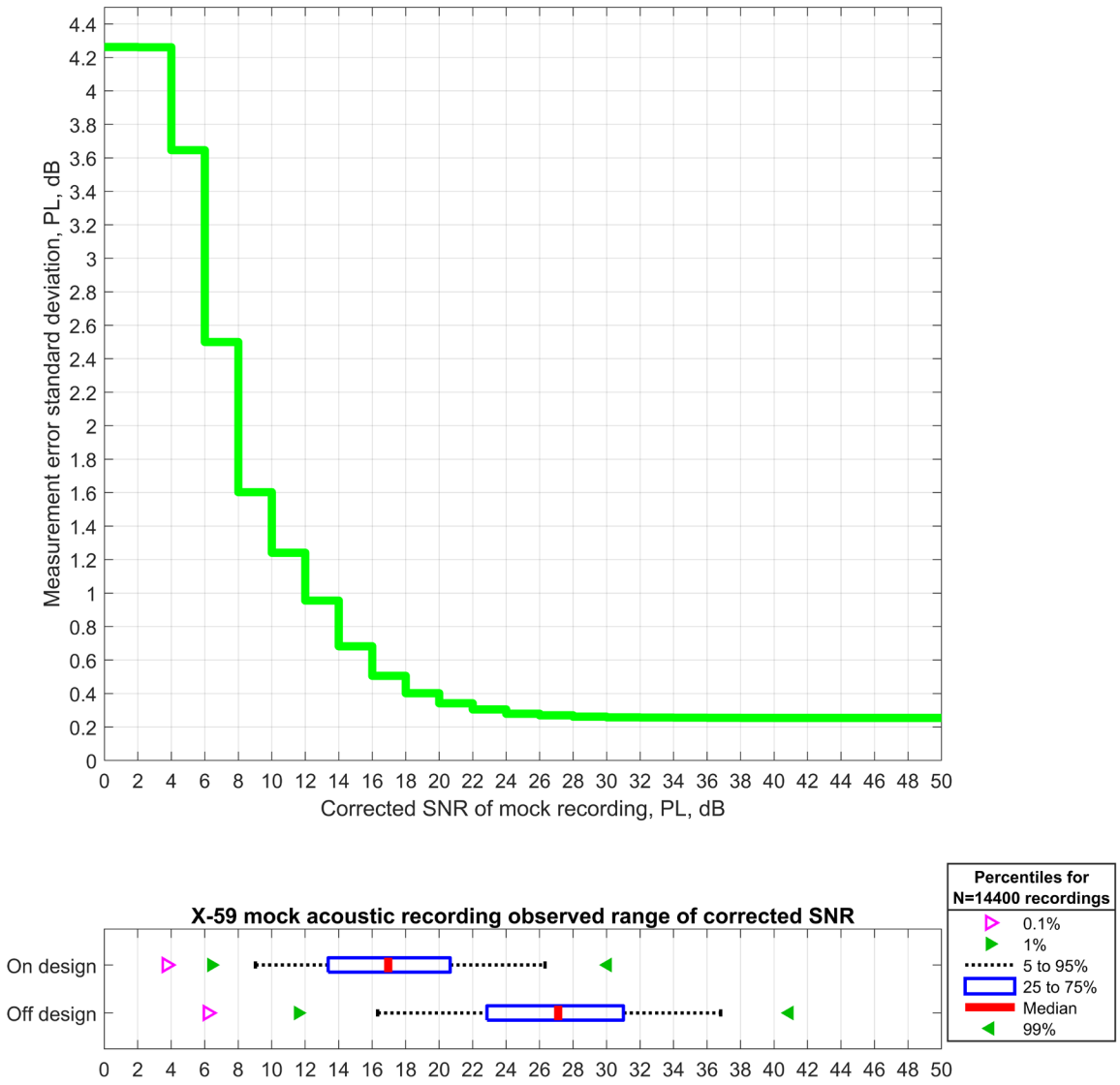


Figure 12: Total combined measurement error standard deviation.

B. Contribution proportions

It might be useful in some cases for analysts to understand the proportion of the total variance that is explained by each source of uncertainty. For example, a rank order of source significance may be used to identify ways to mitigate the effect of dominant sources while avoiding allocating resources to reduce sources that already contribute little to the overall measurement error. Thus, an analysis of variance was performed on the Monte Carlo dataset to determine the relative contribution of each uncertainty source for each metric type and level. An example result of this analysis is plotted in Figure 13 for Perceived Level. The curves identified in the legend are ordered in the same manner as the lines appear from top to bottom within the plot.

The contribution of each source to the total variance changes with corrected SNR since the background noise related measurement errors are a function of SNR (e.g., see Section III.A). Thus, the contribution of background noise to the total error is high when SNR is low and it is low when SNR is high (Figure 13, dashed black line). Consequently, other sources will contribute more to the total variance when SNR is high. Specifically, the calibration uncertainty, the microphone ambient temperature effects, and the windscreen effects become significant as SNR increases and the effects of background noise decrease. Importantly, Figure 13 should be analyzed while considering Figures 11 and 12, which show how the total measurement error varies with changing SNR. Specifically, the total variance, the square of the ordinate in Figure 12, is highest when SNR is low and lowest when SNR is high.

A plot like Figure 13 is useful because it shows which sources are dominant as SNR changes and background noise effects become less dominant. For example, sample rate effects (Figure 13, solid yellow line) never have a significant contribution to the overall uncertainty. Thus, variation in sample rate in the range of ±50 ppm is not important when computing loudness levels of the GRS measurements. Consequently, correcting for GRS sample rate drift is likely not needed if the sample rate uncertainty stays within the ±50 ppm limit cited on the hardware specification sheets. Thus, correcting sample rates using GPS timecode is likely not necessary during X-59 field tests. Using the pre-configured GRS ADC sample rate – e.g., 51,200 Hz – should be sufficient when computing loudness levels. Sources like microphone calibration uncertainty and ambient temperature effects (Figure 13, solid red and green lines, respectively) are expected to be significant when SNR is high, and should be the focus of efforts to reduce uncertainty in the higher SNR range. While windscreen insertion loss effects, which include elevation angle, are expected to become moderately significant when SNR is high (Figure 13, dashed cyan line), the design of the windscreen cannot be changed so the uncertainty caused by this source cannot be reduced.

Separate plots like the one below are included in Appendix 4 for the PL, ISBAP, ASEL, BSEL, CSEL, DSEL, ESEL, and ZSEL metrics. Tabulated proportions for all those metrics are included in Appendix 5, which were used to create the plots in Appendix 4.

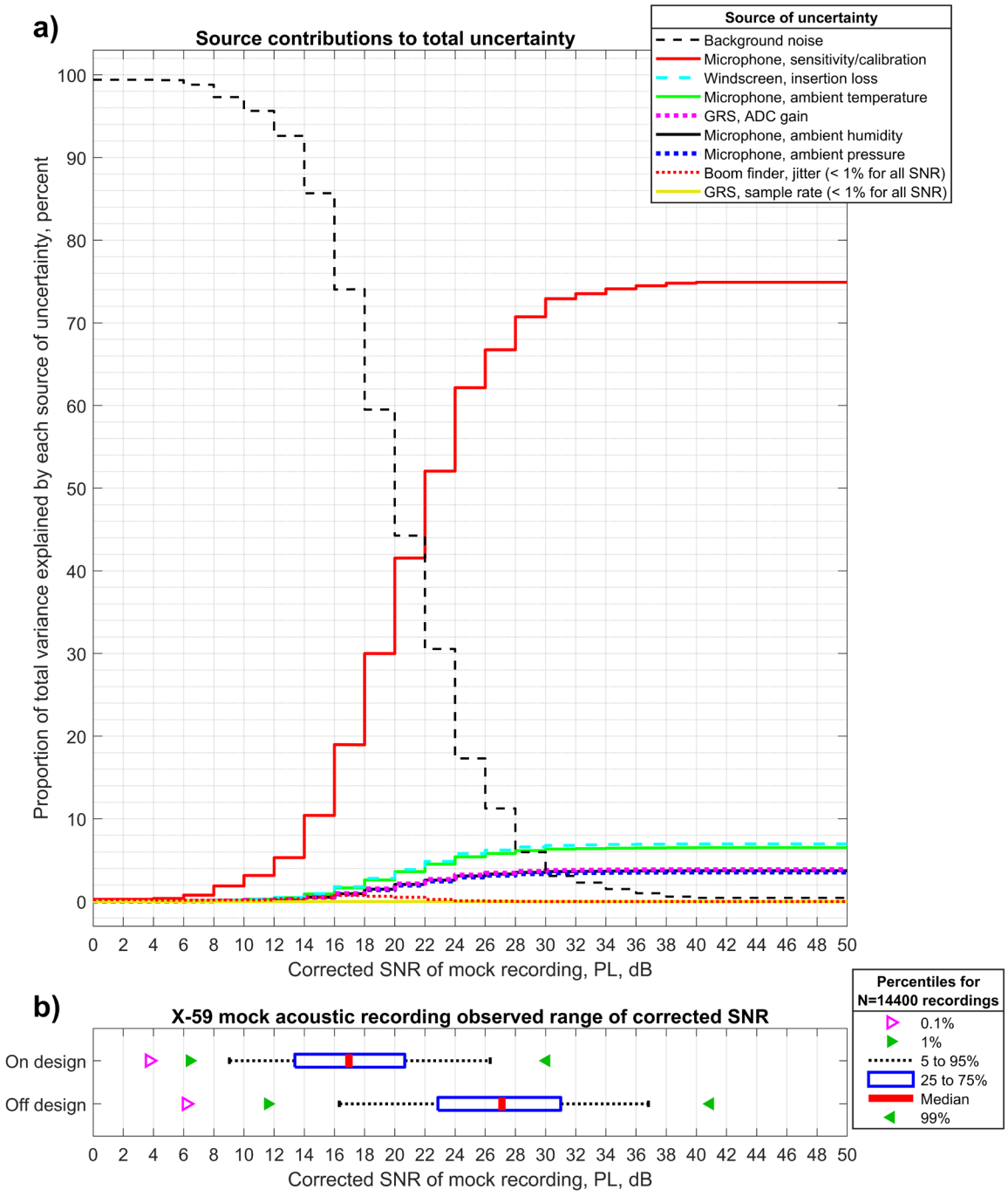


Figure 13: Proportion of the total variance explained by each uncertainty source for the PL noise metric versus the PL corrected SNR of the mock recording.

C. Effects of reduced uncertainty

In the analyses presented above, four components of the total uncertainty stand out as more significant than the other five sources:

- Background noise is dominant when the corrected SNR is low (e.g., see Figure 13a, left-hand side, the dashed black curve),
- As the corrected SNR increases, the uncertainty due to the microphone calibration become increasingly important (Figure 13a, right-hand side, the solid red curve),
- Ambient temperature effects are moderately important when corrected SNR is high (Figure 13a, right-hand side, the solid green curve), and
- Windscreen related uncertainty (Figure 13a, right-hand side, dashed cyan curve) is about as large as ambient temperature effects (solid green curve) when SNR is high.

This knowledge helps to identify methods NASA could use to reduce the total measurement chain uncertainty. Approaches to reduce uncertainty of the first three sources listed above (background noise, calibration, and temperature) and some supporting analyses to identify the effects of the reductions are presented in this section. The windscreen design that will be used with the GRS noise monitors for X-59 measurements cannot be changed, so mitigating uncertainty due to that source is not practical. Also, the contribution of the windscreen source is not as significant for some other noise metrics like BSEL, DSEL, and ESEL (e.g., Appendix 4, Figure 4.4, 4.6, and 4.7). Consequently, effects of reduced windscreen uncertainty are not considered in this section.

One obvious approach to reduce uncertainty would be to make measurements in environments with lower ambient noise levels than the QSF18 test, which were assumed when creating mock recordings above. Lower background noise levels should reduce the impact of this source of uncertainty by changing the proportion of measurements with low SNR. Such efforts may be beneficial when measuring X-59 on-design booms since a large proportion of that boom type will have modestly low SNR if background noise levels are like those of QSF18 (e.g., Figure 13b, on-design box plot). For example, 25% of the on-design X-59 sonic booms that are mixed with background noise from QSF18 have corrected SNR values of 13.5 dB or lower (Figure 13b, left edge of upper blue box), for which the measurement error standard deviation is about 1 dB or more (Figure 12). Measurements made with lower background noise levels are expected to shift the box plot features shown in Figures 11b and 13b rightward, so sonic booms at a particular percentile of corrected SNR would then lie within a bin in Figure 11a with higher SNR and, thus, lower total error. This rightward shift is expected to be particularly beneficial for on-design booms since the measurement error standard deviation curve changes rapidly at low corrected SNR values. For example, a 6 dB increase in SNR for the 25th percentile on-design case, from an SNR of 13.5 to 19.5 dB, would roughly correlate to a change in measurement error standard deviation from about 1 dB to about 0.40 dB (Figure 12 and Appendix 3 Table 3.1) – more than a halving of the total uncertainty. Lower background noise levels are not expected to affect the off-design booms as much since they, generally, have higher corrected SNR values. For example, a 6 dB increase in the off-design corrected SNR 25th percentile from the current 23 dB to 29 dB would change the measurement error standard deviation only slightly, from 0.31 to 0.26 dB (Figure 12 and

Appendix 3 Table 3.1). This is because other sources become dominant at these higher corrected SNR values.

The uncertainty associated with the microphone calibration component could be further reduced by choice of a different calibration method when updating the TEDS data during traceable calibrations. This would reduce the total uncertainty compared to the baseline case shown in Figure 11a for booms with high SNR since this component is significant in that upper SNR range (Figure 13a). The analyses discussed earlier assumed use of an acoustical calibrator, so a standard deviation of 0.22 dB was assumed for this microphone calibration component. If the TEDS sensitivity were instead found using the reciprocity method[5] then the uncertainty is expected to be significantly smaller. Specifically, a standard deviation ranging from 0.015 to 0.025 dB is expected[5], instead of the 0.22 dB assumed previously. That procedural change in the calibration would reduce the effects of the calibration component on measurement error when SNR is high.

Finally, the ambient temperature effect could be reduced if an estimate of the ambient temperature at the time of measurement were used to correct the computed noise levels. For example, the analyses here assumed acoustical measurements would be performed in ambient temperatures ranging from 35 to 110°F, a uniform span of 75°F, and that no temperature compensation would be performed to correct for related changes in sensitivity. This assumption resulted in a uniform gain distribution with range 0.225 dB (see Section II.B). If the ambient temperature could instead be estimated to within ±10°F of the temperature at time of measurement and a suitable temperature compensation applied to the measured data, then that would reduce the span of the assumed gain uncertainty to about 0.06 dB (found from multiplying 20°F by 0.003 dB/°F). Such a compensation would not be possible in real time – if, for example, the metric values are computed by GRS units on the fly. However, that compensation might be possible posttest since detailed weather data will be recorded during each X-59 overflight. However, current X-59 data processing plans do not include such a temperature compensation. The benefits and costs of including such a correction would need to be evaluated to determine if the uncertainty reduction for this component is worth the cost and added data analysis complexity.

To evaluate the effects of reducing the three most significant sources of uncertainty discussed above, the analyses presented earlier were repeated with the following assumptions:

- The QSF18 background noise levels are reduced in level by 6 dB (background noise waveform amplitudes are scaled by one half) when creating the mock recordings to evaluate the effects of the five variable sources of uncertainty,
- Reciprocity is used to update TEDS sensitivities during traceable calibrations, so the standard deviation assumed for the calibration uncertainty component is reduced to from 0.22 to 0.025 dB (normal distribution), and
- A temperature compensation correction with accuracy of ±10°F is applied to recorded data prior to computing final metric values so the temperature effect on microphone sensitivity is reduced from 0.225 to 0.06 dB (uniform distribution).

The results from these updated analyses are plotted below in several ways while considering the Perceived Level metric. For brevity, similar results for the other seven noise metrics are not included in this report. In Figures 14 and 15, a side-by-side comparison is given comparing the baseline results from Sections V.A and V.B to the updated results using the values listed above. The total uncertainty is shown in Figure 14 and the proportional contributions are shown in Figure 15. The left-hand subplots in both figures show the baseline results that were presented in those prior sections. The right-hand subplots show the results for the updated values listed above. The legends in Figure 15a and c are ordered like the lines appear from top to bottom within those subplots, so the two legends have different line orderings.

There are obvious differences when comparing the two total measurement error estimates shown in Figure 14. Specifically, the behavior of the mean bias (red line) is different at low values of corrected SNR. Additionally, the confidence interval (dashed green lines) is smaller at high values of SNR. The effects of reducing these three sources are evident when comparing the proportional contributions shown in Figure 15. Background noise is still dominant at low values of corrected SNR, but the calibration component and ambient temperature component are not as significant at high SNR (comparing Figure 15a versus c).

Small differences in the error estimates are difficult to discern in the side-by-side comparison shown in Figure 14. Thus, the standard deviation and mean bias curves from Figure 14 are compared as overlays in Figures 16a and 17a to help readers visualize the small differences and details in those curves. Specifically, showing the raw standard deviation values in Figure 16a instead of displaying confidence intervals, like in Figure 14, is helpful since the curves in Figure 16a no longer depend on both the mean bias and standard deviation. This makes visual comparisons of the range of measurement errors for the different analysis cases easier. Importantly, three curves are included in both Figure 16a and 17a:

1) The case with baseline values from the prior sections (solid green line),
2) The case where the ambient noise is attenuated and the microphone sensitivity effects are reduced like found in the bulleted list above (dashed blue line), and
3) An additional case where the ambient noise is attenuated but the baseline microphone calibration and temperature uncertainty effects, 0.22 and 0.225 dB, respectively, are used instead of the reduced values (dotted red line).

The third case is included in those two figures to illustrate the expected effect of a reduction in the background noise component only. Also included in Figures 16a and 17a is a gray shaded region towards the left-hand side of the axes. That gray region indicates corrected SNR bins that contain very few observations of measurement error. Thus, the standard deviation and the mean bias may be poorly estimated in that shaded region. For information purposes, the number of observations in the lowest SNR bins are tabulated in Table 12. For the analysis cases with updated values (Table 12, right-most column), less than 1% of all of the mock recordings fell within each of the first three bins that are identified by the shaded region in Figures 16a and 17a. Finally, the four box plots from Figures 14 and 15 are reproduced together in Figures 16b, 16c, 17b and 17c to help readers distinguish the differences in horizontal locations of the boxplot features when comparing

the baseline cases (Figures 16b and 17b) to attenuated analysis cases (Figures 16c and 17c). A rightward shift is visible in the box plot features for that latter case. The box plots shown in subplots 16b and 16c are identical to 17b and 17c, respectively. They are reproduced in both figures so readers can compare the box plot features to both the standard deviation curves and the mean bias curves of those two figures.

The astute reader may wonder why the tabulated percentage values found in Table 12 appear in conflict with the locations of the box plot features in Figures 16b, 16c, 17b and 17c. For example, the table indicates that 1.1%, or 474 (count), of mock recordings of the baseline analysis case fell within the second bin (Table 12, the "2 to 4 dB" bin). Whereas, the box plot features shown in Figures 16b and 17b indicate that the 1st percentile (rightward pointing green arrow) of the on- and off-design mock recording datasets fell at a much higher SNR value, at about 6.5 and 11.5 dB, respectively, when using the baseline background noise levels. Importantly, the table cites the counts and percentages computed across all 43,200 mock recordings from sets 1, 2, and 3 that were described in the first paragraph of Section III.A. As a reminder, the third, contrived set was not included when creating the box plots. Thus, the box plots show the distributions for only the 14,400-waveform subset of the on-design case (set 1) or the 14,400 waveforms of the off-design case (set 2). The third set was only used to improve the estimates of the measurement error when SNR is low, which inflates the proportion of observations in the lower SNR bins for the error estimate cited in Table 12. See Section III.A for additional discussion of set 3.

Decreasing the uncertainty of both the calibration component and the ambient temperature source almost halves the measurement error when corrected SNR is greater than about 24 dB (Figure 16a, solid green line versus dashed blue line). Most of the observed reduction in combined uncertainty at those high values of corrected SNR (Figure 16a, dashed blue line) is due to the reduction in the calibration uncertainty source. When considering the proportion of X-59 booms expected to lie in this SNR range (Figure 16b and c), it may be advisable to pursue such reductions. For example, more than half of the off-design booms are expected to lie in this high-SNR region when background noise levels are like those of QSF18 (Figure 16b, off-design box plot). Requiring calibration providers to use the reciprocity method should not be burdensome to the NASA research team and the added cost should be small relative to using an acoustical calibrator. Additionally, weather data will be collected during X-59 field tests, so incorporating a temperature correction factor when computing levels posttest should be possible. However, reductions in the combined uncertainty due to the ambient temperature source are relatively small in comparison to the calibration source. Even so, these two uncertainty reduction efforts are recommended by the author for use in X-59 field tests since the temperature source might become significant for metrics like BSEL, DSEL, and ESEL (Appendix 4, specifically Figures 4.4, 4.6, and 4.7) once the calibration uncertainty is reduced as compared to the baseline case shown in that appendix.

Inspecting the standard deviation for the three cases (Figure 16a), the scaling applied to the background noise in the updated analyses did not change the relationship of standard deviation with respect to corrected SNR in the range from about +6 to +22 dB corrected SNR (e.g., comparing the solid green line to the other two lines). This

observation is despite the background noise component being the dominant source of measurement error variability in that SNR range (Figure 15, dashed black line). However, there is a minor change in the mean bias between about +6 and +22 dB corrected SNR (Figure 17a, solid green versus dotted red lines). Differences in the bias of about 0.5 dB or less are observed within bins in that SNR range. However, differences in bias on the order of a few tenths of a dB are relatively small so may not be critically important to account for during X-59 tests. The primary effect of decreasing the background noise level in the updated dataset is to shift the distributions of corrected SNR observed across the mock recordings (e.g., Figure 16b versus 16c and Figure 17b versus 17c). Specifically, the box plot features shift rightward by about 4 to 6 dB, which is similar in magnitude to the scalar applied to the background noise waveforms in the updated analyses. For example, the 5th percentile of corrected SNR for on-design booms shifts from about +9 to +13 dB, while the median corrected SNR shifts from about +17 to +23 dB (Figure 16b versus 16c, upper box plot in each subplot). Shifts of similar magnitude are observed when comparing the off-design distributions (Figure 16b versus 16c, lower box plot in each subplot).

The uncertainty estimates presented here were created using mock acoustic recordings that were assembled using snippets of background noise measured during the QSF18 field test. Since the background noise levels observed during the QSF18 test may not be representative of future X-59 deployments, an effort should be made during X-59 field tests to measure the background noise during future deployments and update the uncertainty analysis. All the computational scripts used here to estimate the total uncertainty run relatively quickly. Given properly formatted datasets from future deployments, similar analyses to update the total uncertainty estimates could be completed in an hour or two. The QSF18 background noise dataset contains about 42 hours (total) of recorded data from 12 (count) noise monitors used in that test. So about 3.5 hours of background noise per monitor, where those recordings were spaced out across several days and made at different times during the day. The author recommends similar measurements be made during future test campaigns so the uncertainty can be re-quantified to verify it does not change significantly compared to the results here.

Nonetheless, the uncertainty approximated here should not be significantly different than that of X-59 field tests since scaling the background noise waveforms in the updated analyses did not drastically alter the behavior of the measurement error standard deviation (Figure 16a) or mean bias (Figure 17a). The main effect of changing background noise levels is to shift left or right the distribution of corrected SNR that is observed in the dataset (e.g., Figure 16b versus 16c). Thus, it is believed that the estimates of total uncertainty here are a reasonable approximation of what might be expected during future X-59 field tests.

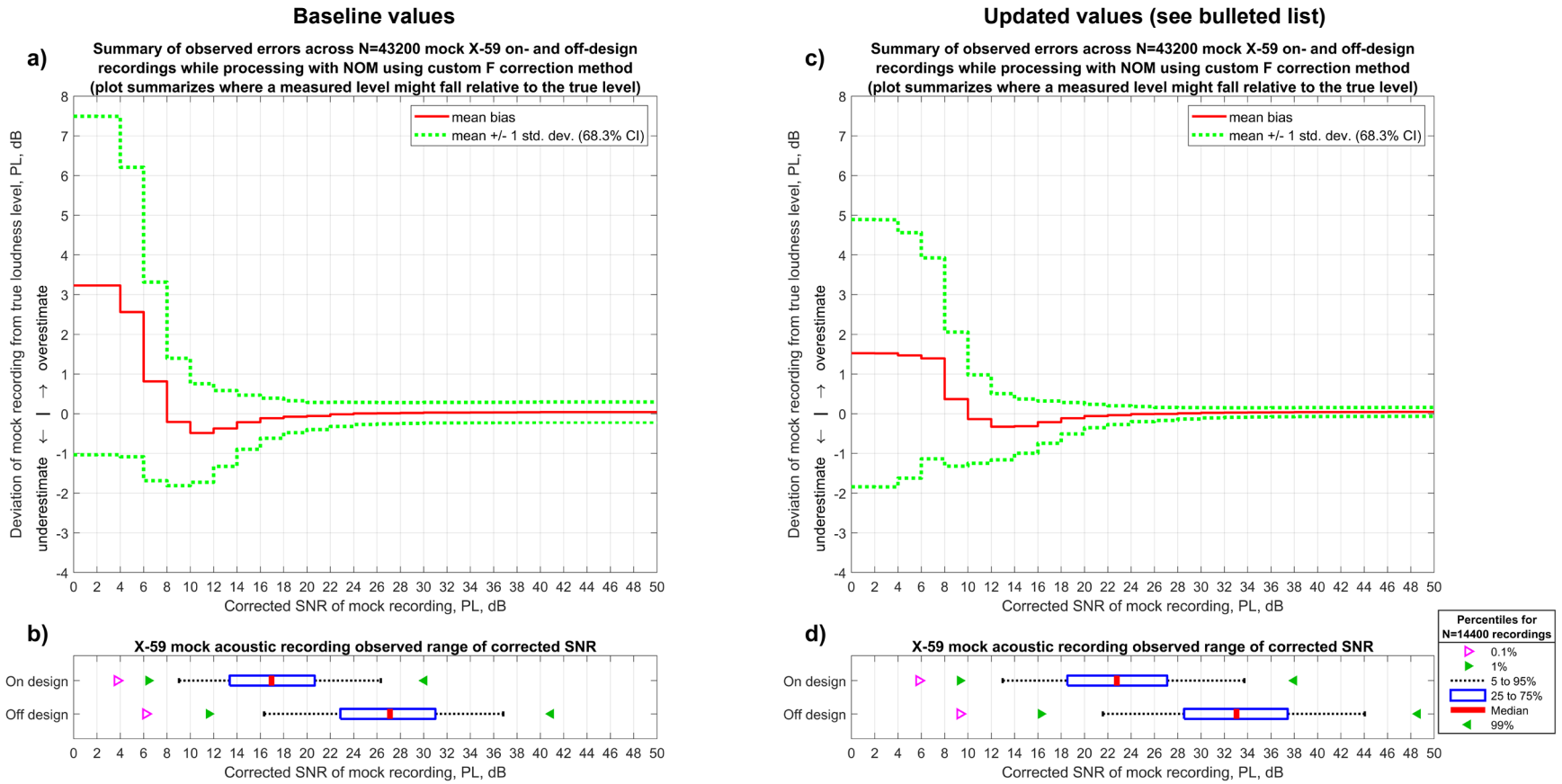


Figure 14: Comparison of baseline measurement error estimate and SNR ranges (left-hand subplots) versus error estimates and SNR ranges while using attenuated background noise levels and smaller microphone-related uncertainties (right-hand subplots).

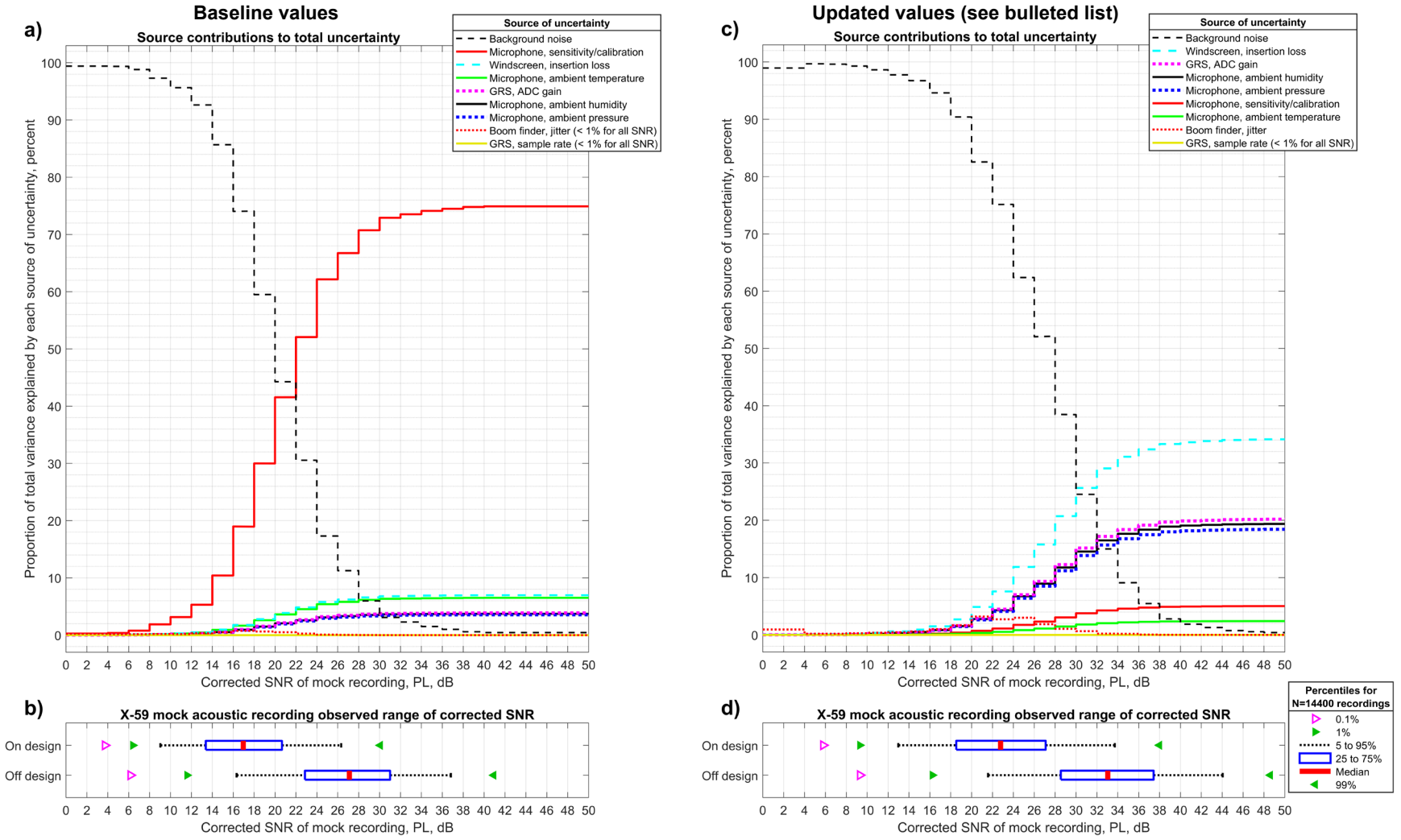


Figure 15: Comparison of baseline proportional contributions and SNR ranges (left-hand subplots) versus proportional contributions and SNR ranges while using smaller microphone-related uncertainties and attenuated background noise levels (right-hand subplots).

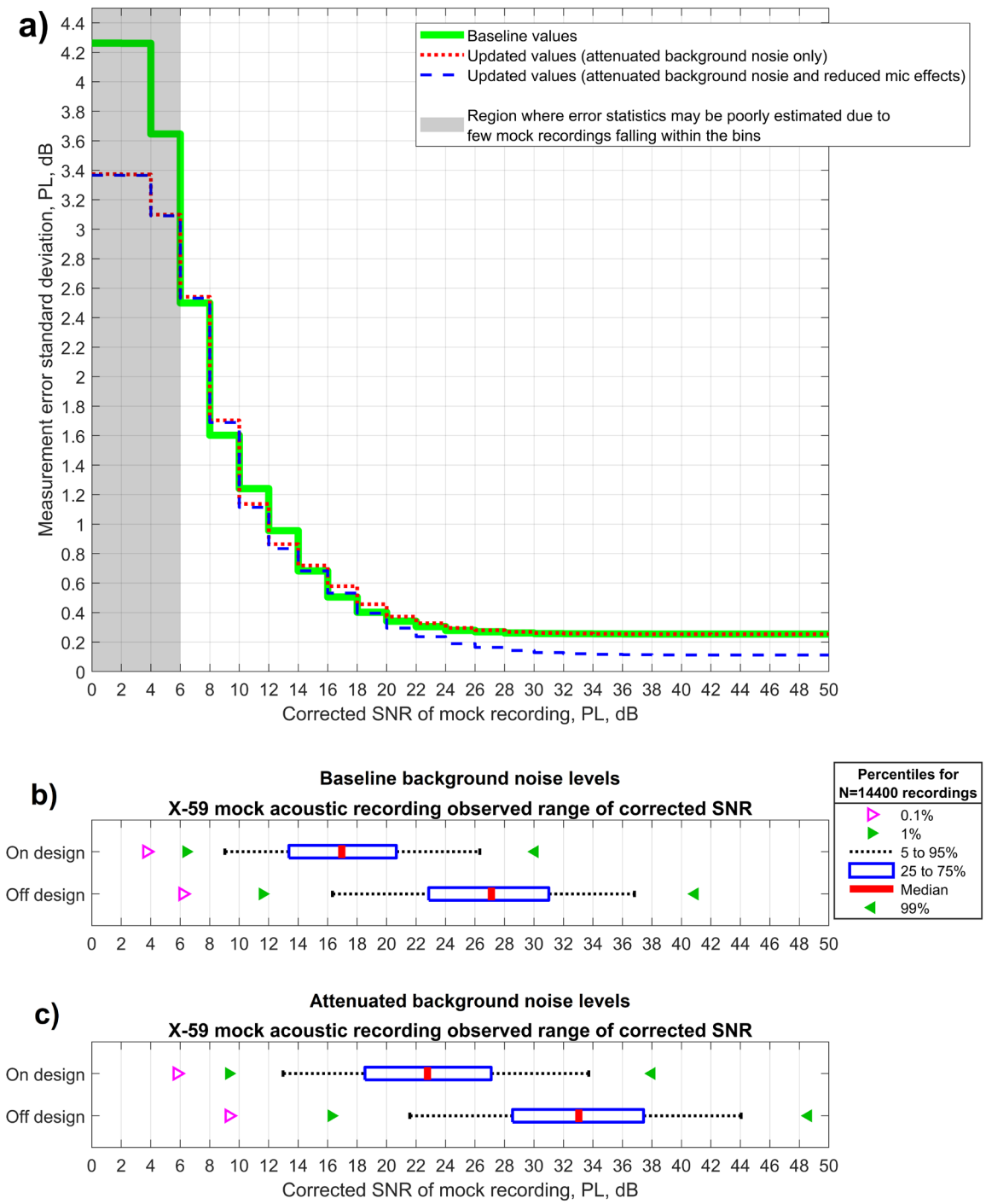


Figure 16: Comparison of the measurement error standard deviations for the baseline values versus using updated values; a) measurement error for three different cases, b) range of corrected SNR with baseline background noise levels, and c) range of corrected SNR with attenuated background noise levels.

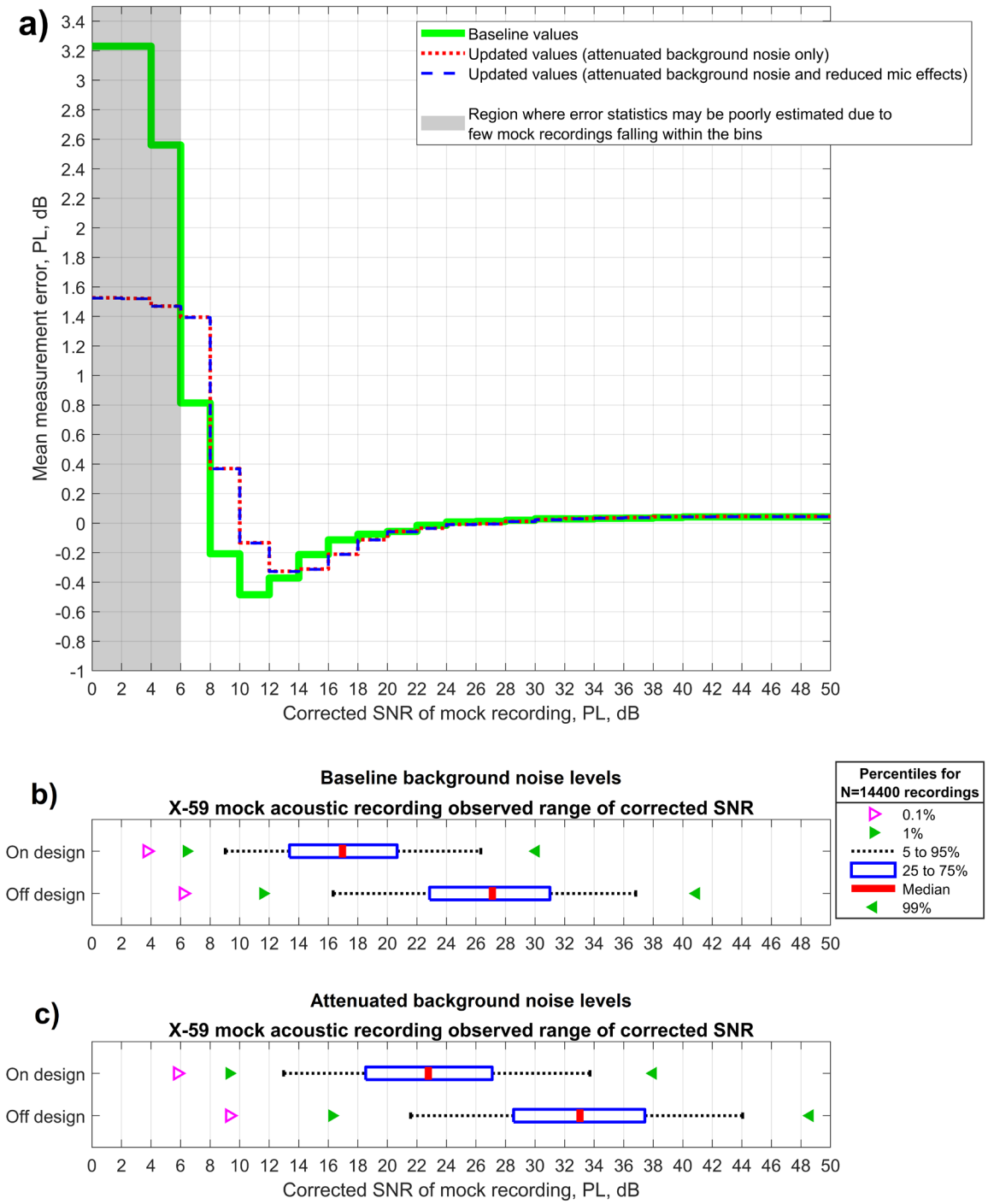


Figure 17: Comparison of the measurement error mean bias for the baseline values versus using updated values; a) measurement error for three different cases, b) range of corrected SNR with baseline background noise levels, and c) range of corrected SNR with attenuated background noise levels.

Table 12: Number and percentage of mock acoustic recordings, of the 43,200 mock recordings analyzed to assess background noise related measurement error, falling within each corrected SNR bin for the PL metric.

Bin	Corrected SNR, PL	Baseline case		With attenuated BG noise	
		Counts	**Percentage**	**Counts**	**Percentage**
1	0 to 2 dB[13]	< 50	< 0.12	< 50	< 0.12
2	2 to 4 dB	474	1.1	108	0.3
3	4 to 6 dB	1706	3.9	481	1.1
4	6 to 8 dB	3693	8.5	1211	2.8
5	8 to 10 dB	4408	10.2	2402	5.6
6	10 to 12 dB	4003	9.3	3401	7.9

[13] Because there are less than 50 mock acoustic recordings falling within this bin, the mean bias and standard deviation of this bin are not calculated from the mock data and instead the values for the 2 to 4 dB bin are used for this bin, and all the bins below it. See related discussion about limiting bins in Section III.A.

VI. CONCLUSIONS

A. Caveats and future work

1. GRS analog to digital converter

Mock acoustic recordings discussed in Section III and Ref. [1] were used to estimate the effects of the variable sources of uncertainty here. Importantly, those mock recordings were assembled using background noise waveforms from NASA's QSF18 field test [14]. Background noise consists of two main components: 1) the acoustical ambient noise from the surrounding environment, and 2) the instrumentation noise associated with the data acquisition hardware. Thus, the instrumentation noise component within the mock recording waveforms here is from the instrumentation used in the QSF18 field test. It is not specific to the GRS hardware – the GRS ADC, the PCB microphone, and the windscreen – that will be used during X-59 overflights. The choice to use QSF18 background noise instead of GRS-specific background noise was made since there is not a sufficiently large database of real-world background noise recordings made with the GRS hardware.

Each GRS input channel is dual range, containing both a 24-bit high-range ADC and a 24-bit low-range ADC that quantize and record the input waveform simultaneously. The high-range ADC has an input voltage range of ±10 V and recent tests have shown it to have an electrical noise floor of about 47 dBA with inputs shorted while assuming an input sensitivity of 10.5 mV/Pa – similar to the PCB microphone. The low-range ADC can measure voltages in the ±0.5 V range with an electrical noise floor of about 26 dBA under similar conditions. Thus, the measurement uncertainty may be different for the two ADC types since the instrumentation noise component of the background noise will be different. If uncertainty estimates are updated in the future using GRS-specific background noise recordings, then computing separate uncertainty estimates for the low- and high-range ADCs is advisable.

2. Microphone

Recent tests have found that using a Brüel and Kjær Type 4193 microphone with low frequency adapter, like the ones used in the QSF18 test, tends to produce more instrumentation noise than when using the GRS low-range ADC and PCB 378M12 microphone combination. Most on-design (quiet) X-59 sonic booms will be measured by the GRS low-range ADC without clipping it. Thus, the instrumentation noise component of the background noise may have been slightly overestimated when using the QSF18 background noise for the mock recordings since the QSF18 recordings used the Type 4193 microphone. This may have led to slightly larger uncertainty estimates than if background noise snippets containing GRS-specific instrumentation noise were used. However, the relative importance of instrumentation noise versus acoustical ambient noise to the background noise related uncertainty component is unknown since the two components cannot be separated when creating mock recordings. Thus, the impact on the uncertainty estimates presented earlier is unknown. It is advisable to repeat the uncertainty analyses

presented here when a sufficiently large database of GRS specific background noise is available. That background noise database should include measurements of both the low- and high-range ADC and the PCB microphone. Also, the instrumentation noise component in the QSF18 background noise, which was used as a data source for the mock recordings here, is likely similar in level to the instrumentation noise of the GRS high-range ADC. Thus, the uncertainty estimates here might be a good approximation of the GRS high-range ADC and provide an upper bound for the overall uncertainty of GRS measurements.

The effects of reducing some sources of uncertainty were discussed in Section V.C, where reductions in the background noise level, the microphone calibration uncertainty, and the microphone ambient temperature uncertainty were discussed. The ambient (barometric) pressure effects on the total uncertainty become a significant contributor to the total uncertainty at high SNR values when those three effects are reduced (e.g., see Figure 15c). It may be possible to reduce the uncertainty caused by ambient pressure if a correction to the sound level is made based on the local elevation-related barometric pressure. For example, the range of barometric pressures identified in Section II.D are dominated by the elevation change between the locations cited. If a test site specific, altitude-based barometric pressure compensation were applied to the measured sound levels, the range used to define the uncertainty would be much smaller since it would only need to account for fluctuations in the barometric pressure caused by weather. Implementing an altitude-based barometric pressure correction is recommended for X-59 field tests.

Microphone sensitivities may drift over time. Such effects were not included in the current analyses since the expected magnitude of drift, if any, is unknown. Sensitivity drift should be investigated once a calibration history for the 378M12 microphones is available.

As discussed in Section II.A, it is recommended that the loaded sensitivity be used for 378M12 microphone when converting between voltage units and pressure units, which should result in an unbiased uncertainty for the calibration component – like the 0 dB bias shown in Table 2. If the open-circuit sensitivity is stored in TEDS for the 378M12 microphone, then a correction[6] to convert between open-circuit sensitivity and loaded sensitivity should be applied when converting GRS recordings from voltage to pressure units during X-59 tests.

3. Field test location

The mock recordings used here to estimate background noise effects were measured in Galveston TX during the QSF18 test. These background noise measurements may not be representative of future X-59 field test locations. For example, X-59 phase 2 flights will occur near NASA's Armstrong Flight Research Center (AFRC), where the GRS units will be placed in the desert. It is unknown how the acoustical ambient at that location will compare to that of Galveston TX. Likewise, future X-59 community tests in phase 3 will occur within five select communities around the United States. The acoustical ambient within the chosen communities may differ from that of Galveston TX. Thus, it is advisable to record acoustical ambient during future X-59 field tests so the measurement chain

uncertainty can be updated posttest. If such measurements are made, then a dataset comparable in size to the QSF18 dataset is recommended – which was about 40 hours in total duration, consisting of many individual recordings that were on the order of 2 minutes in duration each, and that were made at different times of day and on different days.

4. Ground impedance

Ground impedance effects were not included in the current uncertainty analysis. Variation caused by different ground impedances is not directly related to the measurement chain, so was deemed outside the scope of the present analyses. While ground impedance will introduce spectral coloration into the measurements and the effects may be important to quantify, the ground impedance that is expected at future measurement sites is currently unknown. For example, it is not known how many GRS units may be placed over soft ground versus hard ground during future tests. This is particularly true for the phase 3 community tests. Ground impedance effects during phase 2 may be less important/significant than in phase 3 since the GRS units will be placed over relatively hard ground in desert areas near AFRC. Quantifying effects of ground impedance is left to future work.

5. Turbulence

Variation due to turbulence is not included here since those propagation effects are not related to the measurement chain so were deemed outside the scope of the current analyses. If turbulence effects on metric level are needed for future comparisons to prediction, then those effects should be modeled separately and included as an additional source of uncertainty.

B. Summary

The uncertainty expected in empirically determined X-59 sonic boom loudness levels was quantified. The measurement error was estimated for ten individual sources of uncertainty (Sections II and III) and the total measurement error was found when combining nine of those sources (Sections IV and V.A). One of the ten sources of uncertainty, the numeric precision used to compute metric values, was excluded from the analyses since the effect of it is very small. The proportional contribution of each source was also quantified so significant sources of uncertainty could be identified (Section V.B). The background noise component, the microphone calibration component, the ambient temperature effects on microphone sensitivity, and the windscreen effects were the four most significant sources of measurement error. Background noise is the dominant source at low SNR values while the other four are dominant when SNR is high.

Methods to reduce three of these sources were discussed in Section V.C, where new values for them were identified and the total measurement error was re-evaluated while assuming the reduced uncertainty values. Reduced uncertainty for the windscreen source was not considered since the windscreen design used by the GRS noise monitors cannot be changed. The effect of reduced background noise manifests primarily as a shift in the

distribution of corrected SNR for the set of recordings. The effect of reduced background noise levels on the behavior of the standard deviation and mean bias at fixed values of corrected SNR is small. Thus, use of the QSF18 background noise dataset likely gives reasonable approximations of the expected measurement error standard deviation and bias for future X-59 tests. The microphone calibration uncertainty can be reduced relative to the baseline analysis case simply by choosing a more accurate method when performing traceable calibrations. Specifically, use of the reciprocity method is recommended. Also, ambient temperature effects can be reduced if the temperature at the time of measurement is estimated and then a correction applied posttest to the measured sound levels. The benefit of reducing the calibration source and ambient temperature source of uncertainty is roughly a halving of the total uncertainty when SNR is high. While reducing these two components of uncertainty using the methods discussed is recommended, the costs of reducing these two components is still unknown and needs to be evaluated before implementing either reduction method.

Overall, the uncertainty estimates provided here are expected to be conservative. Refining these estimates is recommended once more information is known about the details of future X-59 field tests.

Acknowledgements

The author would like to thank Jesse Blaine at Brigham Young University for providing the insertion loss measurements of the COUGAR Gold windscreen, which were used to estimate the measurement error due to the windscreen. The author would also like to thank Will Doebler for the data that helped give insight to the elevation angles expected during X-59 overflights.

References

[1] J. Klos, "An Adaptation of ISO 11204 using Customized Correction Grades to Mitigate Ambient Noise Effects when Computing Sonic Boom Loudness Levels," NASA/TM–20220010779, Hampton, VA, 2022, https://ntrs.nasa.gov/citations/20220010779.

[2] L. J. Cliatt, "Preparations for Quesst Acoustic Validation," in *2023 AIAA SciTech Forum (presentation only)*, National Harbor, MD, 2023, https://ntrs.nasa.gov/citations/20220018155.

[3] J. Rathsam, P. Coen, A. Loubeau, L. Ozoroski and G. Shah, "Scope and goals of NASA's Quesst Community Test Campaign with the X-59 aircraft," in *14th ICBEN Congress on Noise as a Public Health Problem*, Belgrade, Serbia, June 2023, https://ntrs.nasa.gov/citations/20230004142.

[4] N. B. Cruze, "Overview of Community Response Testing Campaign with NASA's X-59 Aircraft," in *UC Davis Aircraft Noise and Emissions Symposium*, Davis, CA, May 2023, https://ntrs.nasa.gov/citations/20230006133.

[5] G. Shah, J. Rathsam and A. Loubeau, "Preparations for Quesst Mission Community Response Testing – Overview and Status," in *2023 AIAA SciTech Forum (presentation only)*, National Harbor, MD, 2023, https://ntrs.nasa.gov/citations/20220018319.

[6] S. V. Lympany and J. A. Page, "Estimating Sonic Boom Metrics Across a Community Using a Kalman Filter," in *183rd Meeting of the Acoustical Society of America*, Nashville, TN, December 2022, https://ntrs.nasa.gov/citations/20220017380.

[7] J. A. Page, J. B. Lonzaga, M. J. Shumway, S. R. Son, R. S. Downs, A. Loubeau and W. J. Doebler, "PCBoom Version 7.3 User's Guide," NASA/TM–20220016207, 2023, https://ntrs.nasa.gov/citations/20220016207.

[8] "Ground Recording System product page," Crystal Instruments, [Online]. Available: https://www.crystalinstruments.com/ground-recorder-system. [Accessed October 2024].

[9] J. D. Blaine, M. Anderson and K. L. Gee, "Development of a Weather Robust Microphone Configuration for Sonic Boom Measurements," in *186th Meeting of the Acoustical Society of America*, Ottawa, CA, May 2024, https://ntrs.nasa.gov/citations/20240005418.

[10] "Type 4231 acoustical calibrator product page," Brüel and Kjær, [Online]. Available: https://www.hbkworld.com/en/products/transducers/acoustic/acoustic-calibrators/microphone/4231. [Accessed October 2024].

[11] "Broomfield, CO Weather History," TWC Product and Technology LLC, [Online]. Available: https://www.wunderground.com/history/monthly/us/co/broomfield/KBJC/date/2024-10. [Accessed November 2024].

[12] "Newport News, VA Weather History," TWC Product and Technology LLC , [Online]. Available: https://www.wunderground.com/history/monthly/us/va/newport-news/KPHF/date/2024-10. [Accessed November 2024].

[13] K. A. Bradley, C. M. Hobbs, C. B. Wilmer, V. W. Sparrow, T. A. Stout, J. M. Morgenstern, K. H. Underwood, D. J. Maglieri, R. A. Cowart, M. T. Collmar, H. Shen and P. Blanc-Benon, "Sonic Booms in Atmospheric Turbulence (SonicBAT): The Influence of Turbulence on Shaped Sonic Booms," NASA CR–2020–220509, 2020, https://ntrs.nasa.gov/citations/20200002482.

[14] J. A. Page, K. K. Hodgdon, R. P. Hunte, D. E. Davis, T. A. Gaugler, R. Downs, R. A. Cowart, D. J. Maglieri, C. Hobbs, G. Baker, M. Collmar, K. A. Bradley, B. Sonak, D. Crom and C. Cutler, "Quiet Supersonic Flights 2018 (QSF18) Test: Galveston, Texas Risk Reduction for Future CommunityTesting with a Low-Boom Flight Demonstration Vehicle," NASA CR-2020-220589, Volume I, 2020, https://ntrs.nasa.gov/citations/20200003223.

[15] S. S. Stevens, "Perceived Level of Noise by Mark VII and Decibels," *J. Acoust. Soc. Am.,* vol. 51, no. 2B, pp. 575-601, 1972.

[16] G. M. J. a. H. G. Leventhall, "Calculation of the perceived level of noise (Pldb) using Stevens' method (Mark VII)," *Applied Acoustics,* vol. 6, no. 1, pp. 23-34, 1973.

[17] K. P. Shepherd and B. M. Sullivan, "A loudness calculation procedure applied to shaped sonic booms," NASA, Technical Report, TP-3134, 1993, https://ntrs.nasa.gov/citations/19920002547.

[18] A. Loubeau, Y. Naka, B. G. Cook, V. W. Sparrow and J. M. Morgenstern, "A new evaluation of noise metrics for sonic booms using existing data," *AIP Conference Proceedings,* vol. 1685, no. 1, 2015, https://doi.org/10.1063/1.4934481.

[19] *ANSI/ASA S1.42-2020, Design Response of Weighting Networks for Acoustical Measurements,* 2020.

[20] *ISO TR 25417, Acoustics - Definitions of Basic Quantities and Terms - First Edition (specifically section 2.6),* 2007.

[21] W. J. Doebler, S. R. Wilson, A. Loubeau and V. W. Sparrow, "Simulation and Regression Modeling of NASA's X-59 Low-Boom Carpets Across America," *Journal of Aircraft,* vol. 60, no. 2, March 2023, https://doi.org/10.2514/1.C036876.

[22] W. J. Doebler and A. Loubeau, "Estimating the noise dose range of the NASA X-59 aircraft in supersonic cruise using PCBoom propagation simulations," *JASA Express Letters,* vol. 3, no. 5, May 2023, https://doi.org/10.1121/10.0019501.

[23] J. Blaine, "Design and testing of an improved weather-resistant windscreen system for microphones (tentative title)," Brigham Young University, Provo, UT, senior thesis, pending publication (est. spring 2025, advisor: Kent Gee).

[24] M. C. Anderson, K. L. Gee, D. J. Novakovich, L. T. Mathews and Z. T. Jones, "Comparing two weather-robust microphone configurations for outdoor measurements," in *Proc. Mtgs. Acoust. 42, 040005, https://doi.org/10.1121/2.0001561*, 2020.

[25] B. M. Harker, S. V. Lympany and J. A. Page, "Performance Evaluation of a Shaped Sonic Boom Detector and Classifier," in *183rd Meeting of the Acoustical Society of America*, Nashville, TN, December 2022, https://ntrs.nasa.gov/citations/20220017378.

Appendix 1: Calculation of corrected SNR with representative data plots

The methods used here to compute the loudness level of a sonic boom while correcting for background noise contamination are documented in Ref. [1]. However, the method to compute corrected SNR, which was introduced in Section III.A above, is not documented within that reference or elsewhere. This appendix provides such documentation for the case when a spectral correction is requested when using NOM[9].

As discussed in Ref. [1], the band levels of the uncorrected sonic boom spectrum are compared to the band levels of the uncorrected preboom background noise spectrum to compute the corrected spectral levels, prior to computing loudness levels. Specifically, the corrected sonic boom spectral sound pressure levels, $L_{B,i,corrected}$, in which i represents the i^{th} one-third-octave band, are computed using the algorithm

$$L_{B,i,corrected} = \begin{cases} L_{B,i} & \text{if } \Delta L_i > 15 \\ 10log_{10}\left(10^{L_{B,i}/10} - 10^{L_A,i/10}\right) & \text{if } X < \Delta L_i \leq 15 \\ L_{B,i} - Y & \text{if } \Delta L_i \leq X \end{cases} \quad (1)$$

where $L_{B,i}$ is the uncorrected sound pressure level of the boom spectrum, $L_{A,i}$ is the level of the preboom background noise, $\Delta L_i = L_{B,i} - L_{A,i}$, and X and Y are the correction-method-specific constants. The quantities L_*, ΔL, X, and Y are in units of decibels. The constants X and Y are set based on the chosen correction method, where choices available in NOM are documented in Table 1 of Ref. [1].

For a spectral correction, like "Custom F" used here, that algorithm in Eq. (1) is applied separately to each i^{th} one-third-octave band. The magnitude of the spectral correction, C_i in decibels, is

$$C_i = L_{B,i} - L_{B,i,corrected} \quad (2)$$

where a unique C_i value is computed for each i^{th} one-third-octave band, and all $C_i \geq 0$ since all $L_{B,i}$ are always greater than $L_{B,i,corrected}$. To compute the "corrected" preboom background noise spectrum – a spectrum that accounts for the effects of the correction values applied to the sonic boom spectrum – the C_i values found above are subtracted from the background noise spectral sound pressure levels

$$L_{A,i,corrected} = L_{A,i} - C_i \quad (3)$$

where $L_{A,i,corrected}$ represents the corrected preboom ambient spectral levels of the i^{th} one-third-octave bands. Thus, the corrected spectrum of the background noise, $L_{A,i,corrected}$, is attenuated relative to the uncorrected spectrum, $L_{A,i}$, by the same C_i values as the boom spectra, $L_{B,i,corrected}$ compared to $L_{B,i}$.

To review, when computing the uncorrected SNR using as-measured $L_{B,i}$ and $L_{A,i}$ values, the signal-plus-noise-to-noise ratio is being estimated since the $L_{B,i}$ values include

both a signal and noise component. Additionally, the $L_{A,i}$ values only approximate the noise component of $L_{B,i}$ since $L_{B,i}$ and $L_{A,i}$ are separated in time (e.g., see Ref [1]). The $L_{B,i,corrected}$ values estimate the component of $L_{B,i}$ that is associated with the signal only by attenuating $L_{B,i}$ using Eq. (1), which approximates the contribution of the noise component and corrects for it. The levels of $L_{B,i,corrected}$ are always less than $L_{B,i}$ since energy is only removed from, never added to, $L_{B,i}$ when using Eq. (1). Consequently, we cannot compare $L_{B,i,corrected}$ directly to $L_{A,i}$ to estimate a signal-to-noise ratio of the corrected spectrum since that would imply a lower signal-to-noise ratio than if $L_{B,i}$ were directly compared to $L_{A,i}$, which would be nonsensical since the purpose of the correction in Eq. (1) is to mitigate the effects of noise. Thus, Eq. (3) is used to attenuate $L_{A,i}$ by the same magnitudes, C_i, that $L_{B,i}$ was attenuated so an updated estimate of the noise spectrum, $L_{A,i,corrected}$, and the loudness levels computed from it can be compared to $L_{B,i,corrected}$ and the associated sonic boom loudness levels when computing the corrected SNR.

Thus, the corrected loudness levels of the preboom background noise are computed from the corrected spectral levels, $L_{A,i,corrected}$, using standard signal processing methods. Additionally, the corrected loudness levels of the sonic boom are computed from the corrected spectral levels, $L_{B,i,corrected}$, using standard methods. Finally, the corrected SNR of a loudness level is found from the difference between the corrected loudness level of the sonic boom minus the corrected loudness level of the preboom background noise. No equations are given for these last computational steps since they are somewhat trivial and well documented elsewhere (e.g., see Table 7). Example plots of loudness level versus corrected SNR are found in Figures 1.1 through 1.8 below for the eight noise metric types, where these data were computed using the mock acoustic recording datasets discussed in Section III.A in the main body. Figure 4 from that earlier section (III.A) is identical to Figure 1.1 below. Additionally, the R^2 values found in the "c" subplots in Figures 1.1 through 1.8 below were summarized Table 8 and discussed in Section III.A.

Readers may request a copy of NOM that implements these calculations, see footnote 9. The corrected SNR value is requested as output when using NOM[9] by choosing output fields with names like *SNR_c_[metricname]*, where *[metricname]* identifies one of the computed noise metrics. The numeric arrays that populate the *SNR_c_[metricname]* fields in the NOM results structure are the corrected SNR for the input waveforms given the background noise waveforms and chosen correction method that were also passed to the software. For example, the values in field *SNR_c_dbpl* are plotted along the abscissa in Figure 2 in Section III.A while using the "Custom F" correction method applied to the spectrum to compute the loudness level values. Please see the NOM[9] help information for more detail on requesting output fields and using the background noise correction methods. Importantly, the corrected SNR depends on the chosen noise metric since the frequency weighting function will impact the ratio of the signal level to the noise level.

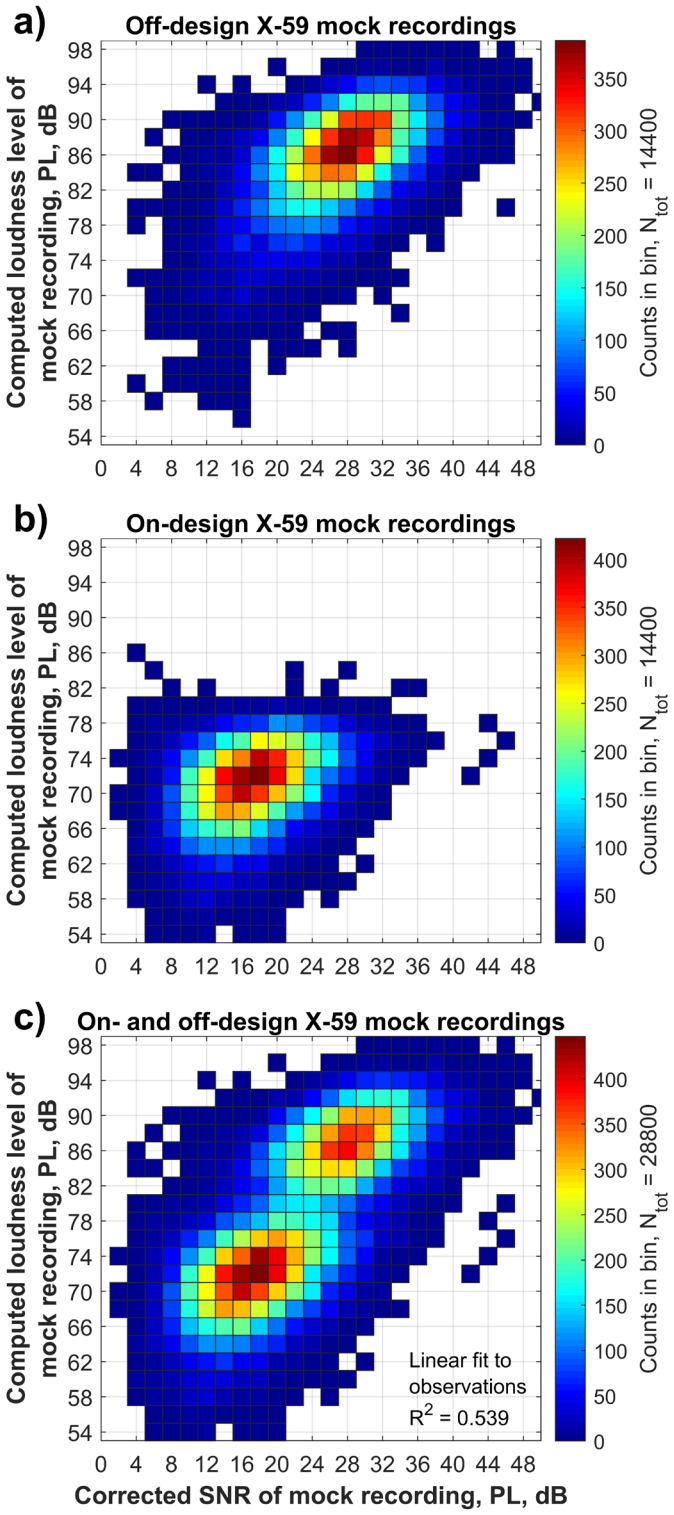


Figure 1.1: Bivariate histograms of Perceived Level versus corrected SNR, where the waveform case is indicated in the subplot title and bin counts are indicated by color as shown in the right-hand-side color bars.

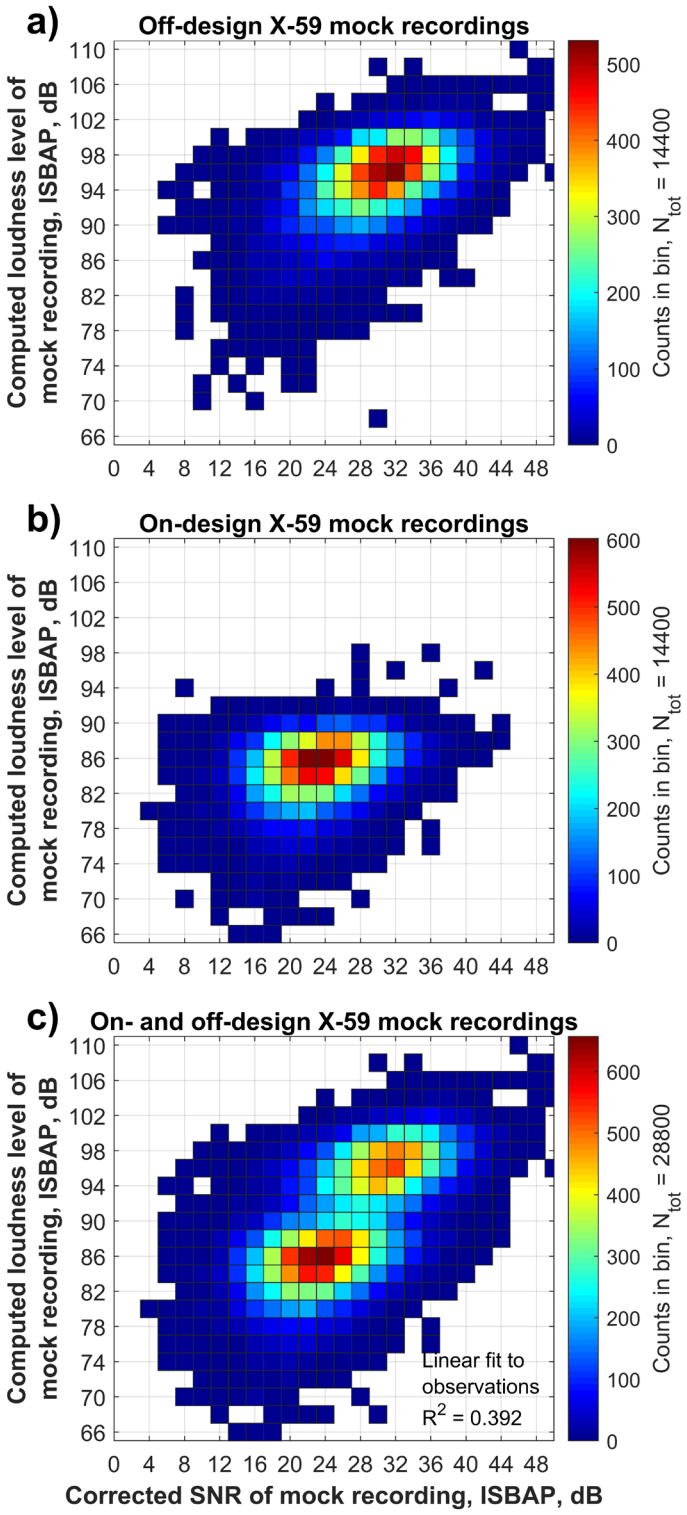


Figure 1.2: Bivariate histograms of ISBAP versus corrected SNR, where the waveform case is indicated in the subplot title and bin counts are indicated by color as shown in the right-hand-side color bars.

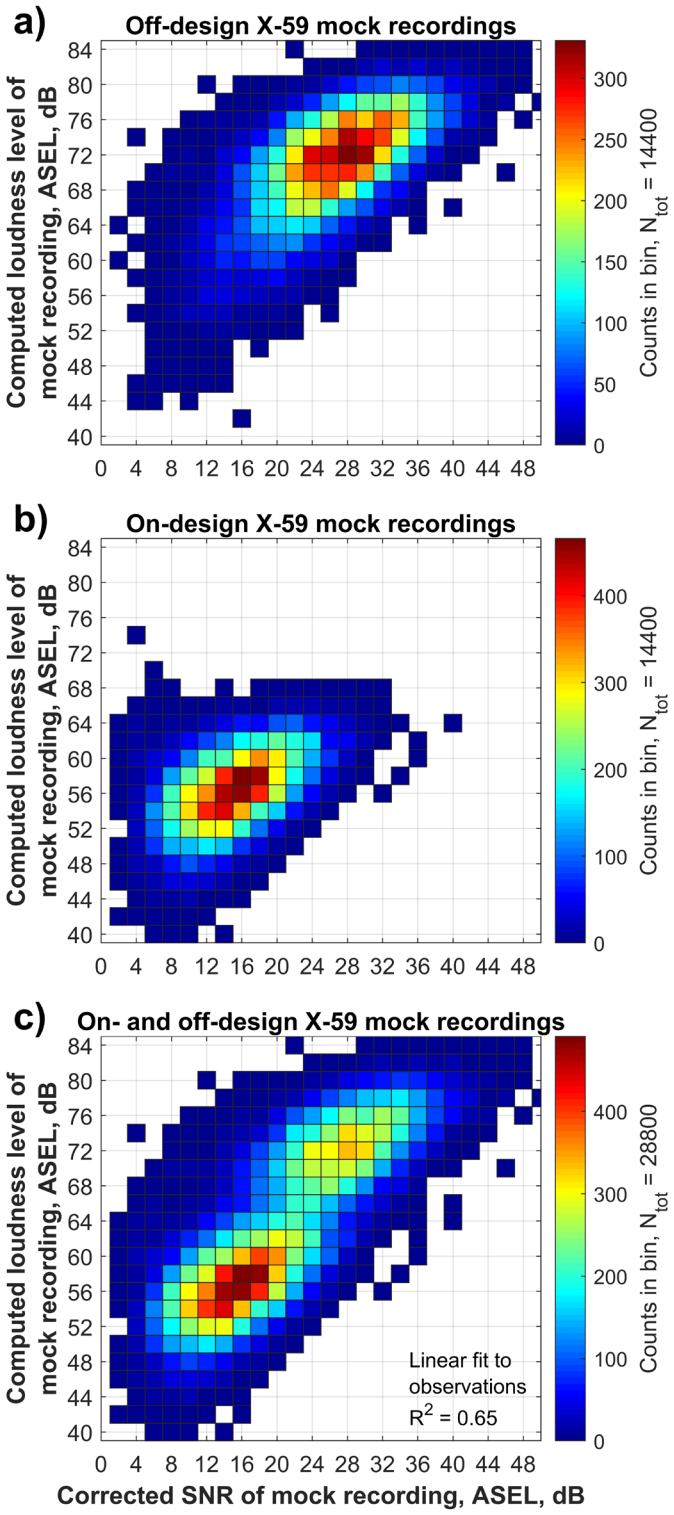


Figure 1.3: Bivariate histograms of ASEL versus corrected SNR, where the waveform case is indicated in the subplot title and bin counts are indicated by color as shown in the right-hand-side color bars.

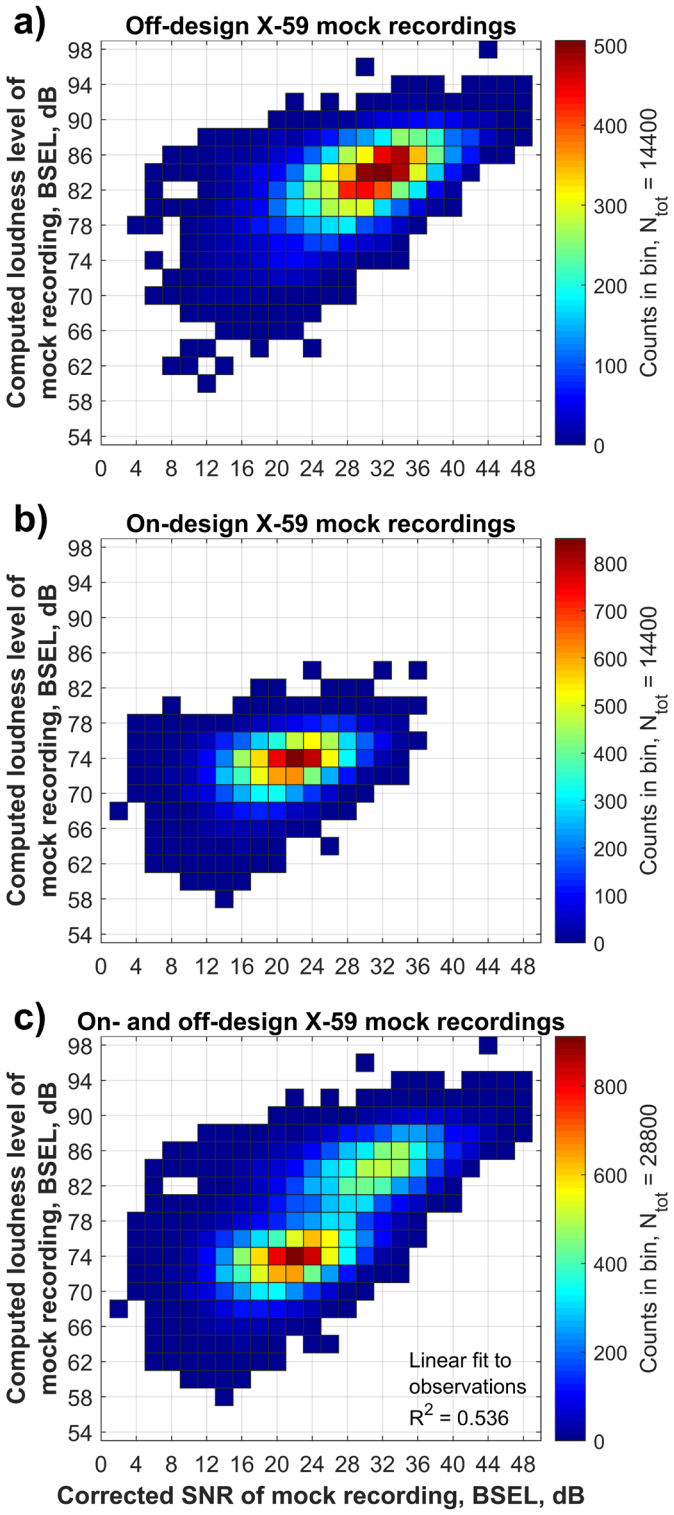


Figure 1.4: Bivariate histograms of BSEL versus corrected SNR, where the waveform case is indicated in the subplot title and bin counts are indicated by color as shown in the right-hand-side color bars.

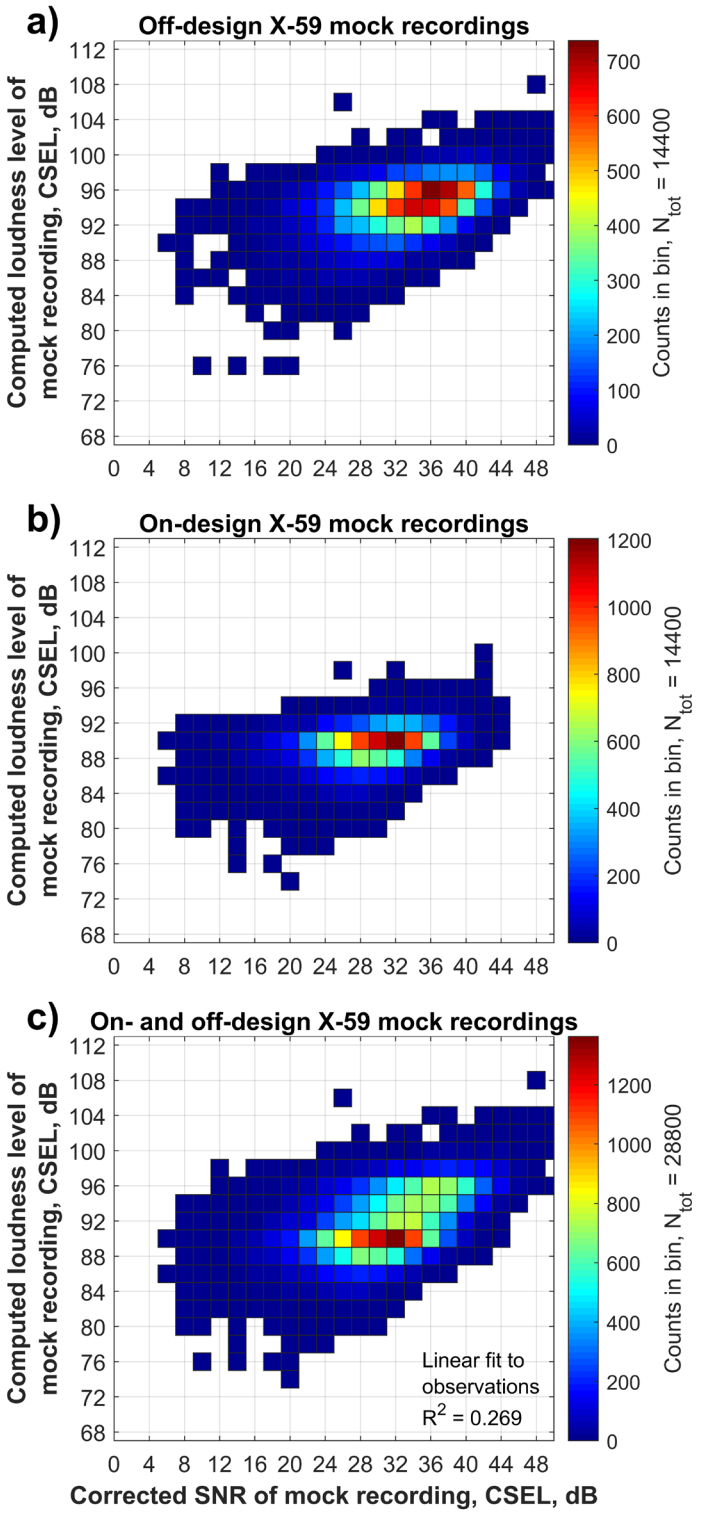


Figure 1.5: Bivariate histograms of CSEL versus corrected SNR, where the waveform case is indicated in the subplot title and bin counts are indicated by color as shown in the right-hand-side color bars.

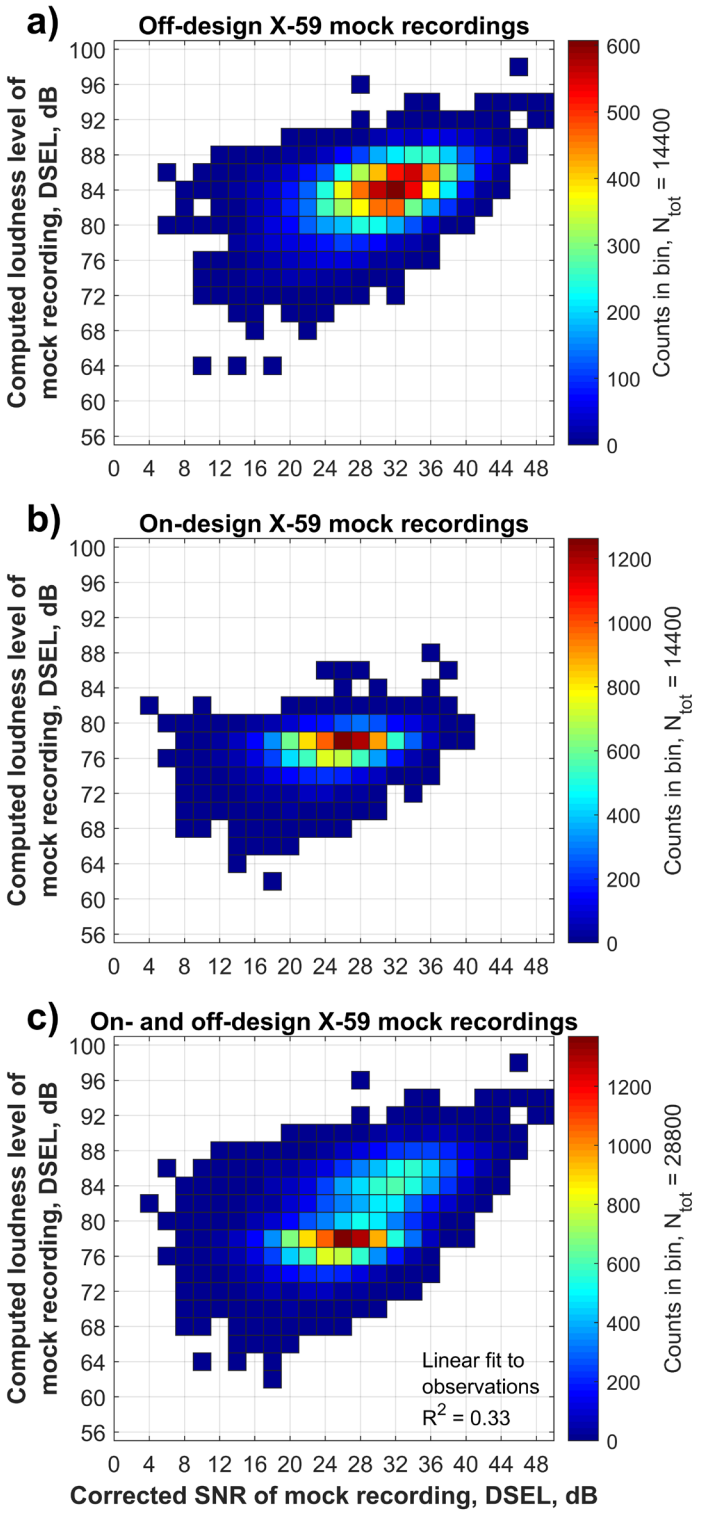


Figure 1.6: Bivariate histograms of DSEL versus corrected SNR, where the waveform case is indicated in the subplot title and bin counts are indicated by color as shown in the right-hand-side color bars.

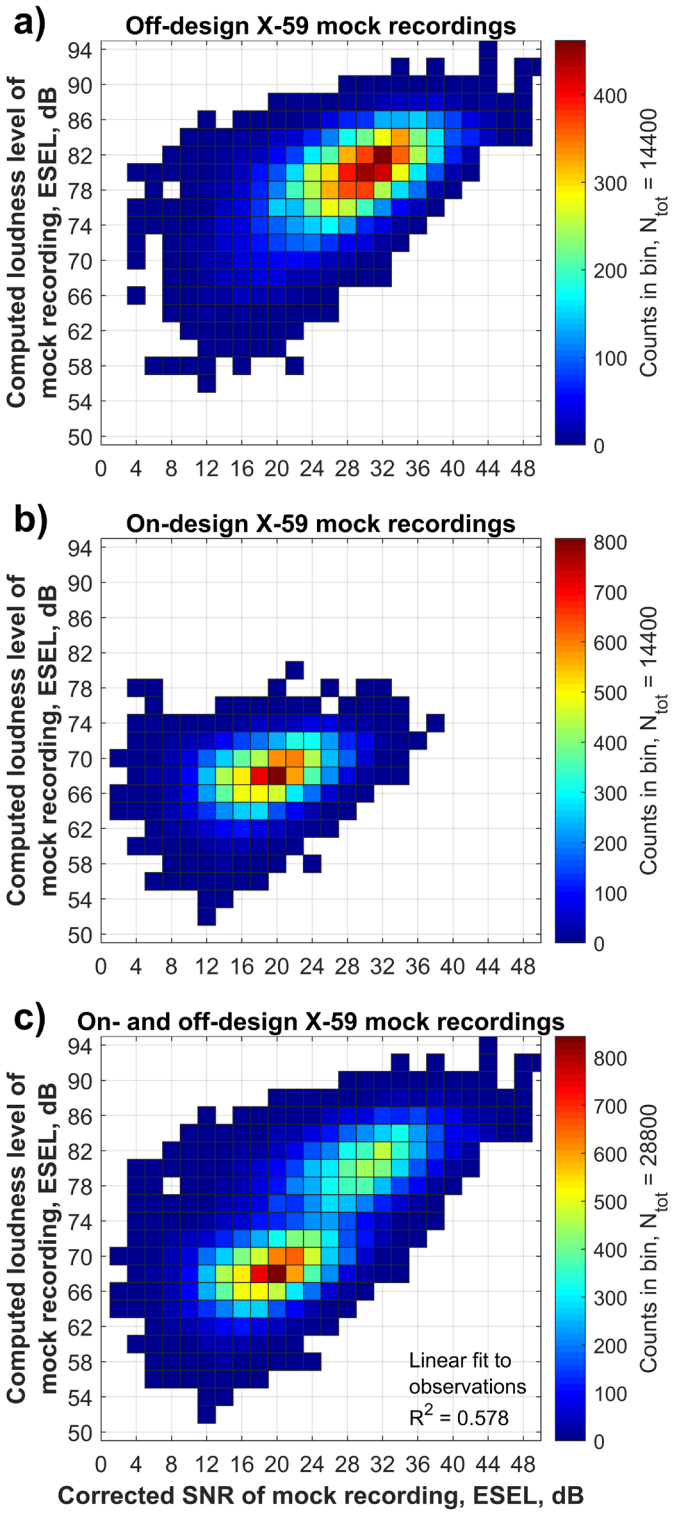


Figure 1.7: Bivariate histograms of ESEL versus corrected SNR, where the waveform case is indicated in the subplot title and bin counts are indicated by color as shown in the right-hand-side color bars.

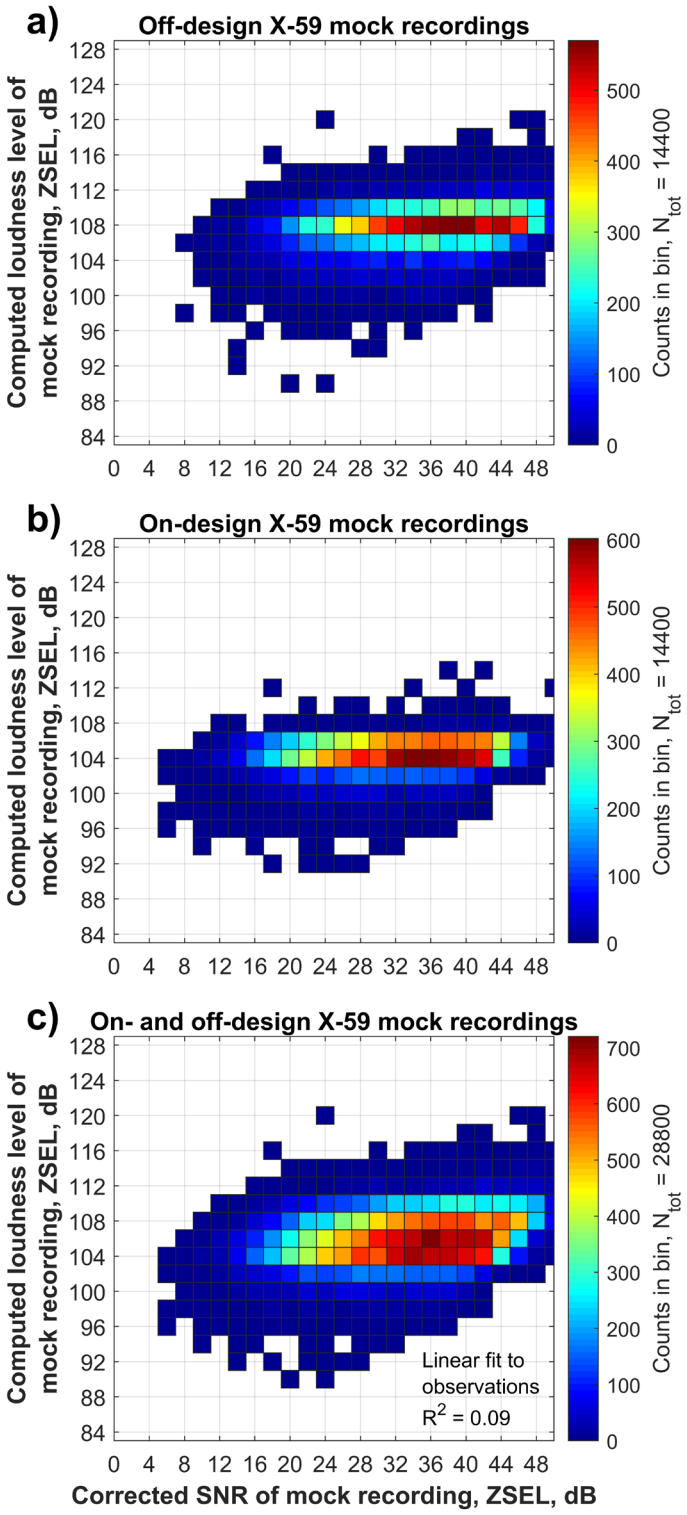


Figure 1.8: Bivariate histograms of ZSEL versus corrected SNR, where the waveform case is indicated in the subplot title and bin counts are indicated by color as shown in the right-hand-side color bars.

Appendix 2: Plots of total measurement error for eight different noise metrics

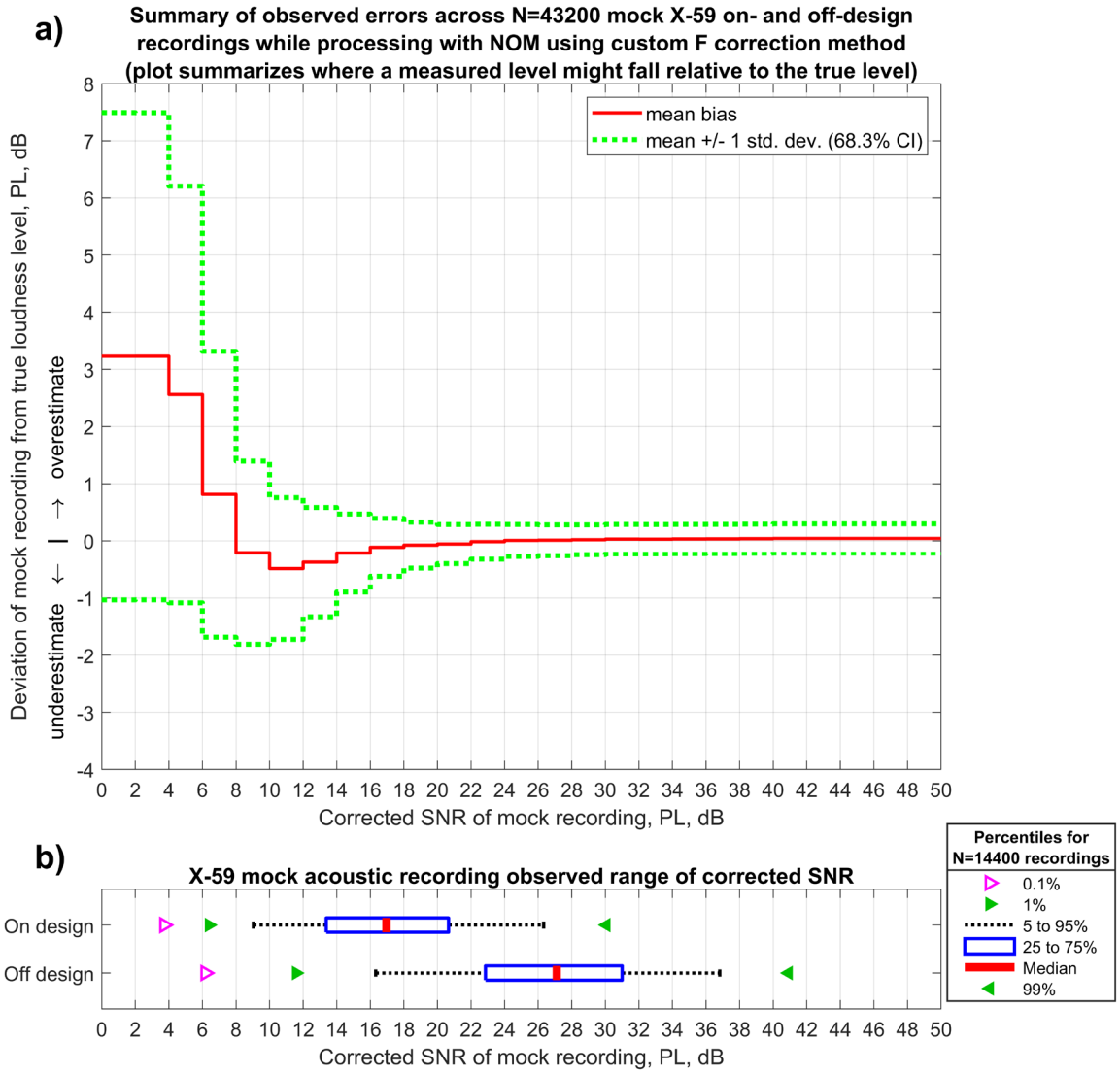


Figure 2.1: Total measurement error for the PL noise metric versus the corrected SNR of PL, a) shows the total measurement error and b) shows the observed distribution of corrected SNR for the on-design and off-design X-59 mock acoustic recordings.

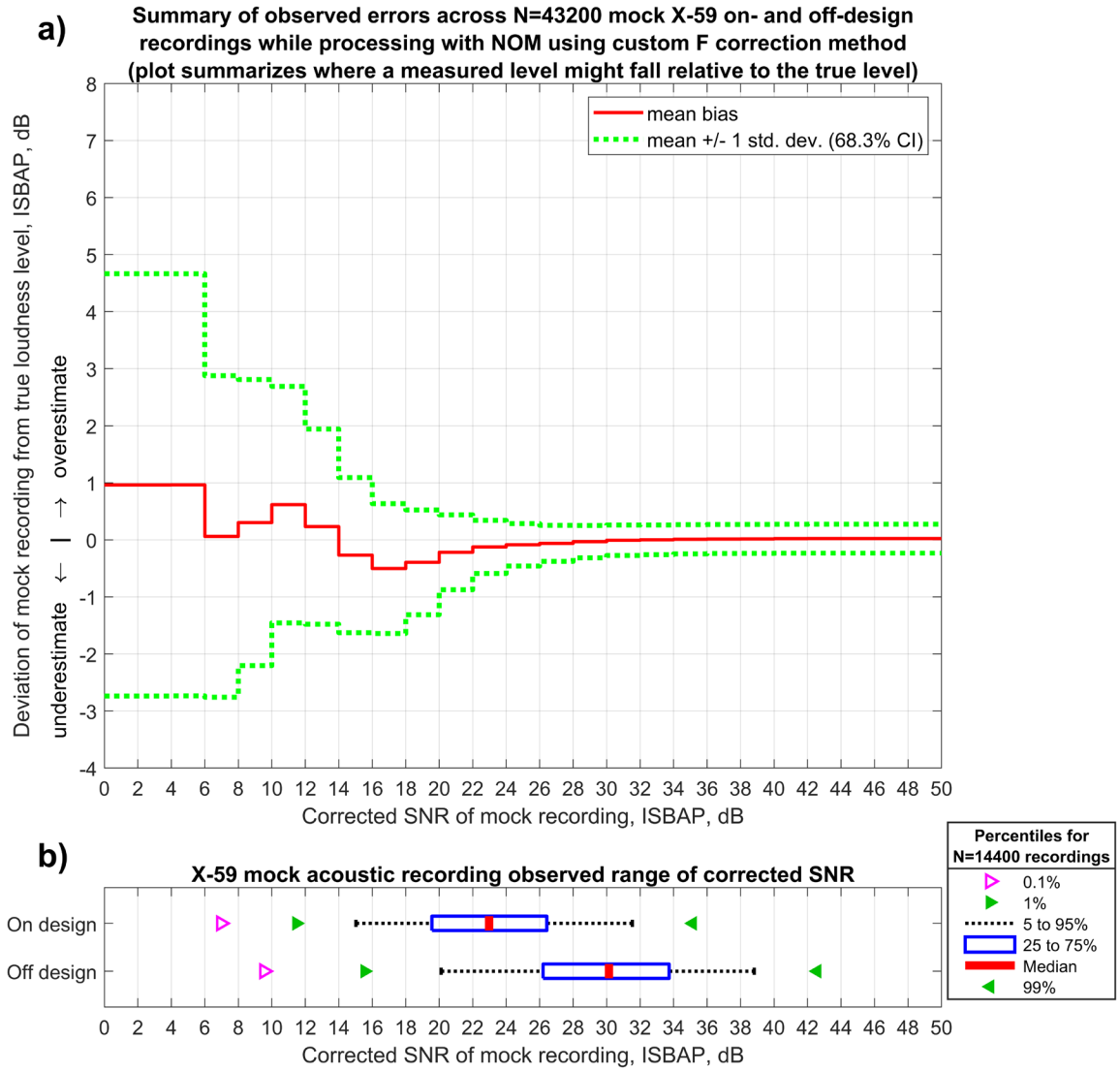


Figure 2.2: Total measurement error for the ISBAP noise metric versus the ISBAP corrected SNR, a) shows the total measurement error and b) shows the observed distribution of corrected SNR for the on-design and off-design X-59 mock acoustic recordings.

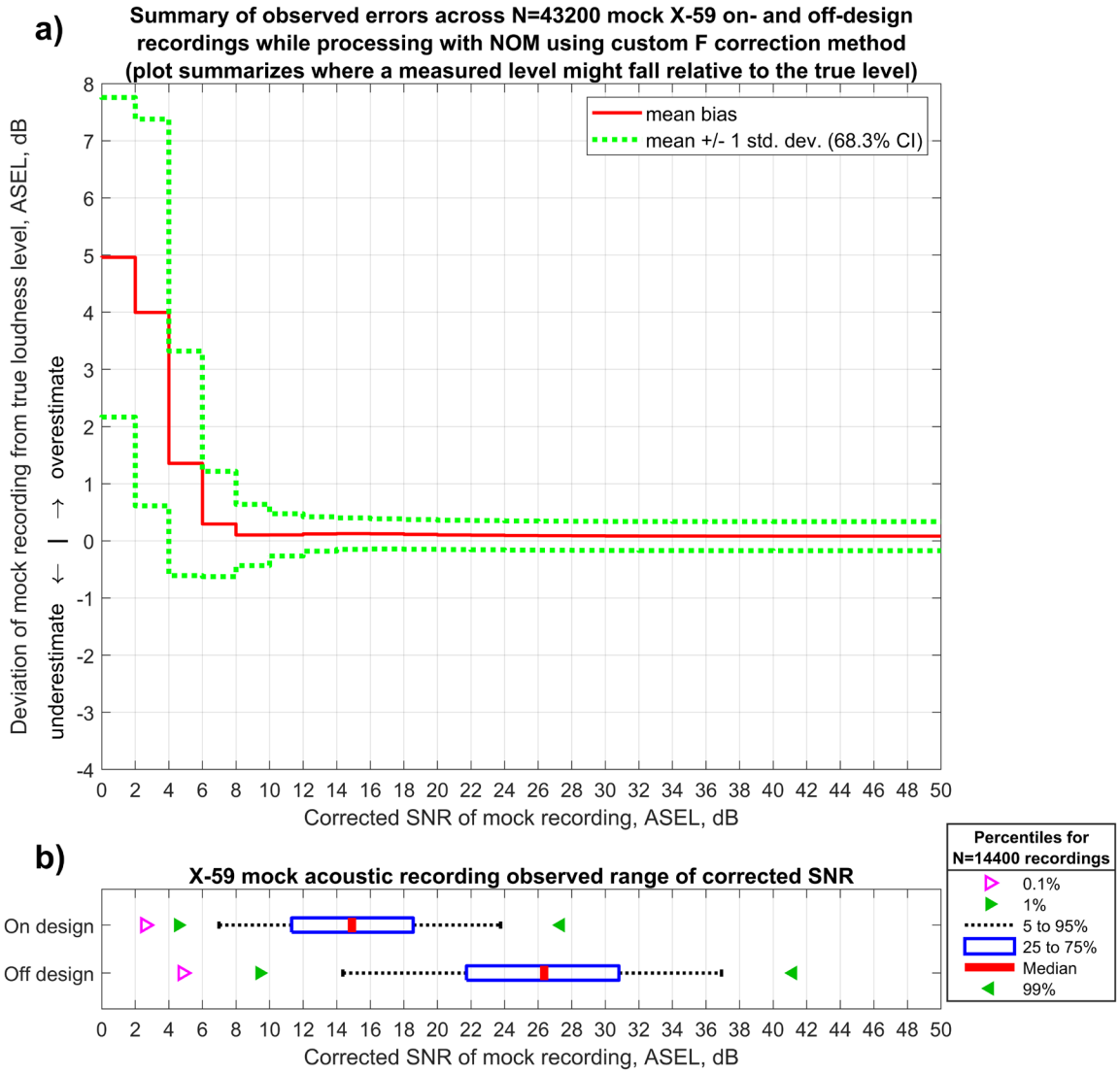


Figure 2.3: Total measurement error for the ASEL noise metric versus the ASEL corrected SNR, a) shows the total measurement error and b) shows the observed distribution of corrected SNR for the on-design and off-design X-59 mock acoustic recordings.

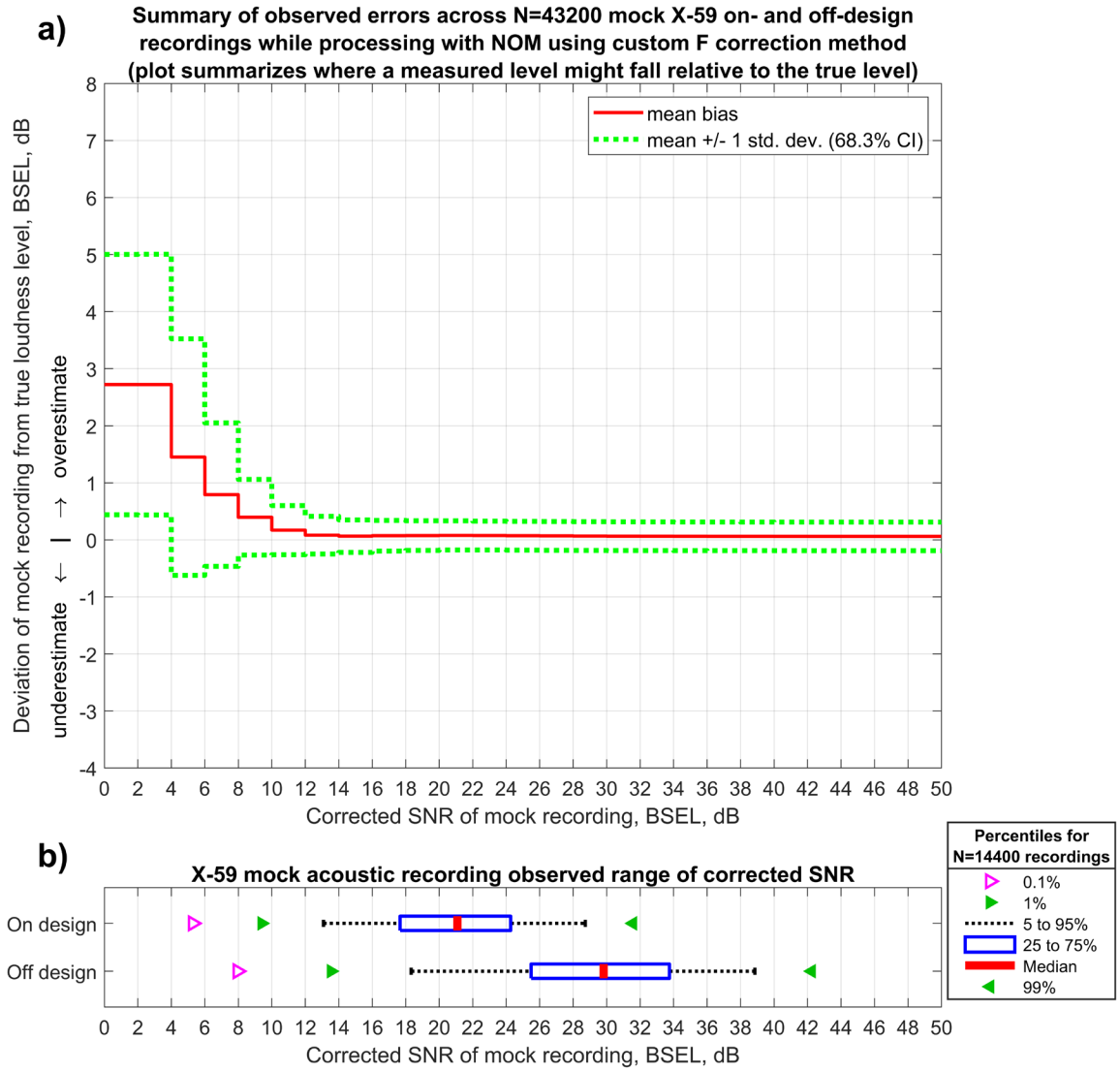


Figure 2.4: Total measurement error for the BSEL noise metric versus the BSEL corrected SNR, a) shows the total measurement error and b) shows the observed distribution of corrected SNR for the on-design and off-design X-59 mock acoustic recordings.

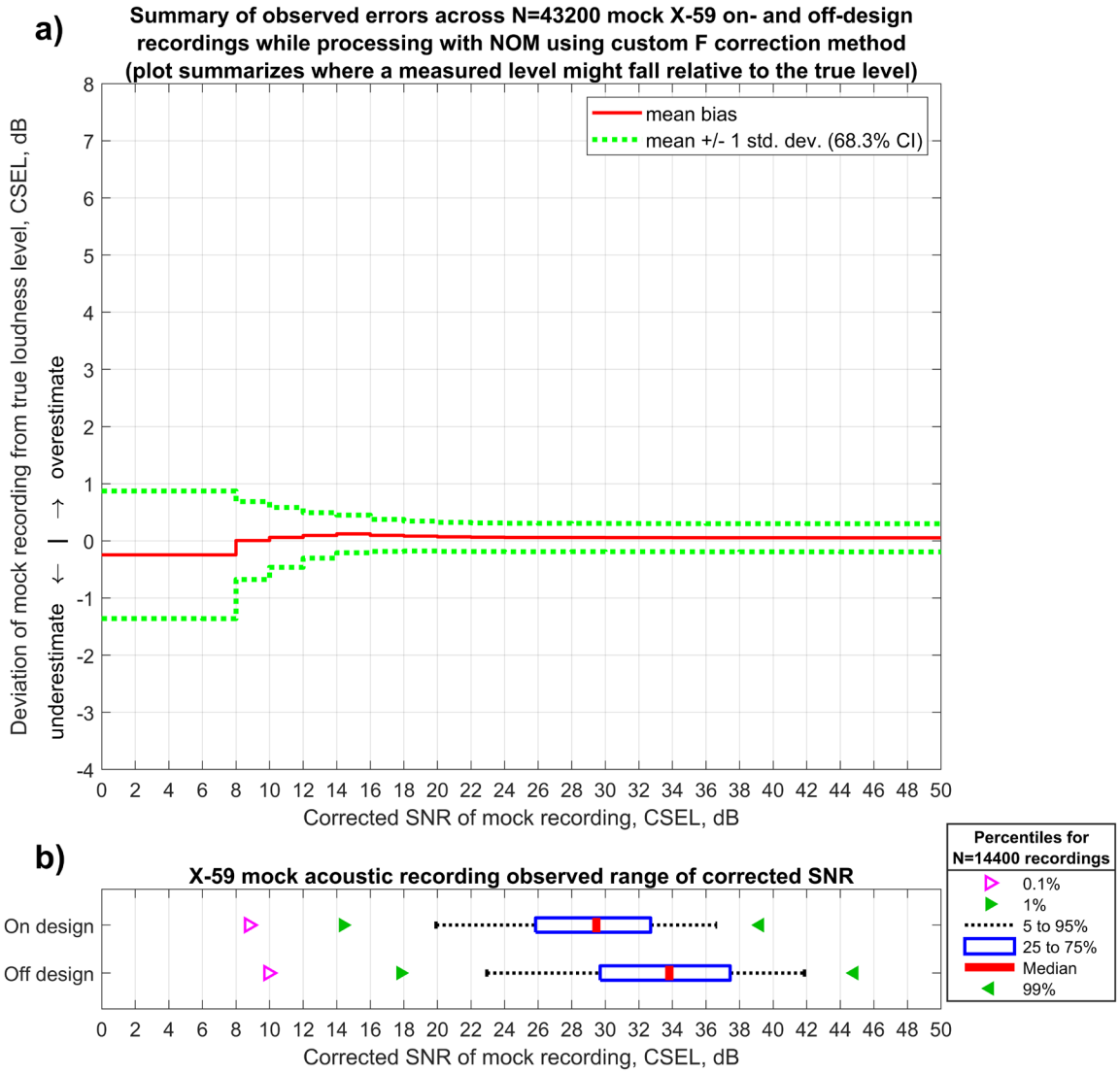


Figure 2.5: Total measurement error for the CSEL noise metric versus the CSEL corrected SNR, a) shows the total measurement error and b) shows the observed distribution of corrected SNR for the on-design and off-design X-59 mock acoustic recordings.

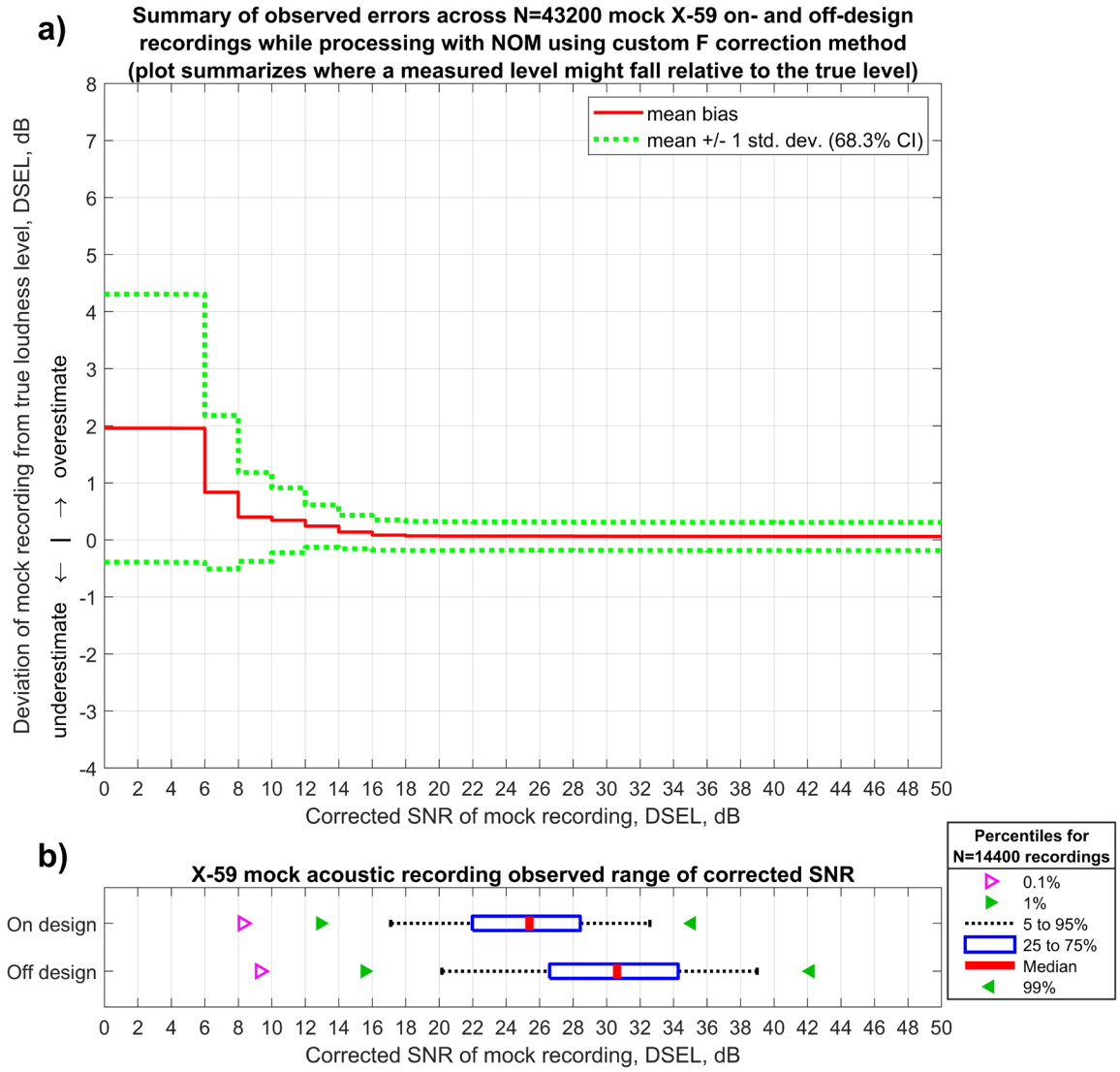


Figure 2.6: Total measurement error for the DSEL noise metric versus the DSEL corrected SNR, a) shows the total measurement error and b) shows the observed distribution of corrected SNR for the on-design and off-design X-59 mock acoustic recordings.

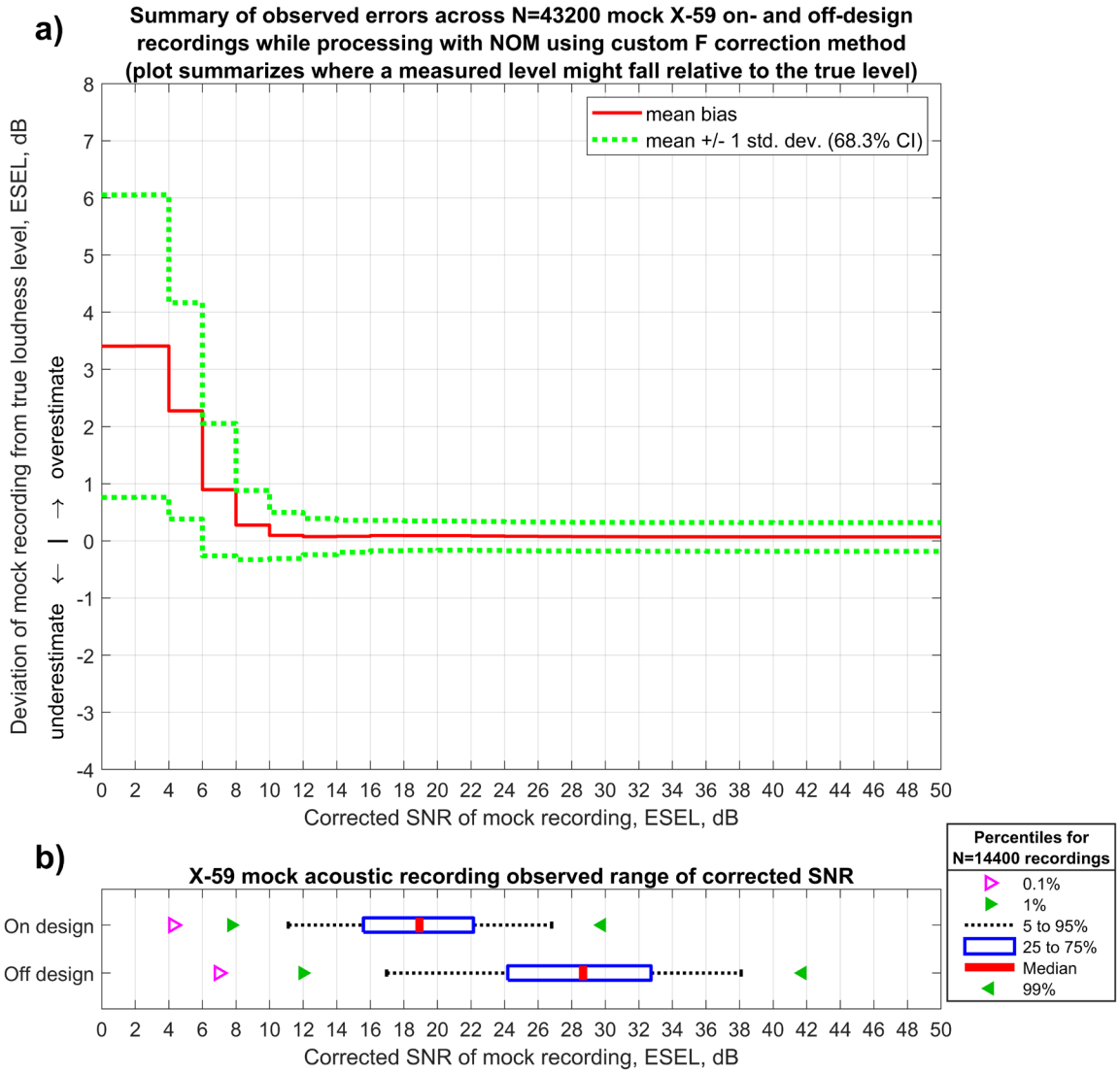


Figure 2.7: Total measurement error for the ESEL noise metric versus the ESEL corrected SNR, a) shows the total measurement error and b) shows the observed distribution of corrected SNR for the on-design and off-design X-59 mock acoustic recordings.

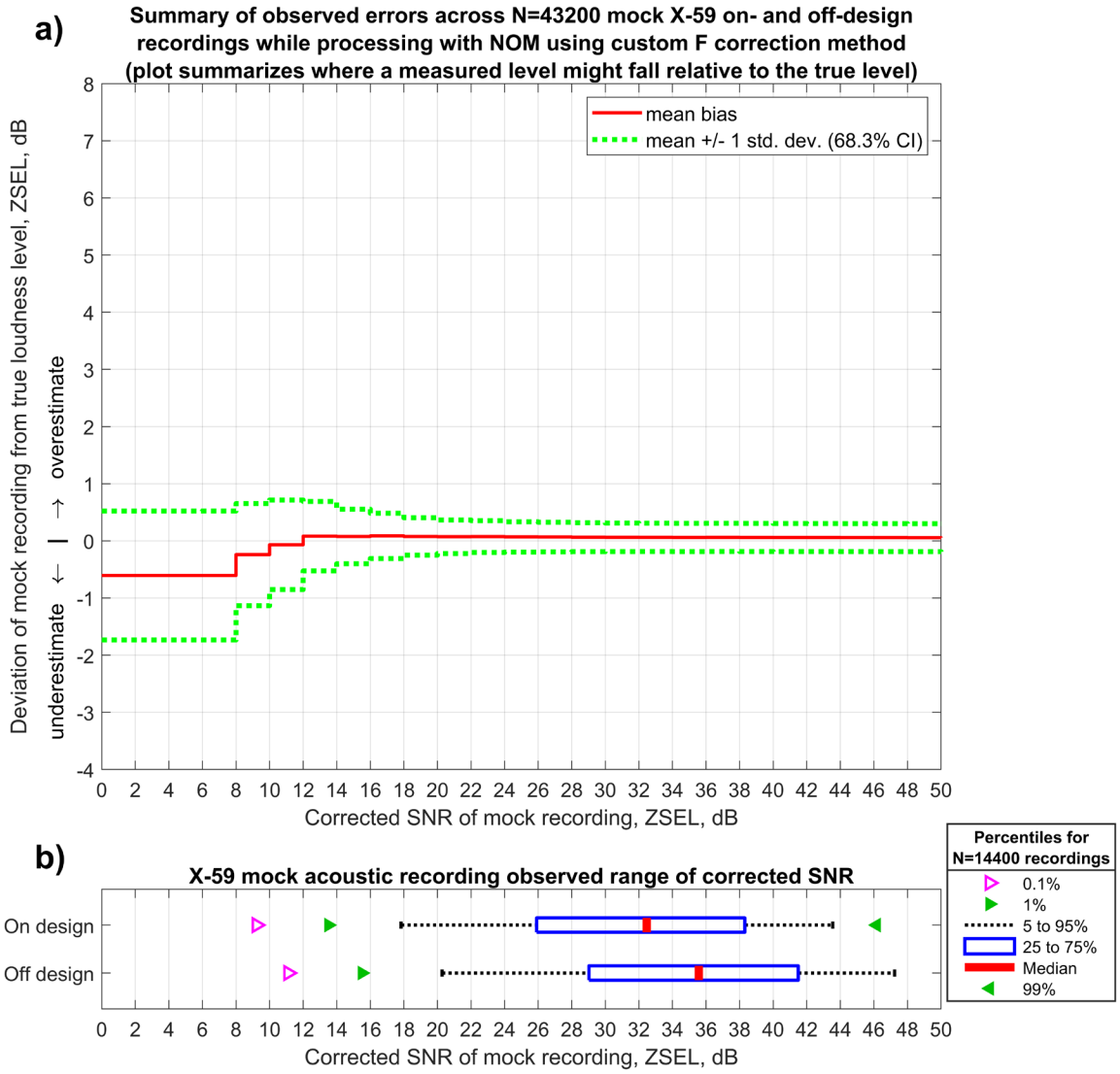


Figure 2.8: Total measurement error for the ZSEL noise metric versus the ZSEL corrected SNR, a) shows the total measurement error and b) shows the observed distribution of corrected SNR for the on-design and off-design X-59 mock acoustic recordings.

Appendix 3: Tabulated total measurement error for eight different noise metrics

Table 3.1: Total measurement error mean and standard deviation for noise metric PL.

Metric: PL	Use condition (Bin Edges, PL)	Mean Bias** dB, PL	Standard Deviation dB, PL
Bin 1	-∞ dB < SNR_c* <= 2 dB	3.23	4.262
Bin 2	2 dB < SNR_c* <= 4 dB	3.23	4.261
Bin 3	4 dB < SNR_c* <= 6 dB	2.561	3.646
Bin 4	6 dB < SNR_c* <= 8 dB	0.814	2.5
Bin 5	8 dB < SNR_c* <= 10 dB	-0.2074	1.603
Bin 6	10 dB < SNR_c* <= 12 dB	-0.4847	1.241
Bin 7	12 dB < SNR_c* <= 14 dB	-0.3713	0.9555
Bin 8	14 dB < SNR_c* <= 16 dB	-0.2127	0.6823
Bin 9	16 dB < SNR_c* <= 18 dB	-0.1131	0.5056
Bin 10	18 dB < SNR_c* <= 20 dB	-0.07479	0.4019
Bin 11	20 dB < SNR_c* <= 22 dB	-0.05595	0.3416
Bin 12	22 dB < SNR_c* <= 24 dB	-0.01421	0.3052
Bin 13	24 dB < SNR_c* <= 26 dB	0.007833	0.2793
Bin 14	26 dB < SNR_c* <= 28 dB	0.01186	0.2696
Bin 15	28 dB < SNR_c* <= 30 dB	0.01943	0.2618
Bin 16	30 dB < SNR_c* <= 32 dB	0.03002	0.2579
Bin 17	32 dB < SNR_c* <= 34 dB	0.02936	0.2568
Bin 18	34 dB < SNR_c* <= 36 dB	0.03279	0.2558
Bin 19	36 dB < SNR_c* <= 38 dB	0.03417	0.2551
Bin 20	38 dB < SNR_c* <= 40 dB	0.03822	0.2546
Bin 21	40 dB < SNR_c* <= 42 dB	0.04235	0.2544
Bin 22	42 dB < SNR_c* <= +∞ dB	0.04234	0.2544

* The corrected SNR, SNR_c, is an output option when using the NOM software. See discussion in Section V.

**The expected measurement error bias relative to truth is tabulated. Use the negative of the tabulated bias value when computing uncertainty for a measured value. E.g., use μ = -3.230000 dB for bin 2 or use μ = +0.212700 dB for bin 8 when computing a confidence interval, *CI*, from $CI = \pm c \times \sigma + \mu$.

Table 3.2: Total measurement error mean and standard deviation for noise metric ISBAP.

Metric: ISBAP	Use condition (Bin Edges, ISBAP)	Mean Bias** dB, ISBAP	Standard Deviation dB, ISBAP
Bin 1	$-\infty$ dB < SNR_c* <= 4 dB	0.964	3.701
Bin 2	4 dB < SNR_c* <= 6 dB	0.965	3.699
Bin 3	6 dB < SNR_c* <= 8 dB	0.06044	2.817
Bin 4	8 dB < SNR_c* <= 10 dB	0.3028	2.507
Bin 5	10 dB < SNR_c* <= 12 dB	0.6176	2.073
Bin 6	12 dB < SNR_c* <= 14 dB	0.2325	1.71
Bin 7	14 dB < SNR_c* <= 16 dB	-0.2677	1.359
Bin 8	16 dB < SNR_c* <= 18 dB	-0.5027	1.138
Bin 9	18 dB < SNR_c* <= 20 dB	-0.3934	0.9182
Bin 10	20 dB < SNR_c* <= 22 dB	-0.2178	0.6569
Bin 11	22 dB < SNR_c* <= 24 dB	-0.1238	0.4664
Bin 12	24 dB < SNR_c* <= 26 dB	-0.08598	0.3717
Bin 13	26 dB < SNR_c* <= 28 dB	-0.06144	0.3163
Bin 14	28 dB < SNR_c* <= 30 dB	-0.03068	0.284
Bin 15	30 dB < SNR_c* <= 32 dB	-0.006772	0.2664
Bin 16	32 dB < SNR_c* <= 34 dB	0.0008078	0.2593
Bin 17	34 dB < SNR_c* <= 36 dB	0.01021	0.2562
Bin 18	36 dB < SNR_c* <= 38 dB	0.01494	0.254
Bin 19	38 dB < SNR_c* <= 40 dB	0.0169	0.2532
Bin 20	40 dB < SNR_c* <= 42 dB	0.02079	0.2523
Bin 21	42 dB < SNR_c* <= 44 dB	0.02272	0.2522
Bin 22	44 dB < SNR_c* <= $+\infty$ dB	0.02274	0.2522

* The corrected SNR, SNR_c, is an output option when using the NOM software. See discussion in Section V.

** The expected measurement error bias relative to truth is tabulated. Use the negative of the tabulated bias value when computing uncertainty for a measured value. E.g., use μ = -0.965000 dB for bin 2 or use μ = +0.502700 dB for bin 8 when computing a confidence interval, *CI*, from $CI = \pm c \times \sigma + \mu$.

Table 3.3: Total measurement error mean and standard deviation for noise metric ASEL.

Metric: ASEL	Use condition (Bin Edges, ASEL)	Mean Bias** dB, ASEL	Standard Deviation dB, ASEL
Bin 1	$-\infty$ dB < SNR_c* <= 0 dB	4.961	2.796
Bin 2	0 dB < SNR_c* <= 2 dB	4.961	2.795
Bin 3	2 dB < SNR_c* <= 4 dB	3.996	3.383
Bin 4	4 dB < SNR_c* <= 6 dB	1.356	1.963
Bin 5	6 dB < SNR_c* <= 8 dB	0.2956	0.921
Bin 6	8 dB < SNR_c* <= 10 dB	0.104	0.5358
Bin 7	10 dB < SNR_c* <= 12 dB	0.105	0.3706
Bin 8	12 dB < SNR_c* <= 14 dB	0.1208	0.3006
Bin 9	14 dB < SNR_c* <= 16 dB	0.1268	0.2749
Bin 10	16 dB < SNR_c* <= 18 dB	0.1229	0.2641
Bin 11	18 dB < SNR_c* <= 20 dB	0.1135	0.2594
Bin 12	20 dB < SNR_c* <= 22 dB	0.1041	0.2568
Bin 13	22 dB < SNR_c* <= 24 dB	0.09904	0.2556
Bin 14	24 dB < SNR_c* <= 26 dB	0.09379	0.2549
Bin 15	26 dB < SNR_c* <= 28 dB	0.09027	0.2545
Bin 16	28 dB < SNR_c* <= 30 dB	0.08798	0.2543
Bin 17	30 dB < SNR_c* <= 32 dB	0.08556	0.2542
Bin 18	32 dB < SNR_c* <= 34 dB	0.08486	0.2541
Bin 19	34 dB < SNR_c* <= 36 dB	0.08471	0.2541
Bin 20	36 dB < SNR_c* <= 38 dB	0.08388	0.2541
Bin 21	38 dB < SNR_c* <= 40 dB	0.08384	0.254
Bin 22	40 dB < SNR_c* <= 42 dB	0.08329	0.254
Bin 23	42 dB < SNR_c* <= 44 dB	0.08325	0.254
Bin 24	44 dB < SNR_c* <= $+\infty$ dB	0.08325	0.254

* The corrected SNR, SNR_c, is an output option when using the NOM software. See discussion in Section V.

** The expected measurement error bias relative to truth is tabulated. Use the negative of the tabulated bias value when computing uncertainty for a measured value. E.g., use μ = -4.961000 dB for bin 2 or use μ = -0.120800 dB for bin 8 when computing a confidence interval, *CI*, from $CI = \pm c \times \sigma + \mu$.

Table 3.4: Total measurement error mean and standard deviation for noise metric BSEL.

Metric: BSEL	Use condition (Bin Edges, BSEL)	Mean Bias** dB, BSEL	Standard Deviation dB, BSEL
Bin 1	$-\infty$ dB < SNR_c* <= 2 dB	2.722	2.282
Bin 2	2 dB < SNR_c* <= 4 dB	2.722	2.284
Bin 3	4 dB < SNR_c* <= 6 dB	1.451	2.073
Bin 4	6 dB < SNR_c* <= 8 dB	0.7926	1.258
Bin 5	8 dB < SNR_c* <= 10 dB	0.3968	0.6634
Bin 6	10 dB < SNR_c* <= 12 dB	0.1709	0.4309
Bin 7	12 dB < SNR_c* <= 14 dB	0.08268	0.3305
Bin 8	14 dB < SNR_c* <= 16 dB	0.0659	0.2849
Bin 9	16 dB < SNR_c* <= 18 dB	0.07293	0.2686
Bin 10	18 dB < SNR_c* <= 20 dB	0.07546	0.2599
Bin 11	20 dB < SNR_c* <= 22 dB	0.07799	0.2555
Bin 12	22 dB < SNR_c* <= 24 dB	0.07621	0.2536
Bin 13	24 dB < SNR_c* <= 26 dB	0.0725	0.2526
Bin 14	26 dB < SNR_c* <= 28 dB	0.06937	0.2518
Bin 15	28 dB < SNR_c* <= 30 dB	0.06663	0.2513
Bin 16	30 dB < SNR_c* <= 32 dB	0.06458	0.2511
Bin 17	32 dB < SNR_c* <= 34 dB	0.06362	0.2509
Bin 18	34 dB < SNR_c* <= 36 dB	0.06273	0.2508
Bin 19	36 dB < SNR_c* <= 38 dB	0.06197	0.2507
Bin 20	38 dB < SNR_c* <= 40 dB	0.06183	0.2506
Bin 21	40 dB < SNR_c* <= 42 dB	0.06153	0.2506
Bin 22	42 dB < SNR_c* <= 44 dB	0.06093	0.2506
Bin 23	44 dB < SNR_c* <= $+\infty$ dB	0.06094	0.2506

* The corrected SNR, SNR_c, is an output option when using the NOM software. See discussion in Section V.

**The expected measurement error bias relative to truth is tabulated. Use the negative of the tabulated bias value when computing uncertainty for a measured value. E.g., use μ = -2.722000 dB for bin 2 or use μ = -0.065900 dB for bin 8 when computing a confidence interval, *CI*, from $CI = \pm c \times \sigma + \mu$.

Table 3.5: Total measurement error mean and standard deviation for noise metric CSEL.

Metric: CSEL	Use condition (Bin Edges, CSEL)	Mean Bias** dB, CSEL	Standard Deviation dB, CSEL
Bin 1	-∞ dB < SNR_c* <= 6 dB	-0.2438	1.116
Bin 2	6 dB < SNR_c* <= 8 dB	-0.2441	1.116
Bin 3	8 dB < SNR_c* <= 10 dB	0.005886	0.6825
Bin 4	10 dB < SNR_c* <= 12 dB	0.06047	0.5238
Bin 5	12 dB < SNR_c* <= 14 dB	0.09478	0.3974
Bin 6	14 dB < SNR_c* <= 16 dB	0.1217	0.3301
Bin 7	16 dB < SNR_c* <= 18 dB	0.09632	0.2805
Bin 8	18 dB < SNR_c* <= 20 dB	0.08362	0.2617
Bin 9	20 dB < SNR_c* <= 22 dB	0.06978	0.2543
Bin 10	22 dB < SNR_c* <= 24 dB	0.06352	0.25
Bin 11	24 dB < SNR_c* <= 26 dB	0.05895	0.2484
Bin 12	26 dB < SNR_c* <= 28 dB	0.05873	0.2476
Bin 13	28 dB < SNR_c* <= 30 dB	0.05841	0.247
Bin 14	30 dB < SNR_c* <= 32 dB	0.05735	0.2466
Bin 15	32 dB < SNR_c* <= 34 dB	0.05696	0.2462
Bin 16	34 dB < SNR_c* <= 36 dB	0.05633	0.2461
Bin 17	36 dB < SNR_c* <= 38 dB	0.05557	0.246
Bin 18	38 dB < SNR_c* <= 40 dB	0.05575	0.2459
Bin 19	40 dB < SNR_c* <= 42 dB	0.05561	0.2459
Bin 20	42 dB < SNR_c* <= 44 dB	0.05511	0.2458
Bin 21	44 dB < SNR_c* <= 46 dB	0.05454	0.2458
Bin 22	46 dB < SNR_c* <= +∞ dB	0.05454	0.2458

* The corrected SNR, SNR_c, is an output option when using the NOM software. See discussion in Section V.

** The expected measurement error bias relative to truth is tabulated. Use the negative of the tabulated bias value when computing uncertainty for a measured value. E.g., use μ = +0.244100 dB for bin 2 or use μ = -0.083620 dB for bin 8 when computing a confidence interval, *CI*, from $CI = \pm c \times \sigma + \mu$.

Table 3.6: Total measurement error mean and standard deviation for noise metric DSEL.

Metric: DSEL	Use condition (Bin Edges, DSEL)	Mean Bias** dB, DSEL	Standard Deviation dB, DSEL
Bin 1	-∞ dB < SNR_c* <= 4 dB	1.958	2.35
Bin 2	4 dB < SNR_c* <= 6 dB	1.955	2.349
Bin 3	6 dB < SNR_c* <= 8 dB	0.8354	1.346
Bin 4	8 dB < SNR_c* <= 10 dB	0.4011	0.7788
Bin 5	10 dB < SNR_c* <= 12 dB	0.3434	0.5678
Bin 6	12 dB < SNR_c* <= 14 dB	0.2409	0.3712
Bin 7	14 dB < SNR_c* <= 16 dB	0.1375	0.2937
Bin 8	16 dB < SNR_c* <= 18 dB	0.08373	0.2648
Bin 9	18 dB < SNR_c* <= 20 dB	0.06851	0.2549
Bin 10	20 dB < SNR_c* <= 22 dB	0.06601	0.2513
Bin 11	22 dB < SNR_c* <= 24 dB	0.06641	0.2488
Bin 12	24 dB < SNR_c* <= 26 dB	0.06694	0.2478
Bin 13	26 dB < SNR_c* <= 28 dB	0.06607	0.2472
Bin 14	28 dB < SNR_c* <= 30 dB	0.0643	0.2469
Bin 15	30 dB < SNR_c* <= 32 dB	0.06301	0.2467
Bin 16	32 dB < SNR_c* <= 34 dB	0.06191	0.2466
Bin 17	34 dB < SNR_c* <= 36 dB	0.061	0.2465
Bin 18	36 dB < SNR_c* <= 38 dB	0.06067	0.2465
Bin 19	38 dB < SNR_c* <= 40 dB	0.06047	0.2464
Bin 20	40 dB < SNR_c* <= 42 dB	0.05985	0.2464
Bin 21	42 dB < SNR_c* <= 44 dB	0.05945	0.2464
Bin 22	44 dB < SNR_c* <= +∞ dB	0.05945	0.2464

* The corrected SNR, SNR_c, is an output option when using the NOM software. See discussion in Section V.

** The expected measurement error bias relative to truth is tabulated. Use the negative of the tabulated bias value when computing uncertainty for a measured value. E.g., use μ = -1.955000 dB for bin 2 or use μ = -0.083730 dB for bin 8 when computing a confidence interval, *CI*, from $CI = \pm c \times \sigma + \mu$.

Table 3.7: Total measurement error mean and standard deviation for noise metric ESEL.

Metric: ESEL	Use condition (Bin Edges, ESEL)	Mean Bias** dB, ESEL	Standard Deviation dB, ESEL
Bin 1	-∞ dB < SNR_c* <= 2 dB	3.406	2.645
Bin 2	2 dB < SNR_c* <= 4 dB	3.409	2.645
Bin 3	4 dB < SNR_c* <= 6 dB	2.275	1.892
Bin 4	6 dB < SNR_c* <= 8 dB	0.8964	1.158
Bin 5	8 dB < SNR_c* <= 10 dB	0.2765	0.6058
Bin 6	10 dB < SNR_c* <= 12 dB	0.09573	0.4029
Bin 7	12 dB < SNR_c* <= 14 dB	0.07444	0.317
Bin 8	14 dB < SNR_c* <= 16 dB	0.07964	0.2793
Bin 9	16 dB < SNR_c* <= 18 dB	0.09308	0.2643
Bin 10	18 dB < SNR_c* <= 20 dB	0.09176	0.2574
Bin 11	20 dB < SNR_c* <= 22 dB	0.09149	0.2548
Bin 12	22 dB < SNR_c* <= 24 dB	0.08563	0.2531
Bin 13	24 dB < SNR_c* <= 26 dB	0.08019	0.2522
Bin 14	26 dB < SNR_c* <= 28 dB	0.07694	0.2516
Bin 15	28 dB < SNR_c* <= 30 dB	0.07394	0.2513
Bin 16	30 dB < SNR_c* <= 32 dB	0.07273	0.2511
Bin 17	32 dB < SNR_c* <= 34 dB	0.07023	0.2509
Bin 18	34 dB < SNR_c* <= 36 dB	0.07042	0.2509
Bin 19	36 dB < SNR_c* <= 38 dB	0.06965	0.2508
Bin 20	38 dB < SNR_c* <= 40 dB	0.06937	0.2508
Bin 21	40 dB < SNR_c* <= 42 dB	0.06905	0.2508
Bin 22	42 dB < SNR_c* <= 44 dB	0.06869	0.2507
Bin 23	44 dB < SNR_c* <= +∞ dB	0.06869	0.2507

* The corrected SNR, SNR_c, is an output option when using the NOM software. See discussion in Section V.

**The expected measurement error bias relative to truth is tabulated. Use the negative of the tabulated bias value when computing uncertainty for a measured value. E.g., use μ = -3.409000 dB for bin 2 or use μ = -0.079640 dB for bin 8 when computing a confidence interval, *CI*, from $CI = \pm c \times \sigma + \mu$.

Table 3.8: Total measurement error mean and standard deviation for noise metric ZSEL.

Metric: ZSEL	Use condition (Bin Edges, ZSEL)	Mean Bias** dB, ZSEL	Standard Deviation dB, ZSEL
Bin 1	-∞ dB < SNR_c* <= 6 dB	-0.6059	1.128
Bin 2	6 dB < SNR_c* <= 8 dB	-0.6058	1.128
Bin 3	8 dB < SNR_c* <= 10 dB	-0.2409	0.8935
Bin 4	10 dB < SNR_c* <= 12 dB	-0.06825	0.7842
Bin 5	12 dB < SNR_c* <= 14 dB	0.08263	0.6077
Bin 6	14 dB < SNR_c* <= 16 dB	0.07712	0.4773
Bin 7	16 dB < SNR_c* <= 18 dB	0.08733	0.3961
Bin 8	18 dB < SNR_c* <= 20 dB	0.07677	0.3272
Bin 9	20 dB < SNR_c* <= 22 dB	0.07275	0.2939
Bin 10	22 dB < SNR_c* <= 24 dB	0.07486	0.2786
Bin 11	24 dB < SNR_c* <= 26 dB	0.06928	0.2649
Bin 12	26 dB < SNR_c* <= 28 dB	0.06798	0.2588
Bin 13	28 dB < SNR_c* <= 30 dB	0.0639	0.2522
Bin 14	30 dB < SNR_c* <= 32 dB	0.06214	0.2492
Bin 15	32 dB < SNR_c* <= 34 dB	0.06156	0.2473
Bin 16	34 dB < SNR_c* <= 36 dB	0.05956	0.2463
Bin 17	36 dB < SNR_c* <= 38 dB	0.06085	0.2458
Bin 18	38 dB < SNR_c* <= 40 dB	0.05938	0.2454
Bin 19	40 dB < SNR_c* <= 42 dB	0.05886	0.2452
Bin 20	42 dB < SNR_c* <= 44 dB	0.05866	0.245
Bin 21	44 dB < SNR_c* <= 46 dB	0.05797	0.245
Bin 22	46 dB < SNR_c* <= 48 dB	0.05768	0.2449
Bin 23	48 dB < SNR_c* <= 50 dB	0.05656	0.2449
Bin 24	50 dB < SNR_c* <= 52 dB	0.05599	0.2449
Bin 25	52 dB < SNR_c* <= +∞ dB	0.05599	0.2449

* The corrected SNR, SNR_c, is an output option when using the NOM software. See discussion in Section V.

**The expected measurement error bias relative to truth is tabulated. Use the negative of the tabulated bias value when computing uncertainty for a measured value. E.g., use μ = +0.605800 dB for bin 2 or use μ = -0.076770 dB for bin 8 when computing a confidence interval, *CI*, from $CI = \pm c \times \sigma + \mu$.

Appendix 4: Plots of the proportion of the total variance explained by each uncertainty source for eight different noise metrics

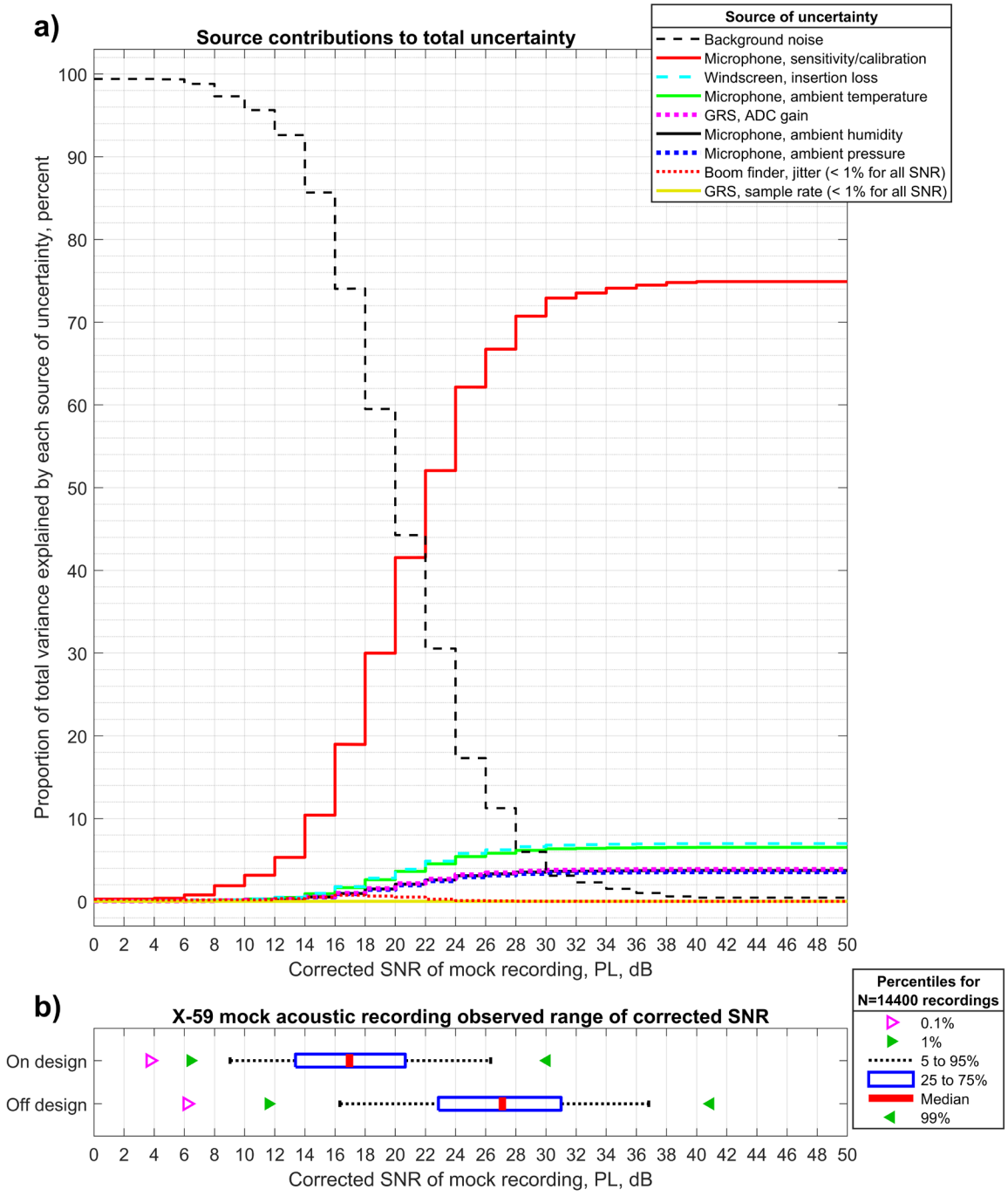


Figure 4.1: Proportion of the total variance explained by each uncertainty source for the PL noise metric versus the PL corrected SNR of the mock recording.

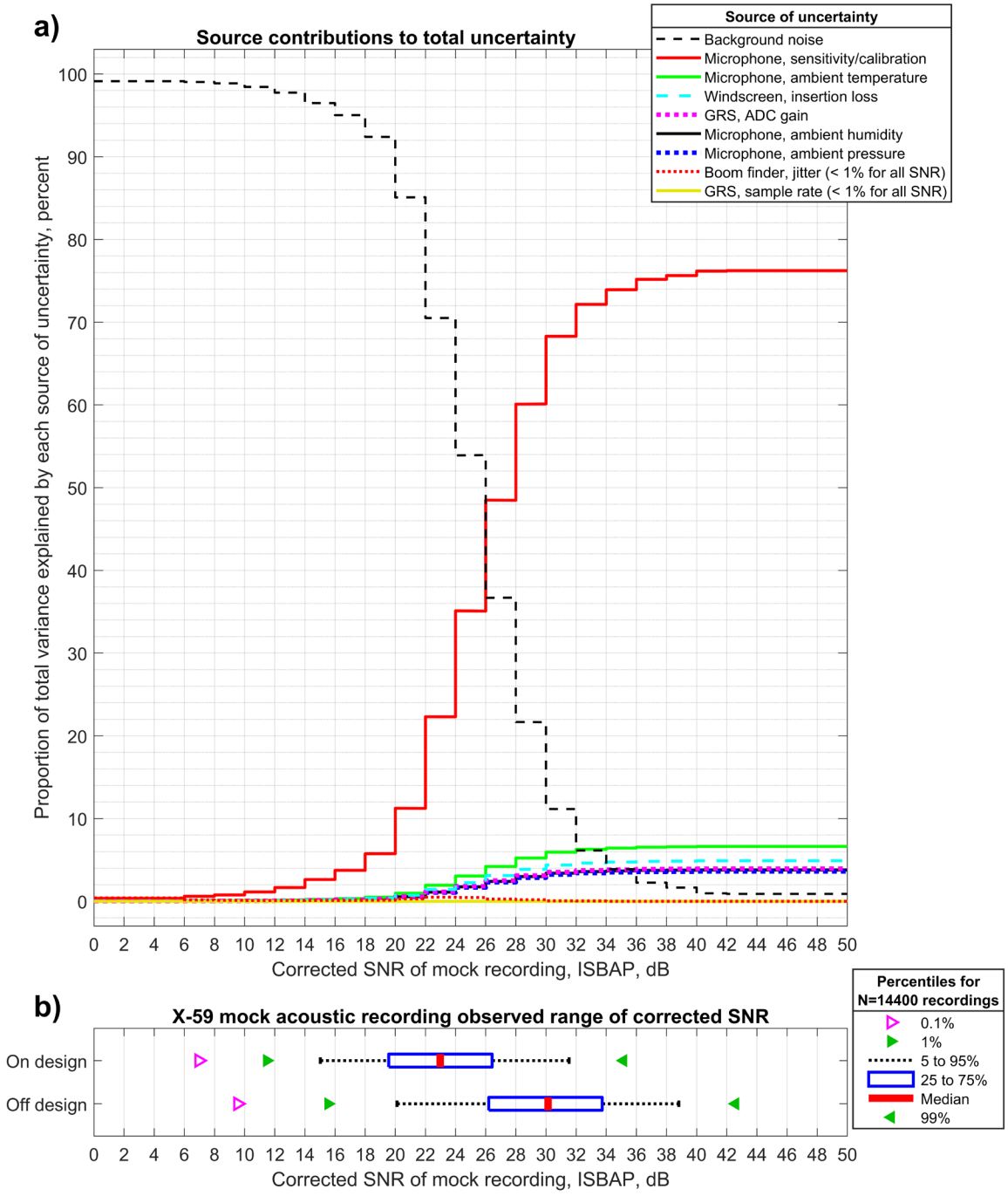


Figure 4.2: Proportion of the total variance explained by each uncertainty source for the ISBAP noise metric versus the ISBAP corrected SNR of the mock recording.

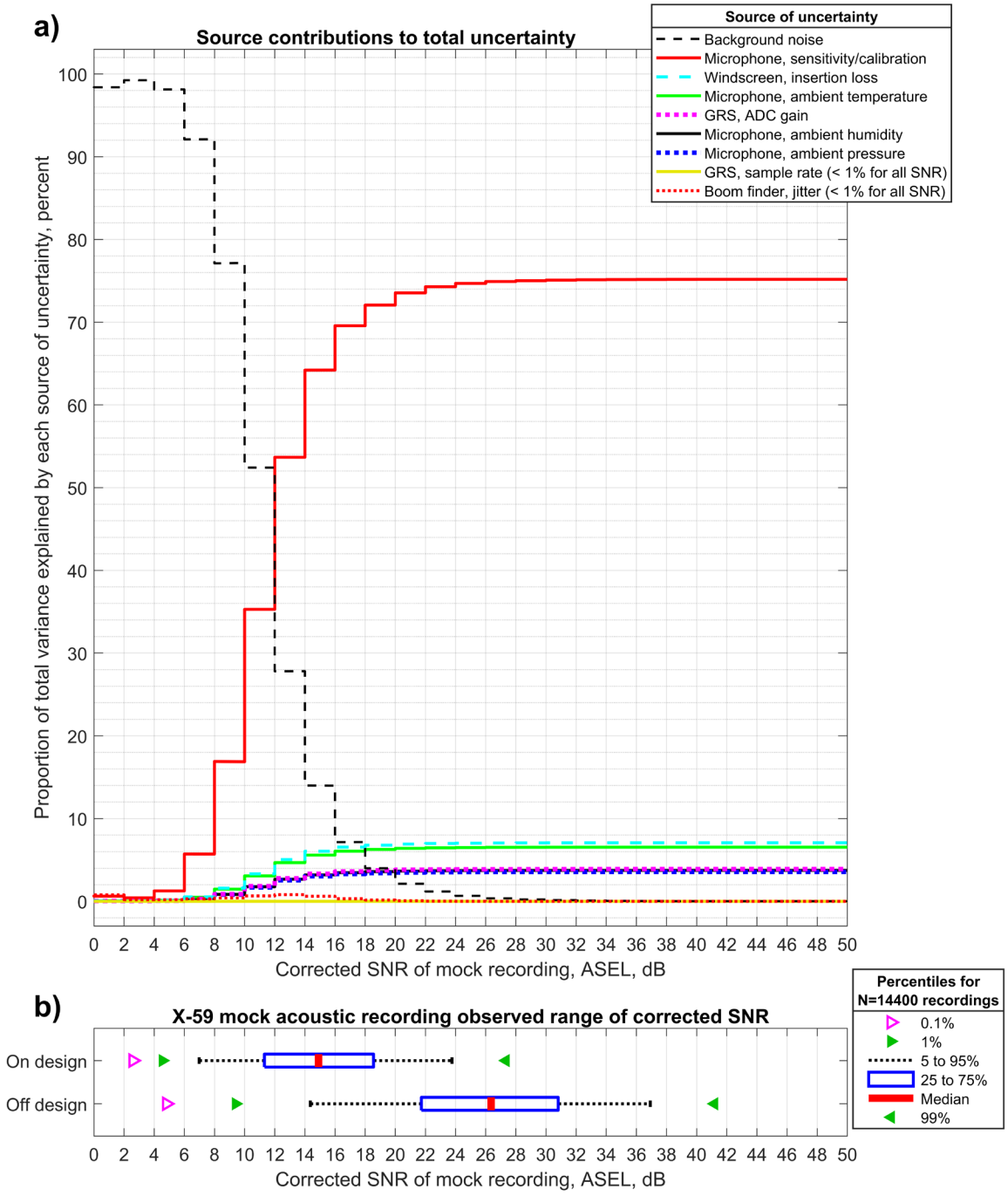


Figure 4.3: Proportion of the total variance explained by each uncertainty source for the ASEL noise metric versus the ASEL corrected SNR of the mock recording.

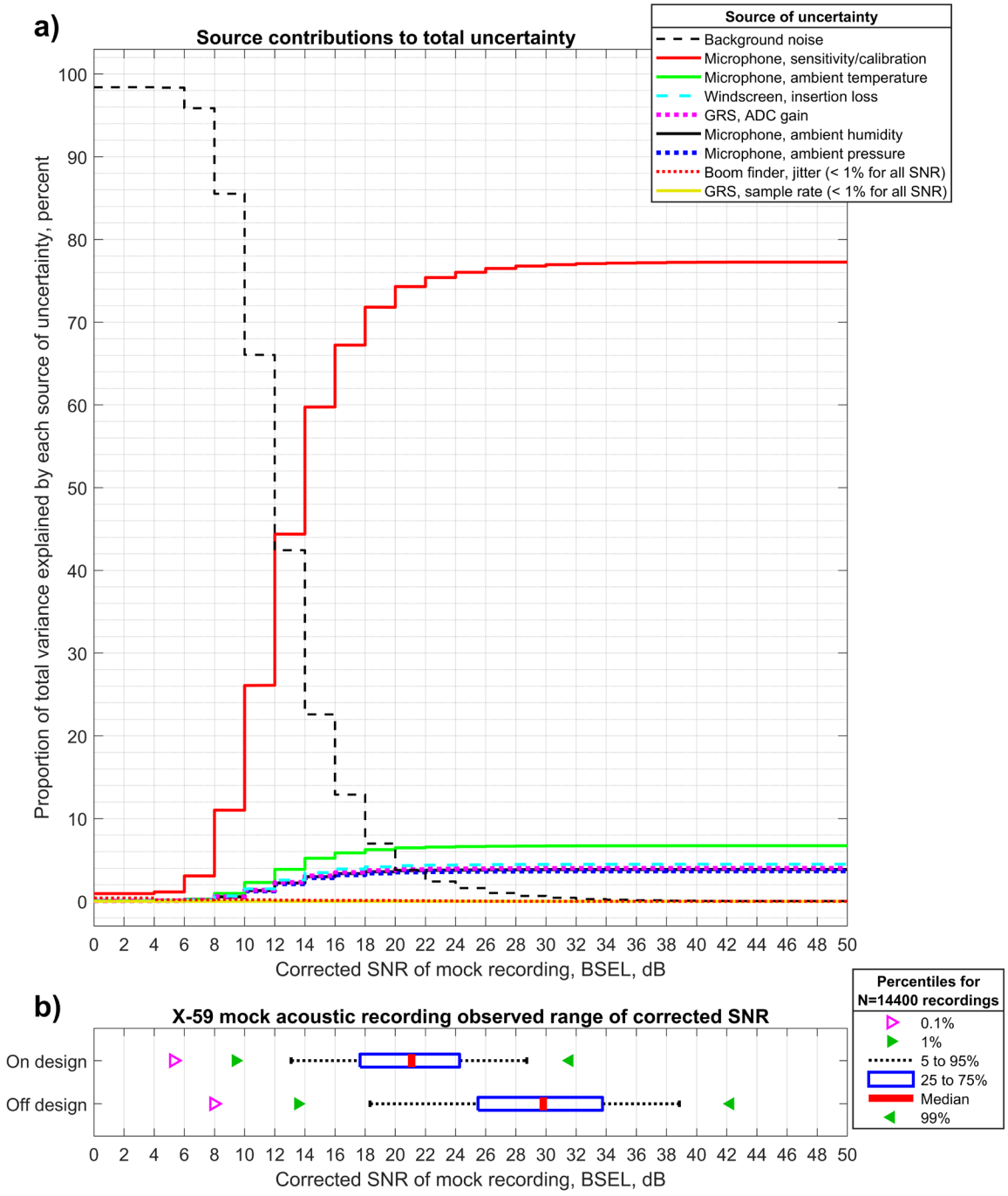


Figure 4.4: Proportion of the total variance explained by each uncertainty source for the BSEL noise metric versus the BSEL corrected SNR of the mock recording.

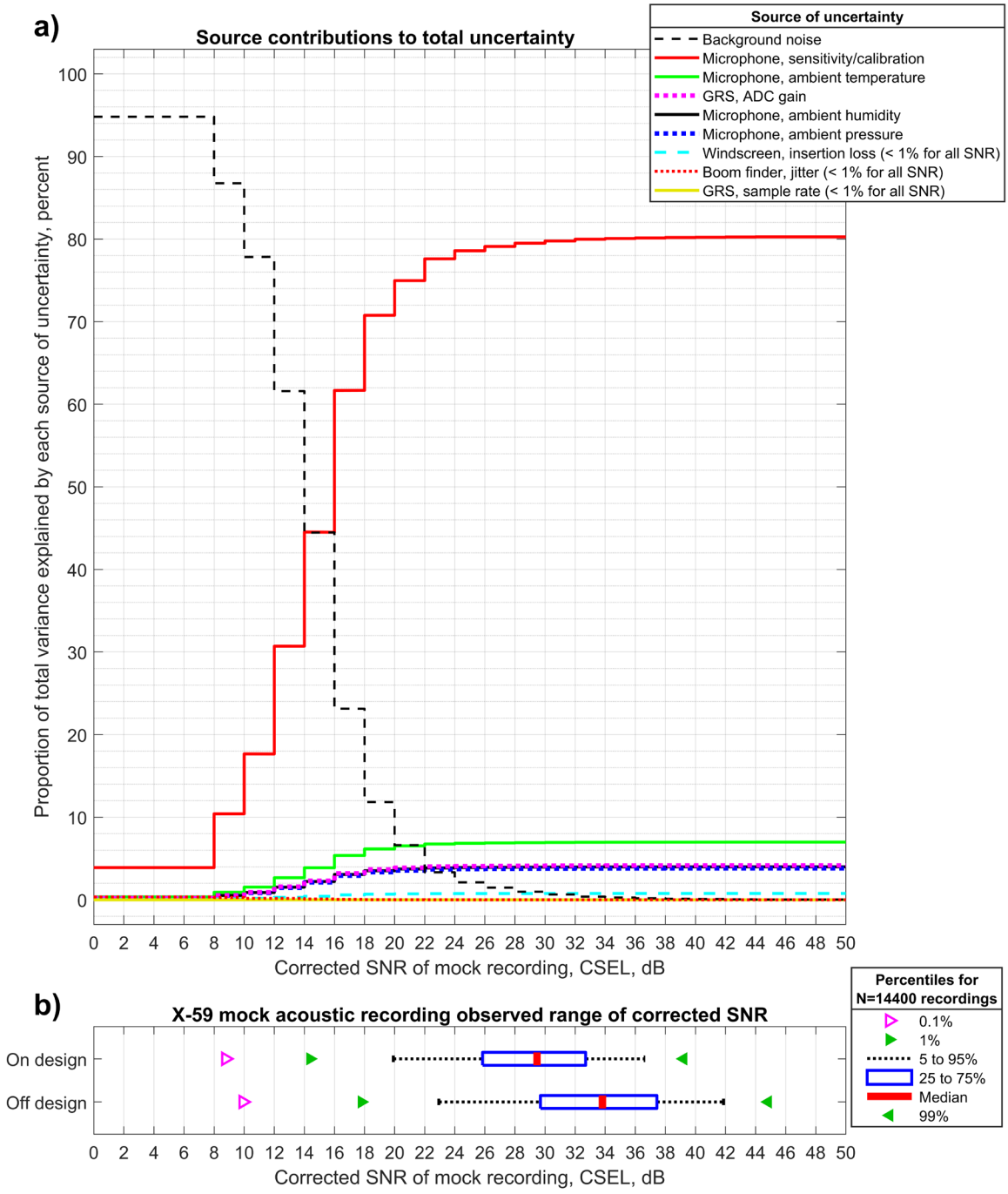


Figure 4.5: Proportion of the total variance explained by each uncertainty source for the CSEL noise metric versus the CSEL corrected SNR of the mock recording.

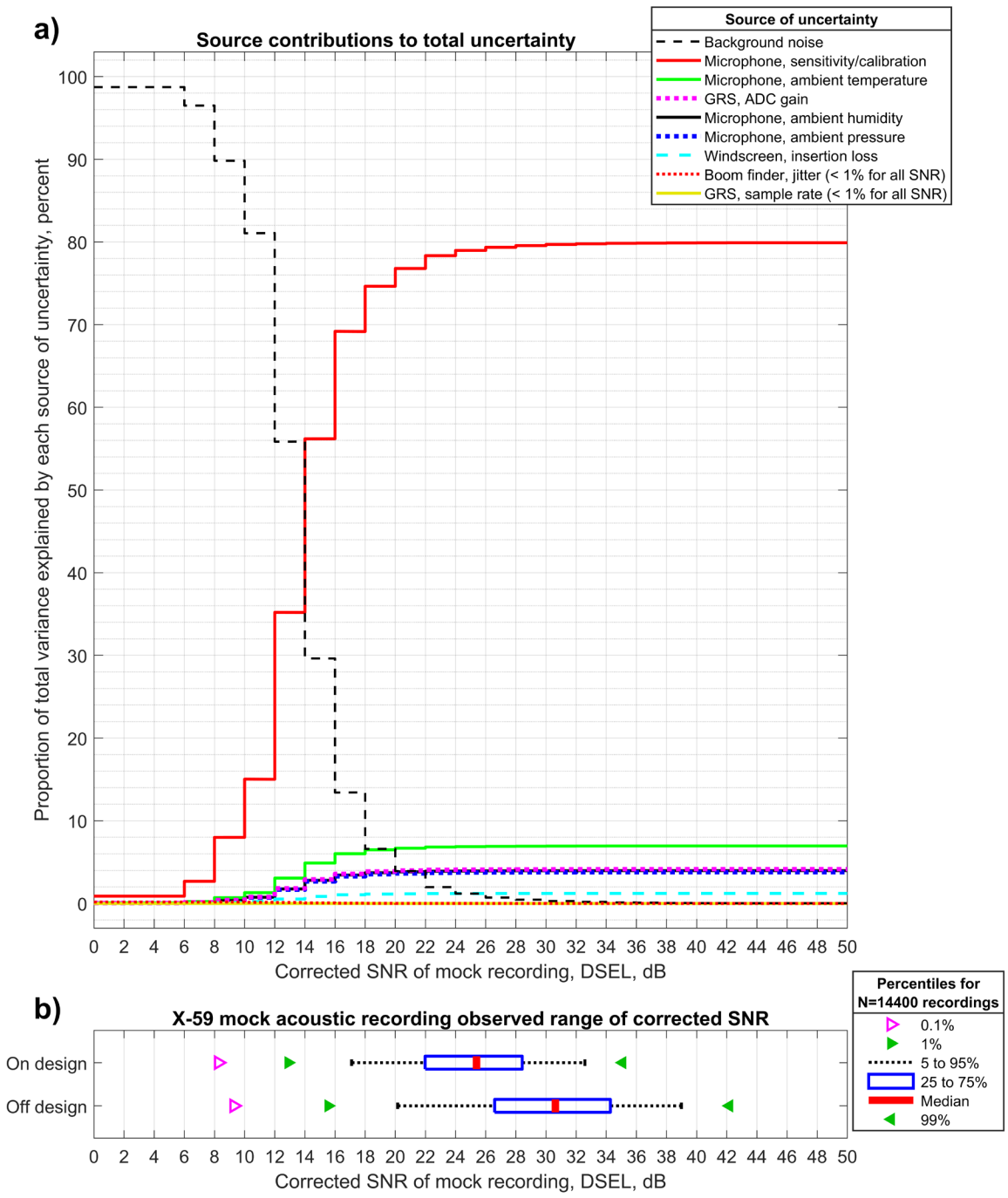


Figure 4.6: Proportion of the total variance explained by each uncertainty source for the DSEL noise metric versus the DSEL corrected SNR of the mock recording.

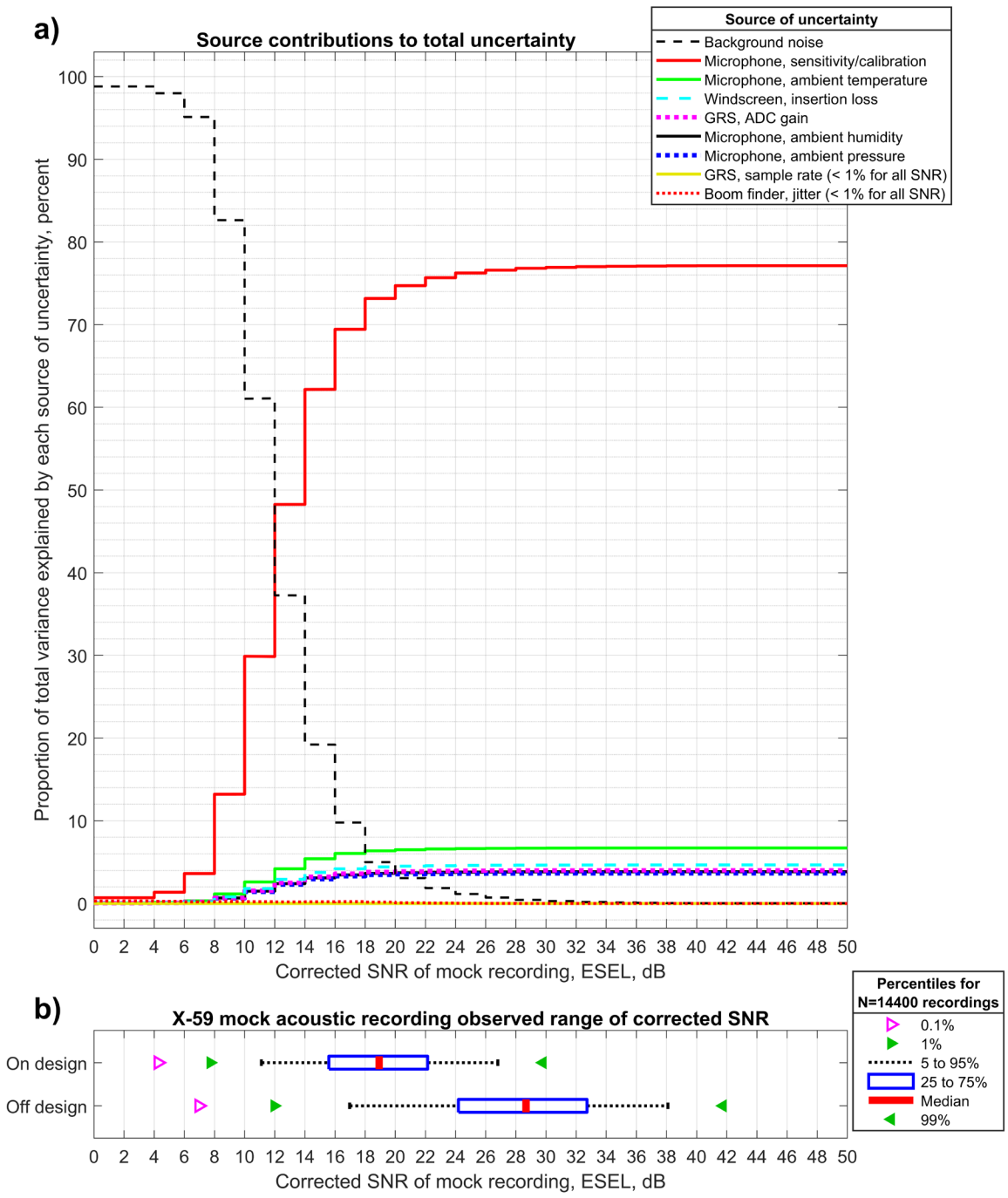


Figure 4.7: Proportion of the total variance explained by each uncertainty source for the ESEL noise metric versus the ESEL corrected SNR of the mock recording.

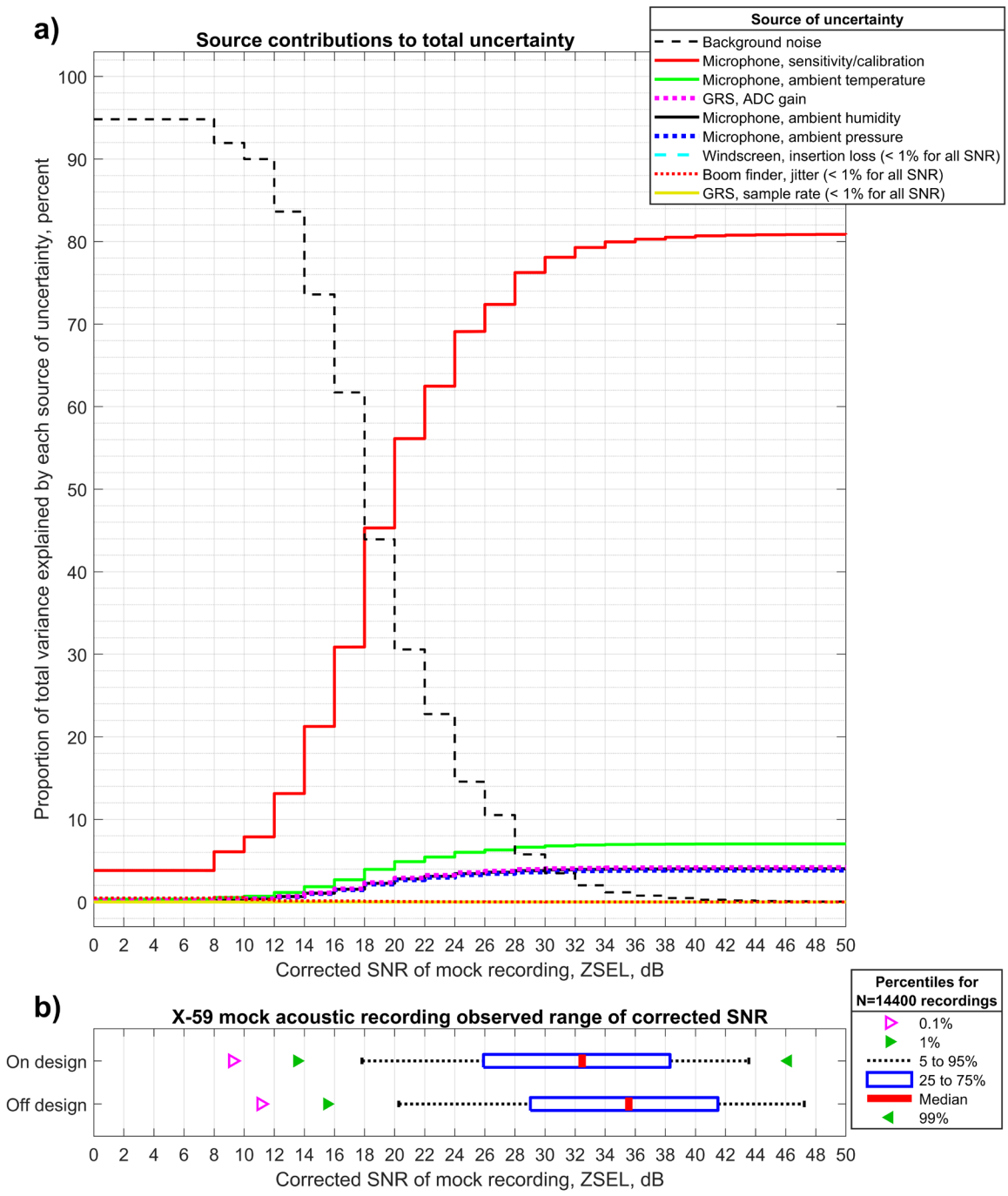


Figure 4.8: Proportion of the total variance explained by each uncertainty source for the ZSEL noise metric versus the ZSEL corrected SNR of the mock recording.

Appendix 5: Tabulated proportion of the total variance explained by each uncertainty source for eight different noise metrics

Table 5.1: Proportion of the total variance explained by each uncertainty source for the PL noise metric for each corrected SNR bin, where the lower and upper edge of each bin is identified in column two.

Metric: PL	Use condition (Bin Edges, PL)	Background noise % of total	Mic calibration % of total	Mic amb temp % of total	ADC gain % of total	Mic amb RH % of total	Windscreen IL % of total	Mic amb press % of total	Window jitter % of total	GRS sample rate** % of total
Bin 1	-∞ dB < SNR_c* <= 2 dB	99.4	0.267	0.0232	0.0138	0.0133	0.0249	0.0126	0.243	3.87e-07
Bin 2	2 dB < SNR_c* <= 4 dB	99.4	0.267	0.0232	0.0138	0.0133	0.0249	0.0126	0.243	3.87e-07
Bin 3	4 dB < SNR_c* <= 6 dB	99.4	0.365	0.0317	0.0189	0.0181	0.034	0.0173	0.16	5.29e-07
Bin 4	6 dB < SNR_c* <= 8 dB	98.8	0.775	0.0675	0.0402	0.0385	0.0722	0.0367	0.161	1.12e-06
Bin 5	8 dB < SNR_c* <= 10 dB	97.3	1.89	0.164	0.0978	0.0937	0.176	0.0892	0.193	2.73e-06
Bin 6	10 dB < SNR_c* <= 12 dB	95.6	3.15	0.274	0.163	0.157	0.293	0.149	0.178	4.56e-06
Bin 7	12 dB < SNR_c* <= 14 dB	92.6	5.31	0.462	0.275	0.264	0.494	0.251	0.327	7.69e-06
Bin 8	14 dB < SNR_c* <= 16 dB	85.7	10.4	0.906	0.54	0.518	0.97	0.493	0.487	1.51e-05
Bin 9	16 dB < SNR_c* <= 18 dB	74.1	19	1.65	0.984	0.943	1.77	0.897	0.74	2.75e-05
Bin 10	18 dB < SNR_c* <= 20 dB	59.5	30	2.61	1.56	1.49	2.79	1.42	0.631	4.35e-05
Bin 11	20 dB < SNR_c* <= 22 dB	44.3	41.6	3.62	2.16	2.07	3.87	1.97	0.51	6.02e-05
Bin 12	22 dB < SNR_c* <= 24 dB	30.6	52.1	4.53	2.7	2.59	4.85	2.46	0.255	7.54e-05
Bin 13	24 dB < SNR_c* <= 26 dB	17.3	62.2	5.41	3.22	3.09	5.79	2.94	0.0847	9.01e-05
Bin 14	26 dB < SNR_c* <= 28 dB	11.3	66.7	5.81	3.46	3.32	6.22	3.16	0.0418	9.67e-05
Bin 15	28 dB < SNR_c* <= 30 dB	5.98	70.7	6.15	3.67	3.52	6.59	3.35	0.0171	0.000102
Bin 16	30 dB < SNR_c* <= 32 dB	3.09	72.9	6.34	3.78	3.62	6.79	3.45	0.00354	0.000106
Bin 17	32 dB < SNR_c* <= 34 dB	2.29	73.5	6.4	3.81	3.65	6.85	3.48	0.00237	0.000107
Bin 18	34 dB < SNR_c* <= 36 dB	1.5	74.1	6.45	3.84	3.68	6.9	3.51	0.00244	0.000107
Bin 19	36 dB < SNR_c* <= 38 dB	1.01	74.5	6.48	3.86	3.7	6.94	3.52	0.00125	0.000108
Bin 20	38 dB < SNR_c* <= 40 dB	0.587	74.8	6.51	3.88	3.72	6.97	3.54	0.000766	0.000108
Bin 21	40 dB < SNR_c* <= 42 dB	0.441	74.9	6.52	3.89	3.72	6.98	3.54	0.000587	0.000109
Bin 22	42 dB < SNR_c* <= +∞ dB	0.441	74.9	6.52	3.89	3.72	6.98	3.54	0.000587	0.000109

* The corrected SNR, SNR_c, is an output option when using the NOM software. See discussion in Section V.

**Using single precision instead of double precision when computing loudness levels is expected to contribute less to the total variance than the GRS sample rate effect, so precision effects were excluded from these analyses.

Table 5.2: Proportion of the total variance explained by each uncertainty source for the ISBAP noise metric for each corrected SNR bin, where the lower and upper edge of each bin is identified in column two.

Metric: ISBAP	Use condition (Bin Edges, ISBAP)	Background noise % of total	Mic calibration % of total	Mic amb temp % of total	ADC gain % of total	Mic amb RH % of total	Windscreen IL % of total	Mic amb press % of total	Window jitter % of total	GRS sample rate** % of total
Bin 1	-∞ dB < SNR_c* <= 4 dB	99.1	0.354	0.0308	0.0184	0.0176	0.0227	0.0167	0.41	3.44e-07
Bin 2	4 dB < SNR_c* <= 6 dB	99.1	0.354	0.0308	0.0184	0.0176	0.0228	0.0168	0.41	3.44e-07
Bin 3	6 dB < SNR_c* <= 8 dB	99	0.611	0.0532	0.0317	0.0304	0.0392	0.0289	0.168	5.94e-07
Bin 4	8 dB < SNR_c* <= 10 dB	98.9	0.771	0.0671	0.04	0.0383	0.0495	0.0365	0.125	7.5e-07
Bin 5	10 dB < SNR_c* <= 12 dB	98.4	1.13	0.0981	0.0585	0.0561	0.0724	0.0534	0.0953	1.1e-06
Bin 6	12 dB < SNR_c* <= 14 dB	97.8	1.66	0.144	0.086	0.0824	0.106	0.0784	0.0948	1.61e-06
Bin 7	14 dB < SNR_c* <= 16 dB	96.5	2.63	0.228	0.136	0.131	0.169	0.124	0.104	2.55e-06
Bin 8	16 dB < SNR_c* <= 18 dB	95	3.74	0.326	0.194	0.186	0.241	0.177	0.102	3.64e-06
Bin 9	18 dB < SNR_c* <= 20 dB	92.4	5.75	0.5	0.298	0.286	0.369	0.272	0.129	5.59e-06
Bin 10	20 dB < SNR_c* <= 22 dB	85.1	11.2	0.978	0.583	0.559	0.722	0.532	0.297	1.09e-05
Bin 11	22 dB < SNR_c* <= 24 dB	70.5	22.3	1.94	1.16	1.11	1.43	1.06	0.496	2.17e-05
Bin 12	24 dB < SNR_c* <= 26 dB	53.9	35.1	3.05	1.82	1.74	2.25	1.66	0.455	3.41e-05
Bin 13	26 dB < SNR_c* <= 28 dB	36.7	48.5	4.22	2.52	2.41	3.11	2.29	0.267	4.71e-05
Bin 14	28 dB < SNR_c* <= 30 dB	21.7	60.1	5.23	3.12	2.99	3.86	2.84	0.194	5.84e-05
Bin 15	30 dB < SNR_c* <= 32 dB	11.2	68.3	5.94	3.54	3.39	4.39	3.23	0.0502	6.64e-05
Bin 16	32 dB < SNR_c* <= 34 dB	6.15	72.2	6.28	3.74	3.59	4.63	3.41	0.0375	7.02e-05
Bin 17	34 dB < SNR_c* <= 36 dB	3.88	73.9	6.43	3.83	3.67	4.75	3.5	0.00668	7.19e-05
Bin 18	36 dB < SNR_c* <= 38 dB	2.25	75.2	6.54	3.9	3.74	4.83	3.56	0.00368	7.31e-05
Bin 19	38 dB < SNR_c* <= 40 dB	1.66	75.6	6.58	3.92	3.76	4.86	3.58	0.00202	7.35e-05
Bin 20	40 dB < SNR_c* <= 42 dB	0.956	76.2	6.63	3.95	3.79	4.89	3.6	0.00111	7.41e-05
Bin 21	42 dB < SNR_c* <= 44 dB	0.892	76.2	6.63	3.95	3.79	4.9	3.61	0.000577	7.41e-05
Bin 22	44 dB < SNR_c* <= +∞ dB	0.892	76.2	6.63	3.95	3.79	4.9	3.61	0.000577	7.41e-05

* The corrected SNR, SNR_c, is an output option when using the NOM software. See discussion in Section V.

**Using single precision instead of double precision when computing loudness levels is expected to contribute less to the total variance than the GRS sample rate effect, so precision effects were excluded from these analyses.

Table 5.3: Proportion of the total variance explained by each uncertainty source for the ASEL noise metric for each corrected SNR bin, where the lower and upper edge of each bin is identified in column two.

Metric: ASEL	Use condition (Bin Edges, ASEL)	Background noise % of total	Mic calibration % of total	Mic amb temp % of total	ADC gain % of total	Mic amb RH % of total	Windscreen IL % of total	Mic amb press % of total	Window jitter % of total	GRS sample rate** % of total
Bin 1	-∞ dB < SNR_c* <= 0 dB	98.4	0.62	0.0539	0.0322	0.0308	0.0583	0.0293	0.78	1.06e-06
Bin 2	0 dB < SNR_c* <= 2 dB	98.4	0.62	0.054	0.0322	0.0308	0.0584	0.0294	0.78	1.06e-06
Bin 3	2 dB < SNR_c* <= 4 dB	99.2	0.424	0.0369	0.022	0.0211	0.0399	0.02	0.189	7.24e-07
Bin 4	4 dB < SNR_c* <= 6 dB	98.1	1.26	0.109	0.0652	0.0625	0.118	0.0595	0.196	2.15e-06
Bin 5	6 dB < SNR_c* <= 8 dB	92.1	5.72	0.497	0.297	0.284	0.538	0.27	0.298	9.78e-06
Bin 6	8 dB < SNR_c* <= 10 dB	77.1	16.9	1.47	0.876	0.839	1.59	0.799	0.405	2.89e-05
Bin 7	10 dB < SNR_c* <= 12 dB	52.4	35.3	3.07	1.83	1.75	3.32	1.67	0.644	6.04e-05
Bin 8	12 dB < SNR_c* <= 14 dB	27.8	53.7	4.67	2.78	2.67	5.05	2.54	0.805	9.18e-05
Bin 9	14 dB < SNR_c* <= 16 dB	14	64.2	5.59	3.33	3.19	6.04	3.04	0.609	0.00011
Bin 10	16 dB < SNR_c* <= 18 dB	7.15	69.6	6.05	3.61	3.46	6.55	3.29	0.317	0.000119
Bin 11	18 dB < SNR_c* <= 20 dB	4	72.1	6.27	3.74	3.58	6.78	3.41	0.152	0.000123
Bin 12	20 dB < SNR_c* <= 22 dB	2.12	73.5	6.4	3.81	3.66	6.92	3.48	0.0655	0.000126
Bin 13	22 dB < SNR_c* <= 24 dB	1.18	74.3	6.46	3.85	3.69	6.99	3.51	0.0212	0.000127
Bin 14	24 dB < SNR_c* <= 26 dB	0.654	74.7	6.5	3.87	3.71	7.03	3.53	0.0067	0.000128
Bin 15	26 dB < SNR_c* <= 28 dB	0.354	74.9	6.52	3.89	3.72	7.05	3.54	0.00214	0.000128
Bin 16	28 dB < SNR_c* <= 30 dB	0.227	75	6.53	3.89	3.73	7.06	3.55	0.00096	0.000128
Bin 17	30 dB < SNR_c* <= 32 dB	0.139	75.1	6.53	3.89	3.73	7.06	3.55	0.000434	0.000128
Bin 18	32 dB < SNR_c* <= 34 dB	0.0828	75.1	6.54	3.9	3.73	7.07	3.55	0.000217	0.000128
Bin 19	34 dB < SNR_c* <= 36 dB	0.0496	75.2	6.54	3.9	3.74	7.07	3.56	0.000177	0.000129
Bin 20	36 dB < SNR_c* <= 38 dB	0.0322	75.2	6.54	3.9	3.74	7.07	3.56	0.000119	0.000129
Bin 21	38 dB < SNR_c* <= 40 dB	0.0128	75.2	6.54	3.9	3.74	7.07	3.56	6.6e-05	0.000129
Bin 22	40 dB < SNR_c* <= 42 dB	0.011	75.2	6.54	3.9	3.74	7.07	3.56	4.66e-05	0.000129
Bin 23	42 dB < SNR_c* <= 44 dB	0.00911	75.2	6.54	3.9	3.74	7.07	3.56	1.54e-05	0.000129
Bin 24	44 dB < SNR_c* <= +∞ dB	0.00912	75.2	6.54	3.9	3.74	7.07	3.56	1.54e-05	0.000129

* The corrected SNR, SNR_c, is an output option when using the NOM software. See discussion in Section V.

**Using single precision instead of double precision when computing loudness levels is expected to contribute less to the total variance than the GRS sample rate effect, so precision effects were excluded from these analyses.

Table 5.4: Proportion of the total variance explained by each uncertainty source for the BSEL noise metric for each corrected SNR bin, where the lower and upper edge of each bin is identified in column two.

Metric: BSEL	Use condition (Bin Edges, BSEL)	Background noise % of total	Mic calibration % of total	Mic amb temp % of total	ADC gain % of total	Mic amb RH % of total	Windscreen IL % of total	Mic amb press % of total	Window jitter % of total	GRS sample rate** % of total
Bin 1	-∞ dB < SNR_c* <= 2 dB	98.4	0.931	0.081	0.0483	0.0463	0.054	0.044	0.398	8.77e-07
Bin 2	2 dB < SNR_c* <= 4 dB	98.4	0.929	0.0809	0.0482	0.0462	0.0539	0.044	0.397	8.75e-07
Bin 3	4 dB < SNR_c* <= 6 dB	98.3	1.13	0.0981	0.0585	0.0561	0.0654	0.0534	0.195	1.06e-06
Bin 4	6 dB < SNR_c* <= 8 dB	95.9	3.06	0.267	0.159	0.152	0.178	0.145	0.169	2.89e-06
Bin 5	8 dB < SNR_c* <= 10 dB	85.5	11	0.958	0.571	0.547	0.639	0.521	0.221	1.04e-05
Bin 6	10 dB < SNR_c* <= 12 dB	66	26.1	2.27	1.35	1.3	1.51	1.23	0.187	2.46e-05
Bin 7	12 dB < SNR_c* <= 14 dB	42.4	44.4	3.86	2.3	2.21	2.57	2.1	0.132	4.18e-05
Bin 8	14 dB < SNR_c* <= 16 dB	22.6	59.7	5.2	3.1	2.97	3.47	2.83	0.106	5.63e-05
Bin 9	16 dB < SNR_c* <= 18 dB	12.9	67.2	5.85	3.49	3.34	3.9	3.18	0.102	6.34e-05
Bin 10	18 dB < SNR_c* <= 20 dB	6.98	71.8	6.25	3.73	3.57	4.17	3.4	0.0991	6.77e-05
Bin 11	20 dB < SNR_c* <= 22 dB	3.79	74.3	6.47	3.85	3.69	4.31	3.51	0.0734	7e-05
Bin 12	22 dB < SNR_c* <= 24 dB	2.4	75.4	6.56	3.91	3.75	4.37	3.57	0.0493	7.1e-05
Bin 13	24 dB < SNR_c* <= 26 dB	1.6	76	6.62	3.94	3.78	4.41	3.6	0.0251	7.16e-05
Bin 14	26 dB < SNR_c* <= 28 dB	1.01	76.5	6.66	3.97	3.8	4.44	3.62	0.0127	7.21e-05
Bin 15	28 dB < SNR_c* <= 30 dB	0.644	76.8	6.68	3.98	3.82	4.45	3.63	0.00699	7.23e-05
Bin 16	30 dB < SNR_c* <= 32 dB	0.421	77	6.7	3.99	3.83	4.46	3.64	0.0024	7.25e-05
Bin 17	32 dB < SNR_c* <= 34 dB	0.26	77.1	6.71	4	3.83	4.47	3.65	0.000923	7.26e-05
Bin 18	34 dB < SNR_c* <= 36 dB	0.18	77.1	6.71	4	3.83	4.47	3.65	0.000572	7.27e-05
Bin 19	36 dB < SNR_c* <= 38 dB	0.125	77.2	6.72	4	3.84	4.48	3.65	0.00033	7.27e-05
Bin 20	38 dB < SNR_c* <= 40 dB	0.0701	77.2	6.72	4.01	3.84	4.48	3.65	0.000233	7.28e-05
Bin 21	40 dB < SNR_c* <= 42 dB	0.0454	77.2	6.72	4.01	3.84	4.48	3.65	0.000136	7.28e-05
Bin 22	42 dB < SNR_c* <= 44 dB	0.0296	77.3	6.72	4.01	3.84	4.48	3.66	0.000102	7.28e-05
Bin 23	44 dB < SNR_c* <= +∞ dB	0.0296	77.3	6.72	4.01	3.84	4.48	3.66	0.000102	7.28e-05

* The corrected SNR, SNR_c, is an output option when using the NOM software. See discussion in Section V.

**Using single precision instead of double precision when computing loudness levels is expected to contribute less to the total variance than the GRS sample rate effect, so precision effects were excluded from these analyses.

Table 5.5: Proportion of the total variance explained by each uncertainty source for the CSEL noise metric for each corrected SNR bin, where the lower and upper edge of each bin is identified in column two.

Metric: CSEL	Use condition (Bin Edges, CSEL)	Background noise % of total	Mic calibration % of total	Mic amb temp % of total	ADC gain % of total	Mic amb RH % of total	Windscreen IL % of total	Mic amb press % of total	Window jitter % of total	GRS sample rate** % of total
Bin 1	-∞ dB < SNR_c* <= 6 dB	94.8	3.89	0.339	0.202	0.193	0.0374	0.184	0.342	1.91e-06
Bin 2	6 dB < SNR_c* <= 8 dB	94.8	3.89	0.338	0.202	0.193	0.0374	0.184	0.342	1.91e-06
Bin 3	8 dB < SNR_c* <= 10 dB	86.8	10.4	0.906	0.54	0.517	0.1	0.492	0.281	5.1e-06
Bin 4	10 dB < SNR_c* <= 12 dB	77.8	17.7	1.54	0.916	0.878	0.17	0.835	0.169	8.66e-06
Bin 5	12 dB < SNR_c* <= 14 dB	61.6	30.7	2.67	1.59	1.53	0.295	1.45	0.165	1.51e-05
Bin 6	14 dB < SNR_c* <= 16 dB	44.5	44.5	3.87	2.31	2.21	0.428	2.11	0.091	2.18e-05
Bin 7	16 dB < SNR_c* <= 18 dB	23.1	61.7	5.37	3.2	3.07	0.593	2.92	0.0452	3.02e-05
Bin 8	18 dB < SNR_c* <= 20 dB	11.8	70.8	6.16	3.67	3.52	0.68	3.35	0.0215	3.47e-05
Bin 9	20 dB < SNR_c* <= 22 dB	6.62	75	6.52	3.89	3.73	0.72	3.55	0.0112	3.68e-05
Bin 10	22 dB < SNR_c* <= 24 dB	3.33	77.6	6.75	4.03	3.86	0.746	3.67	0.00774	3.8e-05
Bin 11	24 dB < SNR_c* <= 26 dB	2.11	78.6	6.84	4.08	3.91	0.755	3.72	0.00551	3.85e-05
Bin 12	26 dB < SNR_c* <= 28 dB	1.47	79.1	6.88	4.1	3.93	0.76	3.74	0.00432	3.88e-05
Bin 13	28 dB < SNR_c* <= 30 dB	0.978	79.5	6.92	4.12	3.95	0.764	3.76	0.00401	3.9e-05
Bin 14	30 dB < SNR_c* <= 32 dB	0.644	79.8	6.94	4.14	3.97	0.767	3.77	0.00253	3.91e-05
Bin 15	32 dB < SNR_c* <= 34 dB	0.379	80	6.96	4.15	3.98	0.769	3.78	0.00207	3.92e-05
Bin 16	34 dB < SNR_c* <= 36 dB	0.27	80.1	6.97	4.15	3.98	0.77	3.79	0.00127	3.93e-05
Bin 17	36 dB < SNR_c* <= 38 dB	0.183	80.1	6.97	4.16	3.98	0.77	3.79	0.000805	3.93e-05
Bin 18	38 dB < SNR_c* <= 40 dB	0.119	80.2	6.98	4.16	3.99	0.771	3.79	0.000485	3.93e-05
Bin 19	40 dB < SNR_c* <= 42 dB	0.087	80.2	6.98	4.16	3.99	0.771	3.79	0.000238	3.93e-05
Bin 20	42 dB < SNR_c* <= 44 dB	0.055	80.2	6.98	4.16	3.99	0.771	3.8	0.000174	3.93e-05
Bin 21	44 dB < SNR_c* <= 46 dB	0.0284	80.3	6.98	4.16	3.99	0.771	3.8	0.000102	3.93e-05
Bin 22	46 dB < SNR_c* <= +∞ dB	0.0284	80.3	6.98	4.16	3.99	0.771	3.8	0.000102	3.93e-05

* The corrected SNR, SNR_c, is an output option when using the NOM software. See discussion in Section V.

**Using single precision instead of double precision when computing loudness levels is expected to contribute less to the total variance than the GRS sample rate effect, so precision effects were excluded from these analyses.

Table 5.6: Proportion of the total variance explained by each uncertainty source for the DSEL noise metric for each corrected SNR bin, where the lower and upper edge of each bin is identified in column two.

Metric: DSEL	Use condition (Bin Edges, DSEL)	Background noise % of total	Mic calibration % of total	Mic amb temp % of total	ADC gain % of total	Mic amb RH % of total	Windscreen IL % of total	Mic amb press % of total	Window jitter % of total	GRS sample rate** % of total
Bin 1	-∞ dB < SNR_c* <= 4 dB	98.7	0.878	0.0764	0.0456	0.0436	0.0133	0.0415	0.169	2.2e-07
Bin 2	4 dB < SNR_c* <= 6 dB	98.7	0.878	0.0764	0.0456	0.0437	0.0133	0.0415	0.17	2.2e-07
Bin 3	6 dB < SNR_c* <= 8 dB	96.5	2.68	0.233	0.139	0.133	0.0407	0.127	0.16	6.7e-07
Bin 4	8 dB < SNR_c* <= 10 dB	89.8	7.99	0.696	0.415	0.397	0.121	0.378	0.174	2e-06
Bin 5	10 dB < SNR_c* <= 12 dB	81.1	15	1.31	0.78	0.747	0.228	0.711	0.137	3.76e-06
Bin 6	12 dB < SNR_c* <= 14 dB	55.9	35.2	3.06	1.83	1.75	0.535	1.67	0.109	8.81e-06
Bin 7	14 dB < SNR_c* <= 16 dB	29.6	56.2	4.89	2.92	2.79	0.854	2.66	0.0623	1.41e-05
Bin 8	16 dB < SNR_c* <= 18 dB	13.4	69.2	6.02	3.59	3.44	1.05	3.27	0.0308	1.73e-05
Bin 9	18 dB < SNR_c* <= 20 dB	6.6	74.6	6.5	3.87	3.71	1.13	3.53	0.0204	1.87e-05
Bin 10	20 dB < SNR_c* <= 22 dB	3.91	76.8	6.68	3.98	3.82	1.17	3.63	0.0131	1.92e-05
Bin 11	22 dB < SNR_c* <= 24 dB	1.97	78.3	6.82	4.06	3.89	1.19	3.71	0.012	1.96e-05
Bin 12	24 dB < SNR_c* <= 26 dB	1.19	79	6.87	4.1	3.93	1.2	3.74	0.0102	1.98e-05
Bin 13	26 dB < SNR_c* <= 28 dB	0.709	79.4	6.91	4.12	3.94	1.21	3.75	0.00746	1.99e-05
Bin 14	28 dB < SNR_c* <= 30 dB	0.458	79.6	6.92	4.13	3.95	1.21	3.76	0.00445	1.99e-05
Bin 15	30 dB < SNR_c* <= 32 dB	0.289	79.7	6.93	4.13	3.96	1.21	3.77	0.00269	1.99e-05
Bin 16	32 dB < SNR_c* <= 34 dB	0.189	79.8	6.94	4.14	3.97	1.21	3.77	0.00186	2e-05
Bin 17	34 dB < SNR_c* <= 36 dB	0.117	79.8	6.95	4.14	3.97	1.21	3.78	0.000815	2e-05
Bin 18	36 dB < SNR_c* <= 38 dB	0.0873	79.9	6.95	4.14	3.97	1.21	3.78	0.000357	2e-05
Bin 19	38 dB < SNR_c* <= 40 dB	0.0544	79.9	6.95	4.14	3.97	1.21	3.78	0.00024	2e-05
Bin 20	40 dB < SNR_c* <= 42 dB	0.0382	79.9	6.95	4.14	3.97	1.21	3.78	0.000152	2e-05
Bin 21	42 dB < SNR_c* <= 44 dB	0.0246	79.9	6.95	4.15	3.97	1.21	3.78	8.3e-05	2e-05
Bin 22	44 dB < SNR_c* <= +∞ dB	0.0246	79.9	6.95	4.15	3.97	1.21	3.78	8.3e-05	2e-05

* The corrected SNR, SNR_c, is an output option when using the NOM software. See discussion in Section V.

**Using single precision instead of double precision when computing loudness levels is expected to contribute less to the total variance than the GRS sample rate effect, so precision effects were excluded from these analyses.

Table 5.7: Proportion of the total variance explained by each uncertainty source for the ESEL noise metric for each corrected SNR bin, where the lower and upper edge of each bin is identified in column two.

Metric: ESEL	Use condition (Bin Edges, ESEL)	Background noise % of total	Mic calibration % of total	Mic amb temp % of total	ADC gain % of total	Mic amb RH % of total	Windscreen IL % of total	Mic amb press % of total	Window jitter % of total	GRS sample rate** % of total
Bin 1	-∞ dB < SNR_c* <= 2 dB	98.8	0.693	0.0603	0.0359	0.0344	0.0418	0.0328	0.295	7.24e-07
Bin 2	2 dB < SNR_c* <= 4 dB	98.8	0.693	0.0603	0.0359	0.0344	0.0418	0.0328	0.295	7.24e-07
Bin 3	4 dB < SNR_c* <= 6 dB	98	1.35	0.118	0.0702	0.0673	0.0817	0.064	0.259	1.41e-06
Bin 4	6 dB < SNR_c* <= 8 dB	95.1	3.62	0.315	0.188	0.18	0.218	0.171	0.198	3.78e-06
Bin 5	8 dB < SNR_c* <= 10 dB	82.6	13.2	1.15	0.686	0.657	0.798	0.625	0.233	1.38e-05
Bin 6	10 dB < SNR_c* <= 12 dB	61.1	29.9	2.6	1.55	1.49	1.8	1.41	0.21	3.12e-05
Bin 7	12 dB < SNR_c* <= 14 dB	37.3	48.3	4.2	2.5	2.4	2.91	2.28	0.188	5.04e-05
Bin 8	14 dB < SNR_c* <= 16 dB	19.2	62.2	5.41	3.22	3.09	3.75	2.94	0.203	6.5e-05
Bin 9	16 dB < SNR_c* <= 18 dB	9.78	69.4	6.04	3.6	3.45	4.19	3.28	0.215	7.26e-05
Bin 10	18 dB < SNR_c* <= 20 dB	4.99	73.2	6.37	3.8	3.64	4.42	3.46	0.16	7.65e-05
Bin 11	20 dB < SNR_c* <= 22 dB	3.06	74.7	6.5	3.88	3.71	4.51	3.53	0.0802	7.81e-05
Bin 12	22 dB < SNR_c* <= 24 dB	1.86	75.7	6.58	3.93	3.76	4.57	3.58	0.0455	7.91e-05
Bin 13	24 dB < SNR_c* <= 26 dB	1.14	76.2	6.63	3.96	3.79	4.6	3.61	0.0233	7.97e-05
Bin 14	26 dB < SNR_c* <= 28 dB	0.711	76.6	6.66	3.97	3.81	4.62	3.62	0.0098	8.01e-05
Bin 15	28 dB < SNR_c* <= 30 dB	0.427	76.8	6.68	3.98	3.82	4.64	3.63	0.00285	8.03e-05
Bin 16	30 dB < SNR_c* <= 32 dB	0.285	76.9	6.69	3.99	3.82	4.64	3.64	0.00109	8.04e-05
Bin 17	32 dB < SNR_c* <= 34 dB	0.168	77	6.7	4	3.83	4.65	3.64	0.000529	8.05e-05
Bin 18	34 dB < SNR_c* <= 36 dB	0.113	77.1	6.71	4	3.83	4.65	3.65	0.000358	8.06e-05
Bin 19	36 dB < SNR_c* <= 38 dB	0.0736	77.1	6.71	4	3.83	4.65	3.65	0.000212	8.06e-05
Bin 20	38 dB < SNR_c* <= 40 dB	0.041	77.1	6.71	4	3.83	4.66	3.65	0.000174	8.06e-05
Bin 21	40 dB < SNR_c* <= 42 dB	0.0267	77.1	6.71	4	3.83	4.66	3.65	8.95e-05	8.06e-05
Bin 22	42 dB < SNR_c* <= 44 dB	0.0188	77.1	6.71	4	3.83	4.66	3.65	5.69e-05	8.06e-05
Bin 23	44 dB < SNR_c* <= +∞ dB	0.0189	77.1	6.71	4	3.83	4.66	3.65	5.69e-05	8.06e-05

* The corrected SNR, SNR_c, is an output option when using the NOM software. See discussion in Section V.

**Using single precision instead of double precision when computing loudness levels is expected to contribute less to the total variance than the GRS sample rate effect, so precision effects were excluded from these analyses.

Table 5.8: Proportion of the total variance explained by each uncertainty source for the ZSEL noise metric for each corrected SNR bin, where the lower and upper edge of each bin is identified in column two.

Metric: ZSEL	Use condition (Bin Edges, ZSEL)	Background noise % of total	Mic calibration % of total	Mic amb temp % of total	ADC gain % of total	Mic amb RH % of total	Windscreen IL % of total	Mic amb press % of total	Window jitter % of total	GRS sample rate** % of total
Bin 1	-∞ dB < SNR_c* <= 6 dB	94.8	3.81	0.331	0.198	0.189	0.000121	0.18	0.478	1.11e-06
Bin 2	6 dB < SNR_c* <= 8 dB	94.8	3.81	0.331	0.198	0.189	0.000121	0.18	0.478	1.11e-06
Bin 3	8 dB < SNR_c* <= 10 dB	91.9	6.07	0.528	0.315	0.302	0.000193	0.287	0.555	1.77e-06
Bin 4	10 dB < SNR_c* <= 12 dB	90	7.88	0.686	0.409	0.392	0.000251	0.373	0.264	2.3e-06
Bin 5	12 dB < SNR_c* <= 14 dB	83.6	13.1	1.14	0.681	0.653	0.000418	0.621	0.145	3.83e-06
Bin 6	14 dB < SNR_c* <= 16 dB	73.6	21.3	1.85	1.1	1.06	0.000677	1.01	0.128	6.21e-06
Bin 7	16 dB < SNR_c* <= 18 dB	61.7	30.9	2.69	1.6	1.53	0.000984	1.46	0.111	9.01e-06
Bin 8	18 dB < SNR_c* <= 20 dB	43.9	45.3	3.94	2.35	2.25	0.00144	2.14	0.068	1.32e-05
Bin 9	20 dB < SNR_c* <= 22 dB	30.6	56.1	4.88	2.91	2.79	0.00179	2.66	0.0419	1.64e-05
Bin 10	22 dB < SNR_c* <= 24 dB	22.8	62.5	5.44	3.24	3.11	0.00199	2.96	0.0271	1.82e-05
Bin 11	24 dB < SNR_c* <= 26 dB	14.6	69.1	6.01	3.58	3.43	0.0022	3.27	0.0196	2.02e-05
Bin 12	26 dB < SNR_c* <= 28 dB	10.5	72.4	6.3	3.75	3.6	0.00231	3.42	0.0144	2.11e-05
Bin 13	28 dB < SNR_c* <= 30 dB	5.76	76.2	6.63	3.96	3.79	0.00243	3.61	0.0111	2.23e-05
Bin 14	30 dB < SNR_c* <= 32 dB	3.48	78.1	6.8	4.05	3.88	0.00249	3.69	0.00879	2.28e-05
Bin 15	32 dB < SNR_c* <= 34 dB	2.01	79.3	6.9	4.11	3.94	0.00253	3.75	0.00682	2.31e-05
Bin 16	34 dB < SNR_c* <= 36 dB	1.16	80	6.96	4.15	3.97	0.00255	3.78	0.00495	2.33e-05
Bin 17	36 dB < SNR_c* <= 38 dB	0.765	80.3	6.99	4.16	3.99	0.00256	3.8	0.00384	2.34e-05
Bin 18	38 dB < SNR_c* <= 40 dB	0.477	80.5	7.01	4.18	4	0.00257	3.81	0.00339	2.35e-05
Bin 19	40 dB < SNR_c* <= 42 dB	0.259	80.7	7.02	4.19	4.01	0.00257	3.82	0.00299	2.36e-05
Bin 20	42 dB < SNR_c* <= 44 dB	0.167	80.8	7.03	4.19	4.01	0.00257	3.82	0.00243	2.36e-05
Bin 21	44 dB < SNR_c* <= 46 dB	0.106	80.8	7.03	4.19	4.02	0.00258	3.82	0.00181	2.36e-05
Bin 22	46 dB < SNR_c* <= 48 dB	0.0727	80.9	7.04	4.19	4.02	0.00258	3.82	0.00115	2.36e-05
Bin 23	48 dB < SNR_c* <= 50 dB	0.0453	80.9	7.04	4.2	4.02	0.00258	3.83	0.000682	2.36e-05
Bin 24	50 dB < SNR_c* <= 52 dB	0.0571	80.9	7.04	4.19	4.02	0.00258	3.83	0.000519	2.36e-05
Bin 25	52 dB < SNR_c* <= +∞ dB	0.0572	80.9	7.04	4.19	4.02	0.00258	3.83	0.00052	2.36e-05

* The corrected SNR, SNR_c, is an output option when using the NOM software. See discussion in Section V.

**Using single precision instead of double precision when computing loudness levels is expected to contribute less to the total variance than the GRS sample rate effect, so precision effects were excluded from these analyses.

This page intentionally left blank.